Imperial College London
Department of Physics

Monopoles, sphalerons and instantons in strong magnetic fields

David L.-J. Ho

Submitted in part fulfilment of the requirements for the degree of
Doctor of Philosophy in Physics of Imperial College London
and the Diploma of Imperial College London, November 2021

Abstract

Magnetic monopoles are hypothetical particles consisting of an isolated north or south magnetic pole without a partner. Though they are currently unobserved, predictions from quantum field theory indicate that if they do exist, they should be produced in north-south pairs by a strong enough magnetic field.

The rate of production of monopoles in weak, constant magnetic fields has been known for decades, but strong fields and fields that change in space and time present significant complications. This thesis calculates the rate of monopole production in time-dependent fields, and in constant fields well beyond the weak-field limit. We find that in field theories admitting monopoles as topological solitons, such as Grand Unified Theories, monopole production occurs by a classical instability when the field exceeds the Ambjørn-Olesen critical field strength. In doing this, we explicitly compute new sphaleron and instanton solutions in Georgi-Glashow SU(2) theory for the first time. The techniques we use to find these solutions are applicable beyond monopole production—we also compute the electroweak sphaleron configuration, responsible for baryon and lepton number violation in the Standard Model, in the background of a strong magnetic field, over the full range of physically relevant field strengths.

Our calculations are motivated by the possibility of producing monopoles in ultrarelativistic heavy ion collisions, which generate some of the strongest magnetic fields in the known Universe. Though a complete calculation of the monopole production cross section in these collisions remains elusive, we present approximations that can reasonably be expected to give a lower bound on the overall production probability, and compute the approximate momentum distribution of the produced particles. This information can be used directly by experimental collaborations to place bounds on monopole masses using data from heavy ion collisions.

Statement of Originality

I declare that the work presented in this thesis is my own unless otherwise stated. Where the work of others has been referenced or quoted, this is attributed as a reference. Some of the work presented here has is based on previously published material:

- Sections **??** to **??** are based on Ref. [**?**], authored in collaboration with Oliver Gould and Arttu Rajantie, and published in Physical Review D. Specifically, the calculation of the electromagnetic fields and numerical computation of the worldline instantons were performed by Oliver Gould.
- Sections **??** to **??** are based on Ref. [**?**], authored in collaboration with Oliver Gould and Arttu Rajantie, and accepted for publication in Physical Review D. Specifically, the work on the locally constant field approximation was contributed by Oliver Gould, and that on the uncertainty principle was contributed by Arttu Rajantie.
- The experimental work described in Section **??** is reported in Ref. [**?**], authored in conjunction with the MoEDAL collaboration and submitted for publication. I helped to contribute the theoretical approximations used to derive the main results of the paper.
- Section **??** is based on Ref. [**?**], authored in collaboration with Arttu Rajantie, and published in Physical Review D.
- Section **??** is based on Ref. [**?**], authored in collaboration with Arttu Rajantie, and published in Physical Review D.
- Chapter **??** is based on Ref. [**?**], authored in collaboration with Arttu Rajantie, and published in Physical Review D.

Acknowledgements

I would like to thank my supervisor, Arttu Rajantie, for his support, advice, and guidance throughout the course of my research. I would also like to thank my PhD student colleagues for helpful discussions on all aspects of physics and beyond.

I am grateful for the funding from the UK Science and Technology Facilities Council (STFC), without which this PhD would not have been possible. The numerical results in Chapter **??** were obtained using computational resources provided by CSC—IT Centre for Science, Finland, and those in Chapters **??** and **??** were obtained using computational resources provided by Imperial College Research Computing Service.

In memory of Gerry Lawrence.

Notation and conventions

Vectors

Points and vectors in spacetime of arbitrary dimension are denoted using unadorned letters, e.g. x, potentially carrying an index (e.g. x_μ). Greek indices from the latter part of the alphabet $\mu, \nu, \rho, \sigma, \ldots$ are used to index spacetime dimensions. Spatial vectors in three dimensions are denoted using a superscript arrow, e.g. $\vec{x}$, $\vec{B}$. Roman indices $i, j, k, \ldots$ are used to index spatial dimensions. Abstract collections of scalar variables that are not explicitly related to space or spacetime are denoted using bold typeface, e.g. $\mathbf{x}, \mathbf{G}$. Greek indices from the first part of the alphabet $\alpha, \beta, \gamma, \ldots$ are used to index these objects.

Units

Unless otherwise specified, natural units are used in which the constants $\hbar$, c, ε_0, μ_0 and k_B are equal to one.

Metric signature

The signature of the Minkowski metric is the "mostly minus" convention $(+, -, -, -)$.

Symbols

The letter m without a subscript always refers to a monopole mass, and g without a subscript always refers to monopole charge.

Every effort has been made to ensure that the symbols in this work are as unambiguous as possible. Due to the finiteness of the Latin and Greek alphabets, there is some inevitable

duplication; we have attempted only to do so where the intended meaning can be inferred easily from context. For reference, a full list of symbols used is provided in Appendix **??**.

Contents

Chapter 1

Introduction

1.1 What are magnetic monopoles?

The nature of magnetism has fascinated humans since ancient times, when naturally occurring magnetite deposits, known as lodestones, were found to attract iron [**?**]. A key feature of the magnetic force is the fact that all magnets observed by humans consist of two inseparable poles. These are commonly given the names "north" and "south" due to the orientation of the Earth's own magnetic field.[1] The concept of a magnetic monopole is straightforward to understand—an isolated north or south pole without a partner. However, according to all available evidence, magnetic monopoles appear not to be included in the building blocks of the Universe.

The nonexistence of magnetic charges may be summarised neatly by the Maxwell equation

$$\vec{\nabla} \cdot \vec{B} = 0; \tag{1.1}$$

the divergence of the magnetic field $\vec{B}$ is everywhere vanishing. An equivalent qualitative statement is that magnetic field lines only form closed loops; they do not start or end. This is in stark contrast to electric field lines, which start and end on electric charges such as electrons or protons. In the language of Maxwell's equations

$$\vec{\nabla} \cdot \vec{E} = \rho_{\mathrm{E}}, \tag{1.2}$$

where $\vec{E}$ denotes the electric field and ρ_{E} is the density of electric charge in natural units.

The apparent lack of magnetic monopoles is an empirical observation: there is no known *a priori* reason why these particles should not exist. A magnetic monopole would interact

[1] The convention is that the north pole of a magnet will point towards the magnetic North Pole of the Earth. This means, somewhat confusingly, that the Earth's magnetic North Pole is in fact a south pole.

with a magnetic field in an analogous way to an electric charge interacting with an electric field, accelerating parallel to the field direction. The magnetic field of a monopole would obey Coulomb's law:

$$\vec{B}(\vec{x}) = \frac{g\vec{x}}{4\pi r^3}, \tag{1.3}$$

where g is the monopole charge and $r = |\vec{x}|$. Over large distances, north and south monopoles would attract each other, and would be each other's antiparticles: they could annihilate, releasing energy in the form of photons. Under the correct conditions, presumably, one could also create monopole-antimonopole (north-south) pairs. This, or indeed any other direct or indirect evidence of the existence of monopoles, has never been observed.

1.2 Why are monopoles important?

Since at least the thirteenth century [**?**], scientific searches for monopoles have returned uniformly negative results, despite extensive efforts (see Section **??** for more details). It is reasonable to question why there should be so much effort spent searching for something that there is no evidence for.

The first—and by many measures the least important—reason why monopoles are believed to exist is due to aesthetics. Should monopoles be found, the theory of electromagnetism would become symmetric under the exchange of electricity and magnetism, interchanging electric charges with their magnetic counterparts. In other words, Eq. (**??**) and Eq. (**??**) would look the same, just with different symbol names. This symmetry is known as electromagnetic duality, and its realisation would be considered by many to be pleasing. Famously, Dirac remarked that he would be "surprised if Nature had made no use of it" [**?**].

Arguments from beauty, however, are not the only motivation for believing that magnetic monopoles should exist. Monopoles are not only permitted, but *predicted* to exist by a wide class of theories extending the Standard Model of particle physics, including all Grand Unified Theories [**?**, **?**]; theories that describe the electromagnetic, strong and weak forces as aspects of the same interaction. In such theories, monopoles exist as topological defects in quantum fields, in analogy to grain boundaries in crystals or vortices in fluids. An argument based on causality, known as the Kibble mechanism [**?**], shows that if these theories describe the Universe, monopoles must have formed during a phase transition shortly after the Big Bang.

Finding a monopole from a Grand Unified Theory would provide an invaluable opportunity: unlike many hypothesised particles beyond the Standard Model, monopoles are expected to be totally stable. This means that if a monopole were found it could be studied at leisure,

and multiple experiments could be performed on the same sample. Furthermore, the microscopic nature of the monopole would offer a chance to probe the nature of the fields from which the monopole is comprised, without requiring impossibly high-energy particle accelerators. The converse prospect is equally exciting: If monopoles were shown conclusively not to exist, it would imply that no Grand Unified Theory could describe the Universe. It would also rule out theories with compact extra dimensions (including string theories), which admit similar monopole solutions [**?**, **?**]. As these theories are some of the leading contenders for extending the Standard Model, such a discovery would revolutionise theoretical high-energy physics.

It is instructive to consider how this latter possibility could come to be demonstrated—negative statements are notoriously difficult to prove. One possible route towards showing that monopoles cannot exist stems from a result known as the Dirac quantisation condition [**?**]. This states that in order for a monopole to be consistent with quantum mechanics, the monopole charge g and the electric charge e must obey the relation

$$eg = 2\pi n, \tag{1.4}$$

where n is an integer. This relation must hold for any pair of electric and magnetically charged particles. As a consequence, if even a single monopole exists in the Universe, all electric charges and magnetic charges must be quantised. This appears to reflect empirical evidence: all observed free particles carry integer multiples of the electron charge.[2] If a continuous spectrum of electric charges were found, or a particle with an electric charge that was an irrational multiple of e, magnetic monopoles would not be consistent with a quantum mechanical description of reality.

1.3 Why are monopoles difficult?

As previously mentioned, all monopole searches carried out so far have failed to find any evidence for the existence of monopoles. In order to interpret these negative findings quantitatively, it is vital to have a firm theoretical understanding of the mechanisms by which monopoles would be produced, if they existed. This theoretical understanding is difficult to obtain, however, due to the strong coupling between the monopole and the electromagnetic field. Eq. (**??**) shows that magnetic charges must come in integer multiples of the Dirac charge

$$g_{\mathrm{D}} = \frac{2\pi}{e}, \tag{1.5}$$

[2]For a discussion of the quantisation condition applied to quarks, see Ref. [**?**].

where e is the magnitude of the electron charge. At zero energy,

$$e \approx 0.303, \tag{1.6}$$

and the electric fine structure constant

$$\alpha = \frac{e^2}{4\pi} \approx \frac{1}{137}. \tag{1.7}$$

As this is much smaller than one, this means that observables in quantum electrodynamics (QED) can be computed perturbatively as a series in increasing powers of α. Including more terms in a perturbation series allows arbitrary accuracy to be obtained, as each power of α contributes less to the overall result. Feynman diagrams are a powerful tool for computing such quantities, and perturbative calculations in QED are some of the most accurate theoretical calculations ever carried out.

This fortuitous feature of electrodynamics is a pitfall of magnetodynamics, the counterpart dealing with magnetic charges. A particle carrying a single unit of Dirac magnetic charge has

$$g \approx 20.7, \tag{1.8}$$

and the magnetic fine structure constant

$$\alpha_{\mathrm{M}} \approx \frac{137}{4}. \tag{1.9}$$

This is much larger than one, so successive terms in a perturbation series increase in magnitude. This means that perturbation theory is totally inapplicable to magnetic monopoles.

The failure of perturbation theory poses a serious problem for the interpretation of experimental results concerning monopoles. For example, consider a particle accelerator experiment, reaching centre of mass energy $\sqrt{s}$, from which no monopoles are detected. There exists some relation between the mass m and charge g of the monopole, the collision energy, and the probability of producing a monopole-antimonopole pair:

$$P(\text{Monopole production}) = f(m, g; \sqrt{s}). \tag{1.10}$$

Assuming the function f is monotonic in m and $\sqrt{s}$, the null result at energy $\sqrt{s}$ can be used to place a lower bound on m for a given g to the desired level of confidence. Currently, however, this function is not reliably known, meaning that existing bounds on monopole masses are questionable.

This thesis documents the progress made towards overcoming these theoretical difficulties, and provides steps towards a truly reliable calculation of the function in Eq. (**??**). The main

mechanism we choose to investigate is the Schwinger effect [**?**, **?**]: the quantum mechanical process by which a field is unstable to decay into charged particle-antiparticle pairs. If magnetic monopoles exist, a sufficiently strong magnetic field should produce them.

1.4 Thesis structure

Immediately following, in Chapter **??**, we provide a brief review of some theoretical aspects of nonperturbative objects in field theory, as well as a summary of the experimental status of magnetic monopoles. The topics reviewed are broad and rich, so only the points most relevant to the work presented in later chapters are discussed; the references in Chapter **??** offer more comprehensive introductions for the interested reader.

In Chapter **??** we review the production of monopoles from magnetic fields in general terms, focusing on instanton methods. We outline the theoretical background behind the methods used in later chapters to obtain the main results of this thesis.

In Chapter **??** we outline important numerical methods used in later parts of the thesis. For the most part, this chapter is also review, though some of the implementations of the algorithms are, to the author's knowledge, novel.

In Chapter **??** we present the results of a series of calculations regarding monopole production in the electromagnetic fields generated in ultrarelativistic heavy ion collisions. A production cross section for monopoles in heavy ion collisions, derived using the worldline approximation, is presented. Though it is found that for ultrarelativistic heavy ion collisions the worldline assumption is not valid, we present arguments as to why the results are likely to provide a lower bound on the cross section. The momentum distribution of the produced particles is also examined, and the resulting approximate distribution is suitable for experimental use in modelling the trajectories of monopoles produced in particle accelerators.

In Chapter **??** we show the first steps taken towards overcoming the limitations of Chapter **??** by relaxing the worldline assumption, and taking the internal structure of the monopoles into account. In order to achieve this, we work in a non-Abelian gauge theory where monopoles are realised as soliton solutions to the field equations with nontrivial topological charge. Using the numerical methods outlined in Chapter **??**, we compute the pair production rate for solitonic monopoles at all relevant field strengths, up to the Ambjørn-Olesen critical field strength where the magnetic field itself becomes unstable [**?**]. At this point we show that if strong enough fields were produced, they would result in production of monopoles via a classical instability, rather than a quantum one.

In Chapter **??** we demonstrate the versatility of the numerical methods developed and employed in this thesis, by using similar techniques to investigate a different nonperturbative phenomenon. We present the results of a study into the effect of a strong magnetic field on sphaleron-induced baryogenesis in the Electroweak theory of the Standard Model. In a similar manner to the result of Chapter **??**, we show that the energy barrier to baryon and lepton number violation vanishes at a critical field strength set by the Higgs mass, again first identified by Ambjørn and Olesen [**?**, **?**].

Finally, in Chapter **??** we present concluding remarks and outline the possible next steps to be taken in future work.

Chapter 2

Nonperturbative objects in field theory

2.1 Elementary monopoles

Starting with the Maxwell equations in terms of electric fields $\vec{E}$ and magnetic fields $\vec{B}$, it is straightforward to include magnetic charges in classical electromagnetism: in units where $\varepsilon_0 = \mu_0 = 1$,

$$\vec{\nabla} \cdot \vec{E} = \rho_{\mathrm{E}}, \tag{2.1}$$

$$\vec{\nabla} \cdot \vec{B} = \rho_{\mathrm{M}}, \tag{2.2}$$

$$\vec{\nabla} \times \vec{E} = -\frac{\partial \vec{B}}{\partial t} - \vec{J}_{\mathrm{M}}, \tag{2.3}$$

$$\vec{\nabla} \times \vec{B} = \frac{\partial \vec{E}}{\partial t} + \vec{J}_{\mathrm{E}}. \tag{2.4}$$

Here ρ and $\vec{J}$ denote charge and current densities respectively, with the subscripts E and M distinguishing between electric and magnetic sources. These modified Maxwell equations are invariant under electromagnetic duality, interchanging electricity and magnetism:

$$\begin{aligned} \vec{E} &\to -\vec{B}, & \vec{B} &\to \vec{E}, \\ \rho_{\mathrm{E}} &\to -\rho_{\mathrm{M}}, & \rho_{\mathrm{M}} &\to \rho_{\mathrm{E}}, \\ \vec{J}_{\mathrm{E}} &\to -\vec{J}_{\mathrm{M}}, & \vec{J}_{\mathrm{M}} &\to \vec{J}_{\mathrm{E}}. \end{aligned} \tag{2.5}$$

However, when formulating electromagnetism in terms of potentials, at first glance it appears that monopoles are forbidden. This is because defining the magnetic field in terms of the 3-potential $\vec{A}$ as $\vec{B} = \vec{\nabla} \times \vec{A}$ requires $\vec{\nabla} \cdot \vec{B} = 0$ identically. Given this fact, the existence of

the Dirac potential [?]

$$\vec{A}(\vec{x}) = \frac{g}{r}\frac{\vec{x}\times\vec{n}}{r-\vec{x}\cdot\vec{n}} \tag{2.6}$$

appears puzzling. Here $\vec{x}$ is a displacement vector from the spatial origin, $r = |\vec{x}|$ and $\vec{n}$ is a constant (arbitrary) unit vector. One can readily verify that (almost everywhere) this potential gives

$$\vec{\nabla}\times\vec{A} = \frac{g\vec{x}}{4\pi r^3}, \tag{2.7}$$

the Coulomb field for a magnetic monopole of charge g. The key to reconciling this with the solenoidal nature of the magnetic field lies in the "almost everywhere" caveat. Along the line where $\vec{x}\cdot\vec{n} \geq 0$, the potential is singular—this is known as the Dirac string. This semi-infinite line may be thought of as the limit of an infinitesimally thin solenoid, carrying a magnetic flux of g inward to the origin and balancing the outward flux of the monopole. Furthermore, the position of the Dirac string can be rotated to any direction in space using a gauge transformation. This means that a Dirac string is not observable; it is purely a gauge object. Using locally defined gauge potentials [?] it is possible to remove the string singularity all together, leaving only the origin where the gauge potential is undefined.[1]

While the fact that the Dirac string is a gauge object precludes its observability in classical electromagnetism, in quantum mechanics this is not a sufficient condition. One way to see this is to consider the Aharonov-Bohm effect: when a particle with electric charge e is transported along a path through a magnetic field with potential $\vec{A}$, its wavefunction picks up a complex phase

$$\Delta\theta = e\int \vec{A}\cdot \mathrm{d}\vec{x}. \tag{2.8}$$

If we consider transporting an electric charge along a closed loop threaded by a Dirac string, we can see using Stokes' theorem that the resultant phase change is $\Delta\theta = eg$. In order for this to be unobservable—i.e. in order for the particle to be a true, spherically symmetric magnetic monopole—this must be an integer multiple of 2π. We therefore arrive at the Dirac quantisation condition [?]

$$eg = 2\pi n, \qquad n \in \mathbb{Z}. \tag{2.9}$$

The existence of a single monopole anywhere in the Universe would require the quantisation of electric charge. It has also been argued [?] that the converse is true: a theoretical explanation of charge quantisation would also predict the existence of monopoles.

Providing the quantisation condition is met, there is no known theoretical inconsistency in including elementary magnetic charges in quantum electrodynamics. Several equivalent

[1] The Coulomb potential of an electric charge is similarly undefined at the origin.

quantum field theoretic descriptions of quantum electromagnetodynamics (QEMD) exist [**?**, **?**, **?**, **?**], and while these are significantly more complicated than theories with only electric (or only magnetic) charges, they have been shown to be both Lorentz and gauge invariant [**?**, **?**]. A comprehensive overview of the classical and quantum treatment of elementary monopoles can be found in Ref. [**?**].

Despite the firm theoretical description of monopoles in quantum field theory, rigorous calculations of observables in QEMD are rare. This is because of another feature of the Dirac quantisation condition. The electric charge e is perturbatively small: at zero energy $e \approx 0.303$, which means that, as stated in Eq. (**??**), the magnetic fine structure constant is

$$\alpha_{\mathrm{M}} = \frac{g^2}{4\pi} = \frac{137}{4} \gg 1. \tag{2.10}$$

This means that the perturbative techniques that enable precision theoretical calculations in QED are inapplicable to magnetic monopoles. Overcoming the difficulties of strong coupling is an ongoing challenge in the theoretical study of magnetic monopoles, and is a key focus of this thesis.

2.2 Solitonic monopoles

The monopoles described in the previous section are known as elementary or Dirac monopoles, due to the fact that they are fundamental particles, like electrons or quarks in the Standard Model. A quantum field theoretic description of elementary monopoles requires the introduction of a new matter field in the Lagrangian, and the bare mass of an elementary monopole is infinite. These qualities are reflected in the fact that the classical description of a Dirac monopole has a singularity at the point where the magnetic charge is located; the Dirac potential (**??**) is defined on $\mathbb{R}^3 - \{0\}$.

Another class of magnetic monopoles arise as solutions to the field equations of certain non-Abelian gauge theories. These monopoles require no new terms to be added to the Lagrangian, and can be thought of as a coherent state of many elementary particles; they are known as solitonic or composite monopoles. Solitonic monopoles are topologically stable objects: although they are not global minima of the energy of a theory, they cannot be continuously deformed to the true vacuum while keeping the energy finite. This means that a monopole solution is stable at both a classical and a quantum level.

The existence of monopole solutions in a gauge theory therefore depends on topological considerations; for finite energy monopoles to exist, the space of finite energy field configurations must be disconnected. The conditions for this to occur are outlined below—for full

details readers are invited to consult Refs. [?, ?, ?, ?, ?] and references therein. Consider a Yang-Mills theory of a gauge field A_μ taking values in the Lie algebra of some gauge group $\mathcal{G}$. Couple this to a scalar field ϕ, transforming under some representation R of $\mathcal{G}$:

$$\phi \to R(\Omega)\phi \tag{2.11}$$

for $\Omega \in \mathcal{G}$. The covariant derivative of ϕ may be defined

$$D_\mu \phi = \partial_\mu \phi + ieR(A_\mu)\phi. \tag{2.12}$$

The canonical Lagrangian is then

$$\mathcal{L} = -\frac{1}{2}\operatorname{Tr} F_{\mu\nu}F^{\mu\nu} + |D_\mu\phi|^2 - V(\phi), \tag{2.13}$$

where $V(\phi)$ is the scalar potential and the field tensor $F_{\mu\nu}$ is defined

$$F_{\mu\nu} = \partial_\mu A_\nu - \partial_\nu A_\mu + ie[A_\mu, A_\nu]. \tag{2.14}$$

Here, the Lie algebra generators T^a are normalised such that

$$\operatorname{Tr} T^a T^b = \frac{1}{2}\delta^{ab}. \tag{2.15}$$

The energy density of the theory is given by

$$\mathcal{E} = |F^{0i}|^2 + |\varepsilon^{ijk}F_{jk}|^2 + |D^0\phi|^2 + |D^i\phi|^2 + V(\phi), \tag{2.16}$$

where i, j, k index spatial indices.

Suppose that the scalar potential V is such that the minima of $V(\phi)$ spontaneously break the symmetry of the gauge group $\mathcal{G}$ to some subgroup $\mathcal{H}$, and choose $V(\phi) = 0$ at these minima.[2] We are interested in finite energy field configurations, so at spatial infinity we require the energy density to vanish:[3] at $r \to \infty$

$$\begin{aligned} F_{\mu\nu} &\to 0, \\ V(\phi) &\to 0, \\ D_\mu\phi &\to 0. \end{aligned} \tag{2.17}$$

The constraint on the scalar field at infinity means that vacuum solutions define a map from spatial infinity to the vacuum manifold:

$$\phi : S^2 \to \mathcal{G}/\mathcal{H}. \tag{2.18}$$

[2]This can always be achieved by adding a constant to V, which does not affect any physical observable.

[3]More precisely, each term in the energy density must decay sufficiently quickly with increasing r so that the energy remains finite.

In order for the theory to admit monopole solutions, there must exist maps of this form that cannot be continually deformed into one another. In mathematical language, such maps must be in different homotopy classes. The set of homotopy classes of maps from the n-sphere to a manifold $\mathcal{M}$ is known as the nth homotopy group, and is denoted by $\pi_n(\mathcal{M})$. For a theory to admit monopoles, we therefore require $\pi_2(\mathcal{G}/\mathcal{H})$ to be nontrivial.

We can make this more concrete by considering a specific gauge theory. For example, in the Standard Model, the Higgs vacuum breaks the electroweak $\mathrm{SU}(2) \times \mathrm{U}(1)$ gauge symmetry to the $\mathrm{U}(1)$ symmetry of electromagnetism. The relevant homotopy group is[4]

$$\pi_2(\mathrm{SU}(2) \times \mathrm{U}(1)/\mathrm{U}(1)) \cong \pi_2(\mathrm{SU}(2)) \cong \pi_2(S^3) \cong 1. \tag{2.19}$$

As the second homotopy group is trivial, there are, sadly, no finite energy solitonic monopoles in the Standard Model.

Surprisingly, under rather general conditions it turns out that $\pi_2(\mathcal{G}/\mathcal{H})$ can be computed without knowledge of the larger gauge group $\mathcal{G}$. If $\mathcal{G}$ is simply connected it can be shown (for proof see, for example, Refs. [**?**, **?**]) that

$$\pi_2(\mathcal{G}/\mathcal{H}) \cong \pi_1(\mathcal{H}). \tag{2.20}$$

This has important consequences for possible extensions to the Standard Model: consider, for example, a Grand Unified Theory based on some simply connected Lie group $\mathcal{G}_{\mathrm{GUT}}$. Despite us not knowing the identity of $\mathcal{G}_{\mathrm{GUT}}$, we know that if such a gauge theory describes the Universe, it must display spontaneous symmetry breaking to give the electromagnetic gauge group $\mathrm{U}(1)_{\mathrm{EM}}$. This means that

$$\pi_2(\mathcal{G}_{\mathrm{GUT}}/\mathrm{U}(1)_{\mathrm{EM}}) \cong \pi_1(\mathrm{U}(1)_{\mathrm{EM}}) \cong \pi_1(S^1) \cong \mathbb{Z}; \tag{2.21}$$

if a Grand Unified Theory based on a semisimple Lie algebra describes the Universe, magnetic monopoles must exist.

2.2.1 The 't Hooft–Polyakov monopole

It is useful to give an explicit example of a solitonic monopole solution. The canonical example is the 't Hooft–Polyakov monopole [**?**, **?**] in Georgi-Glashow SU(2) theory. This has gauge group $\mathcal{G} = \mathrm{SU}(2)$, coupled to an adjoint scalar field Φ. The Lagrangian of the theory is

[4] There is some debate over the quotient factor in the Standard Model gauge group [**?**]. This is omitted here for brevity, as it does not affect any of the physics we discuss.

$$\mathcal{L} = -\frac{1}{2}\,\mathrm{Tr}\,F_{\mu\nu}F^{\mu\nu} + \mathrm{Tr}\,D_\mu\Phi D^\mu\Phi - V(\Phi), \tag{2.22}$$

where

$$D_\mu\Phi = \partial_\mu\Phi + ie[A_\mu, \Phi], \tag{2.23}$$

$$F_{\mu\nu} = \partial_\mu A_\nu - \partial_\nu A_\mu + ie[A_\mu, A_\nu], \tag{2.24}$$

$$V(\Phi) = \lambda\left(\mathrm{Tr}(\Phi^2) - v^2\right)^2 \tag{2.25}$$

The theory has two dimensionless parameters: the gauge coupling e and the scalar self-coupling λ. The dimensionful parameter v sets the scale of the theory. For $v^2 > 0$ the scalar potential induces spontaneous symmetry breaking, giving the scalar field a vacuum expectation value (VEV) $\sqrt{\mathrm{Tr}\,\Phi^2} = v$. This generates a scalar boson mass $m_\mathrm{s} = 2\sqrt{\lambda}v$ and a charged vector boson mass $m_\mathrm{v} = \sqrt{2}ev$. There remains an unbroken U(1) symmetry group corresponding to rotations around the Φ vector; the gauge boson associated with the generator of this symmetry remains massless and takes the role of the electromagnetic photon.

Using the results from the previous section, we can see that the asymptotic scalar field maps spatial infinity to SU(2)/U(1), and so the second homotopy group of the vacuum manifold is

$$\pi_2(\mathrm{SU}(2)/\mathrm{U}(1)) \cong \pi_1(\mathrm{U}(1)) \cong \mathbb{Z}. \tag{2.26}$$

This means that there are a countably infinite number of topologically distinct vacuum sectors that may be associated with an integer indexing the number of times spatial infinity "wraps" around the vacuum manifold. This integer is known as the winding number and can be associated with the magnetic charge.[5] The trivial vacuum has zero winding number, and the 't Hooft–Polyakov monopole solution has a winding number of one.

The 't Hooft–Polyakov monopole solution can be found by considering an ansatz for the scalar field that satisfies the asymptotic vacuum condition $V(\phi) = 0$, and cannot be continuously deformed to the trivial vacuum. This is known as the "hedgehog" ansatz [**?**, **?**]

$$\Phi^a(\vec{x}) = \sqrt{2}vH(r)\frac{x_a}{r^2}, \tag{2.27}$$

where the scalar field components Φ^a are defined by $\Phi = \frac{1}{2}\Phi^a\sigma^a$, with σ^a, $a = 1, 2, 3$ denoting the Pauli matrices. The ansatz is spherically symmetric, and the boundary conditions on the function $H(r)$ can be determined from the condition of finite energy:

$$H(r) \to \begin{cases} 0, & r \to 0, \\ r, & r \to \infty. \end{cases} \tag{2.28}$$

[5] For a concise heuristic argument why this is the case, see Ref. [**?**].

The vacuum condition $D_\mu \Phi = 0$ requires that the gauge fields vary in a way that cancels out the change in direction of the Higgs vector at spatial infinity. The corresponding ansatz for the gauge fields is therefore

$$A_i^a = -\frac{1}{e}\varepsilon_{aij}\left[1 - K(r)\right]\frac{x^j}{r^2}, \qquad A_0^a = 0. \tag{2.29}$$

The boundary conditions on $K(r)$ to ensure finite energy are

$$K(r) \to \begin{cases} 1, & r \to 0, \\ 0, & r \to \infty. \end{cases} \tag{2.30}$$

To determine the complete solution, one can substitute the hedgehog ansatz into the equations of motion and solve the resulting coupled ODEs to determine $H(r)$ and $K(r)$. In general, this must be performed numerically, though in the limit $\lambda \to 0$ an analytical solution can be found [**?**, **?**]. This solution is known as the Bogomolny-Prasad-Sommerfeld (BPS) monopole. For $\lambda \neq 0$, the functions $H(r)$ and $K(r)$ have been calculated to a high level of precision in Ref. [**?**].

The monopole mass can be determined by computing the energy of the 't Hooft–Polyakov monopole solution:

$$m = \frac{4\sqrt{2}\pi v}{e} f(\beta) = \frac{4\pi m_v}{e^2} f(\beta), \tag{2.31}$$

where $\beta = m_\mathrm{s}/m_\mathrm{v}$, the ratio of the scalar and charged vector boson masses. The function $f(\beta)$ is monotonically increasing, with the limits [**?**]

$$\begin{aligned} f(0) &= 1, \\ f(\infty) &= 1.787\ldots \end{aligned} \tag{2.32}$$

The macroscopic properties of the 't Hooft–Polyakov monopole are independent of the precise form of the solution. One can define an electromagnetic field strength tensor by projecting onto the scalar field [**?**]:

$$f_{\mu\nu} = \hat{\Phi}^a F_{\mu\nu}^a + \frac{1}{e}\varepsilon_{abc}\hat{\Phi}^a (D_\mu \hat{\Phi})^b (D_\nu \hat{\Phi})^c, \tag{2.33}$$

where $\hat{\Phi}^a = \Phi^a/\sqrt{\Phi^a \Phi^a}$. By considering the asymptotic fields of the 't Hooft–Polyakov solution, one can see that the magnetic charge of the monopole is

$$g = \frac{4\pi}{e}; \tag{2.34}$$

the 't Hooft–Polyakov monopole carries two units of Dirac charge.

At large distances, the scalar field's magnitude is its VEV, and the gauge fields tend to a pure Coulomb magnetic field; from sufficiently far away solitonic and elementary monopoles are indistinguishable. At smaller distances, however, the scalar field magnitude deviates from the vacuum, and the non-Abelian nature of the gauge fields becomes apparent. This occurs in a spherical region known as the monopole core, with a radius of approximately $r_{\mathrm{M}} \approx m_{\mathrm{v}}^{-1}$. Note that while the electromagnetic field tensor as defined in Eq. (**??**) is singular at the origin, the fields and energy density are all finite and smooth.

2.3 Experimental status of monopole searches

In Section **??** we showed that any Grand Unified Theory (GUT) based on a simply connected gauge group admits 't Hooft–Polyakov monopole solutions. Moreover, a GUT symmetry breaking transition in the early Universe would have created monopoles via the Kibble mechanism [**?**], forming at the intersections of causally disconnected bubbles of symmetry-broken vacuum. This means that all Grand Unified Theories not only permit, but predict the existence of magnetic monopoles. This poses an obvious question—where are they?

The theoretical prediction of GUT monopole density in the Universe, based on a GUT phase transition and expansion of the Universe at the rate set by the Hubble constant, predicts that monopoles should dominate the mass density of the Universe [**?**]. The fact that this is clearly not the case is known as the "monopole problem". One possible solution lies with the inflationary model of cosmology [**?**]—a period of exponential expansion of the Universe after the GUT phase transition would have diluted primordial monopole density to an unobservably small level. Of course, another solution to the problem is that a GUT does not describe the Universe, and that monopoles do not exist.

Despite scepticism about the existence of monopoles, it is undeniably true that there has been considerable experimental effort expended on monopole searches. Practically speaking, monopoles should be fairly easy to identify: they are stable particles, so do not decay, and have clear experimental signatures [**?**, **?**]. Monopoles can be detected both directly through their interactions with experimental apparatus, or indirectly via processes such as the draining of cosmological magnetic fields [**?**] or monopole-catalysed proton decay [**?**, **?**]. The current status of monopole searches is briefly reviewed below—a more comprehensive overview is given in Refs. [**?**, **?**, **?**, **?**].

One logical place to rule out in the search for monopoles is the Earth and its immediate environment. Searches for terrestrial monopoles have encompassed the atmosphere, the

oceans, moon rocks, and meteorites; a review of such searches is found in Ref. [**?**]. These searches have all returned negative results; Ref. [**?**] gives an upper bound of 1.2×10^{-29} monopoles per nucleon.

A second option is to attempt, indirectly, to infer the cosmological monopole flux. One of the earliest and most robust of these attempts is the Parker bound [**?**, **?**], which considers the fact that a significant flux of monopoles would drain the observed galactic magnetic field faster than it could be regenerated. This gives a mass-dependent upper bound of

$$F < \begin{cases} 10^{-15}\ \mathrm{cm}^{-2}\,\mathrm{sr}^{-1}\,\mathrm{s}^{-1}, & m \lesssim 10^{17}\ \mathrm{GeV}, \\ 10^{-15}\left(\frac{m}{10^{17}\ \mathrm{GeV}}\right)\ \mathrm{cm}^{-2}\,\mathrm{sr}^{-1}\,\mathrm{s}^{-1}, & m \gtrsim 10^{17}\ \mathrm{GeV}. \end{cases} \tag{2.35}$$

These bounds may be made stricter by considering the evolution of a smaller seed field in the early Universe; with the conservative estimate of the magnitude of this field of 10^{-11} G, one obtains the extended Parker bound [**?**]

$$F < \begin{cases} 3 \times 10^{-22}\ \mathrm{cm}^{-2}\,\mathrm{sr}^{-1}\,\mathrm{s}^{-1} & m \lesssim 3 \times 10^{10}\ \mathrm{GeV}, \\ 1.2 \times 10^{-16}\left(\frac{m}{10^{17}\ \mathrm{GeV}}\right)\ \mathrm{cm}^{-2}\,\mathrm{sr}^{-1}\,\mathrm{s}^{-1} & m \gtrsim 3 \times 10^{10}\ \mathrm{GeV}. \end{cases} \tag{2.36}$$

In Ref. [**?**], it was shown that this bound may be combined with a consideration of thermal Schwinger production of light monopoles during reheating in the early Universe to constrain monopole masses to

$$m \gtrsim 0.45\ \mathrm{GeV}. \tag{2.37}$$

Another option is to search for monopoles incident on the Earth via cosmic rays. The most stringent bounds to date over a wide range of incident velocities are shown in Fig. **??**. Searches by RICE [**?**] and ANITA-II [**?**] have produced even stricter bounds for ultrarelativistic monopoles ($\gamma > 10^7$); these are not shown in Fig. **??** as they would saturate the horizontal axis.

Earlier experiments searching for monopoles of cosmic origin identified two candidate events with similar signatures to magnetic monopoles [**?**, **?**], but these were not repeatable and are generally considered to be experimental errors. For more discussion of potential monopole candidates, see Ref. [**?**].

The final possibility is that of producing monopoles in particle colliders. The highest energy particle collisions to date have been of order 10^4 GeV. GUT monopoles are expected to have masses of at least 10^{15} GeV, an energy far out of reach for the foreseeable future. However, elementary monopoles with far lower masses could exist, as well as solitonic monopoles in various models that have masses in the TeV range [**?**, **?**, **?**, **?**]. The highest

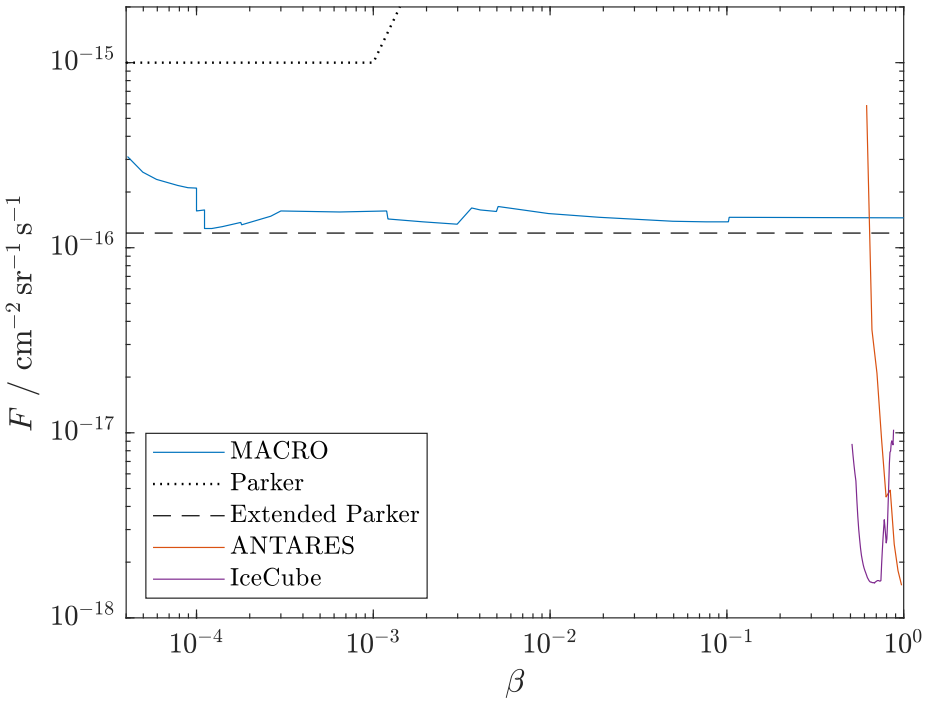

Figure 2.1: Flux bounds as a function of $\beta = v/c$ from cosmic ray experiments [**?**, **?**, **?**], including the Parker bound [**?**] and extended Parker bound [**?**] for reference.

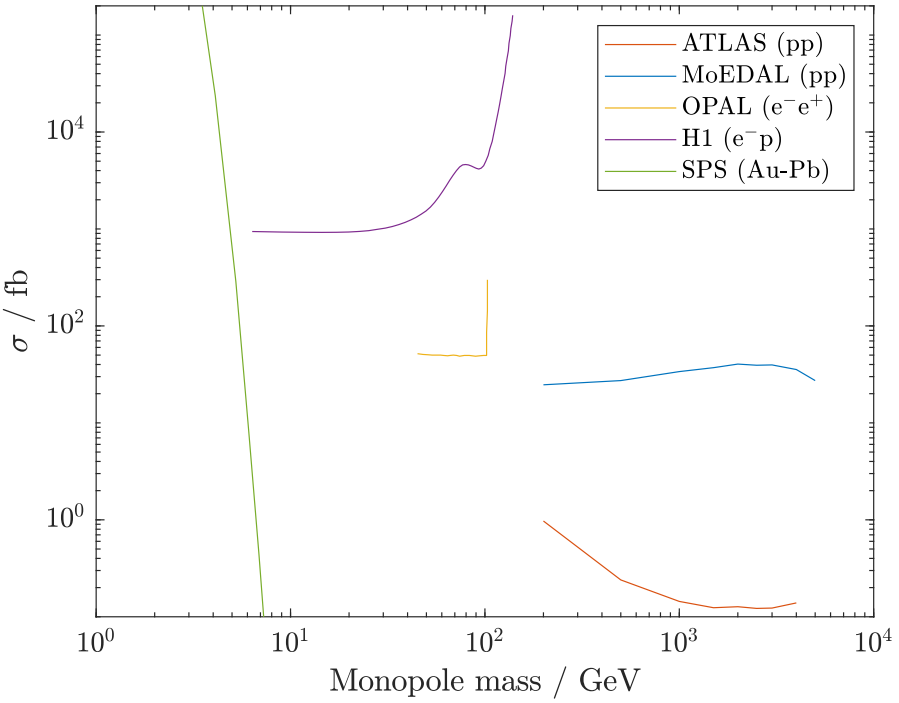

Figure 2.2: Upper limit cross sections as a function of monopole mass from different collider experiments. Data taken from Refs. [?, ?, ?, ?, ?]. All results are for $g = g_{\mathrm{D}}$, except SPS, which is valid for $g > 2g_{\mathrm{D}}$. The SPS results have been included because, at the time of writing, they are the only bounds from a heavy ion collision experiment.

energy monopole searches have been performed in proton-proton collisions by ATLAS [?, ?] and MoEDAL [?, ?, ?]. Searches have also been performed in electron-positron collisions by OPAL [?] and L6-MODAL [?], in electron-proton collisions by H1 [?], in proton-antiproton collisions by CDF [?] and E882 [?], and in heavy ion collisions by SPS [?]. Fig. ?? shows the upper limit cross sections reported from a range of experiments and colliding species. A comprehensive list of the bounds on cross sections and masses from monopole searches can be found in Ref. [?].

Reported mass bounds from particle colliders are subject to significant debate due to the theoretical difficulties in modelling the production of strongly coupled particles. In collisions with a small number of degrees of freedom in the initial state (sometimes known as "few particle collisions"), it is generally believed [?, ?] that the production of solitonic monopoles is suppressed by a factor of

$$\exp\left(-\frac{4}{\alpha}\right) \sim 10^{-238}. \tag{2.38}$$

This is due to the fact that solitons may be thought of as a coherent state of many elementary particles: with a small number of degrees of freedom in the initial state, the formation of a final state with many degrees of freedom is vanishingly unlikely. Even if low-mass solitonic monopoles exist, they are therefore unlikely to be produced in proton-proton, electron-positron or electron-proton collisions. While these arguments do not apply to Dirac monopoles, it has been argued that even elementary monopoles should have a large effective size due to strong coupling effects [?, ?, ?]. This could result in a similar suppression for elementary monopoles (for full details of this argument see Ref. [?]).

In addition to worries about suppression for solitonic monopoles, there is also concern about the methodology used to obtain mass bounds from particle accelerator experiments. The most common model of monopole production used in these experiments is Drell-Yan production, where the annihilation of a quark-antiquark pair produces a monopole-antimonopole pair via a virtual photon (see Fig. ??(a)). Another monopole production channel considered is photon fusion [?] (Fig ??(b)). The production cross sections are computed by taking the electromagnetic duals of tree level results for electric charges, replacing the electric coupling with the magnetic one. This is a perturbative approximation, and as discussed in Section ??, perturbation theory is inapplicable to magnetic monopoles. Mass bounds obtained via perturbative approximations are therefore indicative only, and are best used for comparison between experiments rather than as a concrete prediction.

Clearly, the fact that theoretical understanding of monopole production mechanisms lags behind experiment must be addressed if we are to make full use of the results of past and

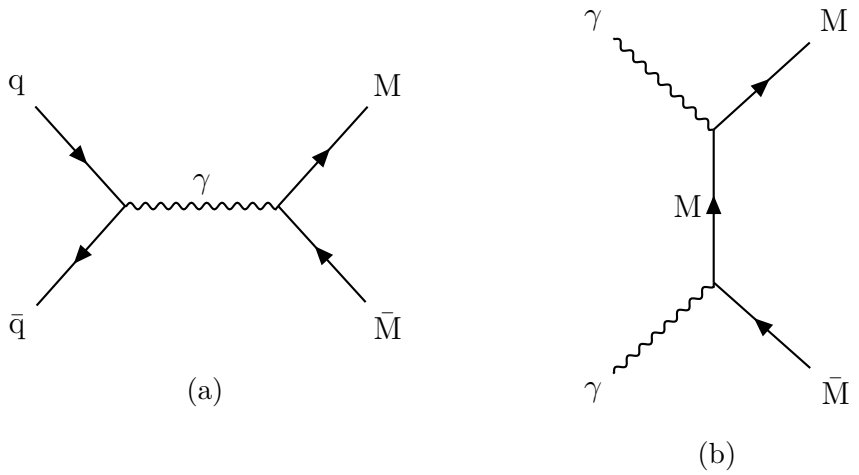

Figure 2.3: Feynman diagrams for production of spin 1/2 magnetic monopoles (analagous diagrams can be drawn for monopoles of any spin) by the Drell-Yan process (a) and photon fusion (b). Note that in a proton-proton collision, the "fusing" photons are virtual, radiated by quarks (not shown here).

future collider searches. One promising area where theoretical advances can be made is monopole production from heavy ion collisions. These have a large number of initial state degrees of freedom, so the arguments for exponential suppression from entropic considerations do not apply. Furthermore, they generate some of the strongest magnetic fields in the known Universe [**?**, **?**], which offers the possibility of magnetic monopoles via the Schwinger effect [**?**, **?**]. This can, in principle, be analysed beyond the limit of perturbative coupling, using methods such as worldline QFT [**?**, **?**] and lattice field theory. In later chapters, we will present the progress we have made towards advancing the theoretical understanding of monopole production from magnetic fields.

2.4 Sphalerons

In Section **??** we showed that Yang-Mills-Higgs theories where the vacuum manifold has a trivial second homotopy group do not admit finite energy solitonic monopole solutions. The electroweak theory of the Standard Model is an example of such a theory. Monopoles, however, are not the only topologically interesting features of gauge theories. Even if the space of finite energy field configurations is connected, there can still be topologically nontrivial paths in field configuration space, which give rise to nonvacuum solutions to the equations of motion with interesting physical consequences.

A relatively simple argument [**?**], applied to field theory in Ref. [**?**], shows that the existence of noncontractible loops passing through the vacuum implies the existence of saddle points of the energy density. The argument is as follows: denote the set of finite energy field configurations by $\mathcal{C}$. Consider a noncontractible loop in field configuration space $\Gamma : S^1 \to \mathcal{C}$, passing through the vacuum. If the vacuum is unique and has energy E_0, the energy along the loop must at some point attain a maximum value $E_{\max}(\Gamma)$. Minimising the value of $E_{\max}(\Gamma)$ over all loops Γ within a homotopy class will yield a saddle point of the energy with a single negative mode.[6] Saddle points of the energy of a field theory are known as sphalerons [**?**], after the Greek $\sigma\phi\alpha\lambda\varepsilon\rho\acute{o}\varsigma$, meaning "slippery" or "ready to fall" [**?**].

The existence of sphalerons in a field theory can be determined using similar topological considerations to those used to determine the existence of monopoles [**?**, **?**]. Recall from Section **??** that in a Yang-Mills-Higgs theory where the gauge group $\mathcal{G}$ is spontaneously broken to a smaller gauge group $\mathcal{H}$, a field configuration in three spatial dimensions defines a map $S^2 \to \mathcal{G}/\mathcal{H}$. A loop in field configuration space therefore defines a map $\Gamma : S^1 \to \mathrm{Maps}(S^2 \to \mathcal{G}/\mathcal{H})$. The set of homotopy classes of these maps is the homotopy group

$$\pi_1\left((\mathrm{Maps}(S^2 \to \mathcal{G}/\mathcal{H})\right). \tag{2.39}$$

If this homotopy group is nontrivial, the theory admits sphaleron solutions.

In the example of Georgi-Glashow SU(2) theory, the vacuum manifold is

$$\mathrm{SU}(2)/\mathrm{U}(1) \cong S^2, \tag{2.40}$$

and the relevant homotopy group is

$$\pi_1\left(\mathrm{Maps}(S^2 \to S^2)\right) \cong \pi_3(S^2) \cong \mathbb{Z}. \tag{2.41}$$

Georgi-Glashow SU(2) theory therefore admits sphaleron solutions, the lowest energy of which was first discovered by Taubes [**?**]. This consists of a monopole-antimonopole pair with a relative twist of π in isospace, which results in a repulsive force that balances the attractive force between the monopoles. In the presence of an magnetic field, a new and distinct sphaleron solution, which is not topological in origin, arises. This will be discussed further in Chapter **??**.

Sphaleron solutions can exist even in theories where $\pi_2(\mathcal{G}/\mathcal{H})$ is trivial, i.e. those without stable soliton solutions. The most physically relevant example of such a theory is electroweak theory; as discussed in Section **??** the vacuum manifold is

$$\mathrm{SU}(2) \times \mathrm{U}(1)/\mathrm{U}(1) \cong \mathrm{SU}(2) \cong S^3. \tag{2.42}$$

[6] Saddle points with more negative modes can be obtained by considering maps from higher spheres to $\mathcal{C}$.

This has a trivial second homotopy group, but

$$\pi_1\left(\mathrm{Maps}(S^2 \to S^3)\right) \cong \pi_3(S^3) \cong \mathbb{Z}. \tag{2.43}$$

There are consequently a countably infinite number of sphaleron solutions to electroweak theory. The lowest-energy of these is the electroweak sphaleron described below. Higher-energy solutions are known as multisphalerons [**?**, **?**], and are mentioned for completeness, but not studied in this work.

2.4.1 The Electroweak sphaleron

The lowest energy saddle point solution to electroweak theory is commonly known as the electroweak sphaleron, and was first identified by Klinkhamer and Manton in Refs. [**?**, **?**]. The sector of the Standard Model Lagrangian of interest here is the electroweak and Higgs sector [**?**, **?**], consisting of an SU(2) gauge field W^a_μ, a U(1) hypercharge gauge field Y_μ, and a scalar Higgs doublet ϕ:

$$\mathcal{L}_{\mathrm{EW}} = -\frac{1}{2}\,\mathrm{Tr}\, G_{\mu\nu}G^{\mu\nu} - \frac{1}{4}Y_{\mu\nu}Y^{\mu\nu} + (D_\mu\phi)^\dagger(D^\mu\phi) - V(\phi), \tag{2.44}$$

where

$$G^a_{\mu\nu} = \partial_\mu W^a_\nu - \partial_\nu W^a_\mu + i g_{\mathrm{EW}} \varepsilon^{abc} W^b_\mu W^c_\nu, \tag{2.45}$$

$$Y_{\mu\nu} = \partial_\mu Y_\nu - \partial_\nu Y_\mu, \tag{2.46}$$

$$D_\mu = \partial_\mu + \tfrac{1}{2} i g_{\mathrm{EW}} W^a_\mu \sigma^a + \tfrac{1}{2} i g'_{\mathrm{EW}} Y_\mu, \tag{2.47}$$

$$V(\phi) = \lambda\left(\phi^\dagger\phi - v^2/2\right)^2; \tag{2.48}$$

σ^a denote the Pauli matrices. There are three dimensionless parameters in the theory: the SU(2) gauge coupling g_{EW}, the U(1) gauge coupling g'_{EW},[7] and the Higgs self-coupling λ. The scale is set by the Higgs vacuum expectation value (VEV) $\sqrt{\phi^\dagger\phi} = v/\sqrt{2}$.

After spontaneous symmetry breaking it is useful to define the weak mixing angle

$$\tan\theta_{\mathrm{W}} = \frac{g'_{\mathrm{EW}}}{g_{\mathrm{EW}}}, \tag{2.49}$$

which quantifies the relationship between the weak isospin and hypercharge gauge couplings. The theory has three massive gauge bosons: the W bosons

$$W^\pm_\mu = W^1_\mu \pm i W^2_\mu \tag{2.50}$$

[7] The subscript distinguishes these couplings from the symbol g used to denote monopole charge in other parts of this thesis.

have mass $m_{\mathrm{W}} = \frac{1}{2} g_{\mathrm{EW}} v$, and the Z boson

$$Z_\mu = W_\mu^3 \cos\theta_{\mathrm{W}} - Y_\mu \sin\theta_{\mathrm{W}} \tag{2.51}$$

has mass $m_{\mathrm{Z}} = m_{\mathrm{W}}/\cos\theta_{\mathrm{W}}$. The photon

$$A_\mu = W_\mu^3 \sin\theta_{\mathrm{W}} + Y_\mu \cos\theta_{\mathrm{W}} \tag{2.52}$$

remains massless. The electric charge is given by

$$e = g_{\mathrm{EW}} \sin\theta_{\mathrm{W}} \approx 0.303. \tag{2.53}$$

Finally, the Higgs field gains a mass $m_{\mathrm{H}} = \sqrt{2\lambda} v$. The physical parameters of the Standard Model are well known [**?**]:

$$m_{\mathrm{W}} \approx 80.4 \text{ GeV}, \tag{2.54}$$

$$m_{\mathrm{H}} \approx 125.2 \text{ GeV}, \tag{2.55}$$

$$\sin^2\theta_{\mathrm{W}} \approx 0.23. \tag{2.56}$$

The sphaleron solution was first found explicitly in the limit $\theta_{\mathrm{W}} \to 0$; a summary of this solution is presented here. In this limit one only needs to consider the SU(2) gauge field, and the sphaleron has spherical symmetry. The authors of Refs. [**?**, **?**] identified an incontractible loop in electroweak theory that may be written in the temporal gauge as [**?**]

$$\begin{aligned} \phi &= \frac{v}{\sqrt{2}} \left[1 - h(r)\right] \begin{pmatrix} 0 \\ \mathrm{e}^{-i\mu} \cos\mu \end{pmatrix} + \frac{v}{\sqrt{2}} U^\infty(\mu) \begin{pmatrix} 0 \\ 1 \end{pmatrix}, \\ W_j &= \frac{i}{g_{\mathrm{EW}}} f(r) U^\infty(\mu) \partial_j U^\infty(\mu)^\dagger, \\ W_0 &= 0, \end{aligned} \tag{2.57}$$

defining the matrix

$$U^\infty(\mu) = \begin{pmatrix} \mathrm{e}^{i\mu}(\cos\mu - i\sin\mu\cos\theta) & \mathrm{e}^{i\varphi}\sin\mu\sin\theta \\ -\mathrm{e}^{-i\varphi}\sin\mu\sin\theta & \mathrm{e}^{i\mu}(\cos\mu + i\sin\mu\cos\theta) \end{pmatrix}. \tag{2.58}$$

Here, θ and φ denote spherical polar coordinate angles, and μ parametrises the loop. The maximum value of the energy along this loop occurs when $\mu = \pi/2$; fixing this value and solving the equations of motion for the radial functions $h(r)$ and $f(r)$ gives the sphaleron solution.

A key feature of the electroweak sphaleron configuration is that its Chern-Simons number

$$N_{\mathrm{CS}} = \frac{1}{8\pi^2} \int_{\mathbb{R}^3} \mathrm{Tr} \left(G \wedge W - \frac{1}{3} W \wedge W \wedge W \right) \tag{2.59}$$

is equal to one half [**?**]. This is physically relevant because when electroweak theory is coupled to fermions in the Standard Model, processes that change Chern-Simons number have been shown to violate baryon and lepton number [**?**, **?**] via the Adler-Bell-Jackiw anomaly [**?**, **?**]. The sphaleron therefore represents the peak-energy configuration along a minimal-energy path that violates baryon and lepton number in the Standard Model. The full details and implications of this are beyond the scope of this thesis, but a pedagogical introduction to electroweak baryogenesis can be found in Ref. [**?**].

The energy of the electroweak sphaleron configuration E_{sph}, for physical values of the Standard Model parameters, is around 9 TeV [**?**, **?**, **?**].[8] This represents the energy required to surmount the sphaleron barrier classically, for example via thermal excitation—the rate of sphaleron transitions at finite temperature is suppressed by a factor of $\exp(-E_{\mathrm{sph}}/T)$. The temperature of the present-day Universe is many orders of magnitude lower than the scale of the sphaleron energy, suggesting that thermal sphaleron transitions are unobservably rare. In fact, at low temperatures the sphaleron rate is determined by a four-dimensional instantonlike configuration,[9] but is still exponentially suppressed. At present, electroweak baryogenesis remains one of the concrete predictions of the Standard Model that has not yet been observed.

The fact the sphaleron energy is comparable to the energy scales of modern particle accelerators is tantalising, but it is believed that there is an exponential suppression of sphaleron transitions in elementary particle collisions [**?**, **?**, **?**] (there is some debate on this matter; see e.g. Refs. [**?**, **?**]). This is due to the large number of final state degrees of freedom compared to a small number of degrees of freedom of the initial state; the same argument was made regarding solitonic monopole production in Section **??**. Heavy ion collisions, which have many degrees of freedom in the initial state, could potentially circumvent this suppression, but the peak energy density in such collisions is around two orders of magnitude lower than the sphaleron energy density [**?**].

[8] Most calculations of the sphaleron energy were performed before the Higgs boson had been observed, so did not use the precise values of the Standard Model parameters. The 9 TeV figure has been extrapolated from the referenced articles; it is useful to note that the effects of nonzero mixing angle give only around a 1% contribution to the energy. The original calculations in Chapter **??**, which use the true Standard Model parameters, corroborate this figure.

[9] There is no true instanton in Electroweak theory in the symmetry-broken phase, but constrained instantons play a similar role. See, for example, Ref. [**?**] for details.

Though the arguments above are presented in the limit of vanishing mixing angle, it is straightforward to generalise to the full electroweak theory, including the U(1) hypercharge coupling. This breaks the spherical symmetry of the sphaleron, reducing it to an axial one, requiring a more complicated ansatz and more sophisticated methods to solve the resulting differential equations. The full numerical calculation has been performed in, for example, Refs. [**?**, **?**].

An important feature that emerges at nonzero θ_{W} is the fact that the sphaleron obtains a significant magnetic dipole moment [**?**, **?**, **?**, **?**, **?**]. This suggests that the energy of the sphaleron can be lowered by aligning it with an external magnetic field. This phenomenon is investigated using lattice field theory in Chapter **??**.

2.4.2 Nontopological sphalerons

Not all sphalerons in field theory are topological in nature. The existence of a noncontractible loop in field configuration space guarantees[10] the existence of a saddle point of the energy functional, but saddle points can exist independently of such loops. The most physically important of these are saddle points that lie on a path between *distinct* extrema of the energy, rather than loops which connect the vacuum to itself.

These sphaleron solutions are analogous to transition states in chemical reactions; for a system to transition classically from a high-energy metastable state to a lower-energy one, it must pass through the sphaleron configuration. As with the electroweak sphaleron, the physically important saddle points have a single negative mode, and the energy of the sphaleron configuration can be used to determine the rate of thermal excitation over the barrier, which is proportional to $\exp(-E_{\mathrm{sph}}/T)$. In Section **??** we investigate one such field configuration, which connects a metastable state—a constant, homogeneous magnetic field—with a lower energy one—a state containing a monopole-antimonopole pair. The sphaleron mediates pair production of monopoles from a magnetic field via the thermal Schwinger effect (for more details see Chapter **??**).

If the initial and final state are both minima, and the field configuration space is suitably smooth, the sphaleron lying between the two states can be found using a straightforward adaptation of the procedure outlined earlier for noncontractible loops. As the field configuration space is smooth, any path between two minima must have a maximum-energy configuration

[10] with certain caveats, detailed in Ref. [**?**]. Notably, the path cannot be simply a gauge transformation—in Chapter **??** we will see that the path outlined in Section **??** falls into this trap in the background of very strong magnetic fields.

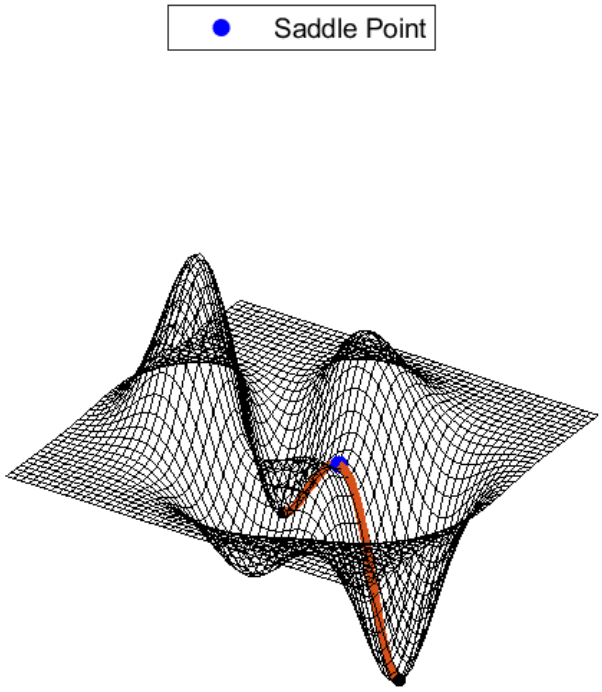

Figure 2.4: Example of a saddle point lying on a path between two distinct minima.

along it; minimising this maximum energy gives sphaleron configuration. An example of a saddle point lying on a path between two distinct minima can be seen in Fig. **??**. However, as the initial and final states are not the same, one has to be careful to ensure that the higher energy state is indeed a minimum of the energy. If the initial state is itself a saddle point, there can be a path to the final state that monotonically decreases in energy, descending along the negative mode of the initial state. This is precisely what occurs in Chapter **??**, when at sufficiently high field strengths the vacuum becomes unstable and coincides with the Schwinger sphaleron.

2.5 Instantons

The sphalerons described in Section **??** are time-independent solutions to the equations of motion. The sphaleron energy determines the classical rate of thermal excitation over an

energy barrier. Classically surmounting an energy barrier is not, however, the only way that a system can transition between states: there is also the possibility of quantum tunnelling. This is the dominant transition phenomenon at low temperatures.

Like the thermal excitation rate, the tunnelling rate can also be computed by extremising the action. Instead of a static solution, the relevant field configuration is four-dimensional, and is localised in Euclidean time. For this reason, these solutions are known as instantons. Here, we discuss the aspects of instantons most relevant to the work presented in later chapters. A more general and comprehensive introduction can be found in Ref. [**?**].

To see why instantons are relevant to transitions between (meta)stable states, it is necessary to begin with the path integral expression for the transition amplitude between two states $|\Omega_1\rangle$ and $|\Omega_2\rangle$: in Minkowski space

$$\langle\Omega_2|U(-\infty,\infty)|\Omega_1\rangle = \mathcal{N}\int \mathcal{D}\phi\, \mathrm{e}^{iS/\hbar}. \tag{2.60}$$

Here $U(t_1,t_2)$ is the evolution operator between times t_1 and t_2, S is the action of the theory, and $\mathcal{N}$ is a normalisation factor. The integral $\mathcal{D}\phi$ is over all field configurations satisfying the relevant boundary conditions—note that ϕ is a placeholder variable for all fields in the theory, matter and gauge. We will limit the discussion to computation of the decay probability of some metastable state, the "false vacuum" $|\Omega\rangle$:

$$\begin{aligned} P &= 1 - |\langle\Omega|U(-\infty,\infty)|\Omega\rangle|^2 \\ &= 1 - \exp\left[2\,\mathrm{Im}\, i\log\langle\Omega|U(-\infty,\infty)|\Omega\rangle\right]. \end{aligned} \tag{2.61}$$

This expression may be analytically continued from from real to Euclidean time ($t \to i\tau$) to give [**?**, **?**]

$$P = 1 - \exp\left[2\,\mathrm{Im}\log\langle\Omega|U_\mathrm{E}(-\infty,\infty)|\Omega\rangle\right], \tag{2.62}$$

where U_E is the Euclidean "evolution" operator.

Assuming the transition probability is small, we can expand the exponential to give

$$P \approx -2\,\mathrm{Im}\log\left(\mathcal{N}\int \mathcal{D}\phi\, \mathrm{e}^{-S_\mathrm{E}/\hbar}\right). \tag{2.63}$$

S_E is the Euclidean action; for the remainder of the chapter we will drop the subscript as we shall not return to Minkowski space.

We work in a semiclassical approximation: in the limit $\hbar \to 0$,[11] the path integral is dominated by stationary points of the action—instantons. Denoting these stationary points

[11] In this section we do not use units where $\hbar = 1$, as taking $1 \to 0$ tends to cause discomfort.

by ϕ_n, expanding in powers of $\hbar$ we find [**?**]

$$\mathcal{N}\int \mathcal{D}\phi\, \mathrm{e}^{-S/\hbar} = \sum_n D_n \mathrm{e}^{-S[\phi_n]/\hbar}\left[1+\mathcal{O}(\hbar)\right], \tag{2.64}$$

where the prefactors D_n can be determined by considering fluctuations about the stationary points. Note that this expression includes the contribution from the (false) vacuum, with prefactor D_0.

It is often the case that one stationary point gives the dominant nonvacuum contribution. While the following arguments can be straightforwardly generalised to multiple stationary points, for simplicity we consider the contribution from a single stationary point $\bar{\phi}$. Field configurations consisting of multiple $\bar{\phi}$ solutions widely separated in spacetime—multi-instantons—may be approximately considered to be solutions to the equations of motion. This is known as the dilute instanton gas approximation. Summing over the contributions from all of these configurations, including the false vacuum, gives

$$\mathcal{N}\int \mathcal{D}\phi\, \mathrm{e}^{-S/\hbar} \propto 1 + D\,\mathrm{e}^{-S[\bar{\phi}]/\hbar} + \frac{1}{2!}D^2\,\mathrm{e}^{-2S[\bar{\phi}]/\hbar} + \ldots, \tag{2.65}$$

where the constant of proportionality is purely real, so does not contribute to the imaginary part of the logarithm in Eq. (**??**). The factorial denominators arise from integrating over the positions of the instanton centres; this also gives a spacetime volume factor that (for now) is absorbed into the prefactor. The series is equivalent to a second exponential, which cancels with the aforementioned logarithm to give

$$P \approx -2\,\mathrm{Im}\left(D\,\mathrm{e}^{-S[\bar{\phi}]/\hbar}\right). \tag{2.66}$$

The prefactor D may be calculated using a functional determinant. The first variation of the action vanishes, so the leading order contributions come from the second variation of the action evaluated at the stationary point, a "functional matrix" we denote $S''[\bar{\phi}]$. To leading order in $\hbar$, the path integral is a product of Gaussians, which can be integrated analytically: if all the eigenvalues of $S''[\bar{\phi}]$ are positive, the result is a simple generalisation of the stationary phase approximation for a multivariate function [**?**]:

$$D = \left(\frac{\det S''[\bar{\phi}]}{\det S''[\phi_0]}\right)^{-1/2}, \tag{2.67}$$

where ϕ_0 is the classical field configuration of the false vacuum.

Note, however, that if the eigenvalues of S"$[\phi]$ are all positive, the contribution to the path integral is entirely real, so the solution does not contribute to the probability of false

vacuum decay. Instead, the instantons of interest are saddle points with a single negative mode. General arguments for a wide class of theories suggest that these solutions are the only relevant solutions to tunnelling processes [**?**].

The treatment of the negative mode requires some care; the Gaussian integral over the negative mode diverges and must be evaluated using an analytic continuation. Furthermore, a general instanton solution will have zero modes corresponding to symmetries of the action which are broken by the instanton solution. A more careful treatment (e.g. [**?**, **?**]) gives

$$\mathrm{Im}\, D = -\frac{1}{2}\prod_{\alpha} N_\alpha \left|\frac{\det' S''[\bar{\phi}]}{\det' S''[\phi_0]}\right|^{-1/2}, \tag{2.68}$$

where $\det'$ indicates a determinant ignoring zero modes, and the overall factor of $-1/2$ arises due to the analytic continuation when integrating over the negative mode.[12] In a gauge theory a Faddeev-Popov determinant may also be required. N_α are normalisation factors that arise from integrating over the collective coordinates that arise due to the zero modes; in the case that the theory has spacetime translational symmetry, this contributes a factor of $\mathcal{V}$, the spacetime volume over which the integral is taken. If the spacetime is not closed, this is infinite, so it is more useful to work in terms of probability per unit spacetime volume, defining the "rate"

$$\Gamma = \frac{P}{\mathcal{V}}. \tag{2.69}$$

Instantons play a role in a large number of tunnelling processes, including the decay of the Higgs vacuum [**?**, **?**], baryon number violation [**?**], and, as we will examine in Sections **??** and **??**, monopole production from magnetic fields [**?**, **?**]. In addition, though not explored here, topologically stable instanton solutions in pure Yang-Mills theory known as BPST instantons [**?**] play an important role in the vacuum structure of gauge theories, including confinement in lower-dimensional models of QCD [**?**].

[12] The sign of the prefactor depends on the integration contour, and is chosen such that the overall decay probability is positive.

Chapter 3

Monopole production from magnetic fields

3.1 Schwinger pair production

Our aim is to develop a concrete theoretical understanding of monopole production, taking into account the strong coupling effects that render perturbation theory invalid. In order to do this, we consider a method of monopole production that is amenable to nonperturbative calculation—Schwinger pair production.

The Schwinger effect is the quantum mechanical process by which a field is unstable to decay into charged particle-antiparticle pairs [**?**, **?**, **?**]. The effect is most commonly discussed in reference to the production of electron-positron pairs from an electric field. This process is exponentially suppressed at low field strengths, becoming significant when the electric field approaches the Schwinger limit

$$E_{\text{Schwinger}} \sim \frac{m_{\text{e}}^2}{e}, \tag{3.1}$$

where m_{e} denotes the electron mass. This may be interpreted qualitatively as the field strength where the energy density approaches the value defined by the electron mass and the classical electron radius, or, equivalently, when a virtual electron-positron pair from vacuum fluctuation can draw enough energy from the external field to become real. In physical units, the Schwinger limit for electrons is approximately $10^{18}\ \text{V m}^{-1}$. This is higher than any electric field strength experimentally accessible at present, meaning that even the electric Schwinger effect remains unobserved.

A theoretically rigorous treatment [**?**] can be used to calculate the rate of pair production Γ (defined in Eq. (**??**)) in a constant external field of strength E: for electrons, where the

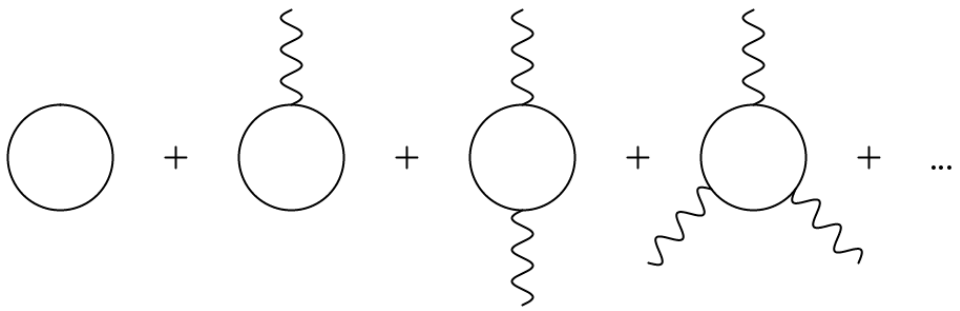

Figure 3.1: Infinite sum of Feynman diagrams contributing to the Schwinger rate (**??**)

charge $e \ll 1$, the approximation

$$\Gamma = \frac{e^2 E^2}{4\pi^3} \sum_{n=1}^{\infty} \frac{1}{n^2} \exp\left(-\frac{\pi m_e^2 n}{eE}\right) \tag{3.2}$$

is valid. The equivalent result for scalar charged particles (assuming the same mass and charge as the electron) is [**?**]

$$\Gamma = \frac{e^2 E^2}{8\pi^3} \sum_{n=1}^{\infty} \frac{(-1)^{n-1}}{n^2} \exp\left(-\frac{\pi m_e^2 n}{eE}\right). \tag{3.3}$$

It is important to note that, despite the fact that Eqs. (**??**) and (**??**) require $e \ll 1$, they are still nonperturbative results: the Schwinger effect is not seen at any order in perturbation theory in e. An equivalent statement is that the Schwinger rate is, in effect, the result of a sum of an infinite number of Feynman diagrams, and truncating this sum at any point gives zero. The diagrams contributing to Eq. (**??**) are those with a single electron loop and any number of external photon legs, shown in Fig. **??**.

By electromagnetic duality, if magnetic monopoles exist, they should be produced by the Schwinger effect in a sufficiently strong magnetic field. However, unlike the result for electric charges, the magnetic Schwinger limit cannot (currently) be expressed in physical units, as the monopole mass is not known. Instead, we can reverse the direction of inference: the nonobservation of the magnetic Schwinger effect can be used to infer a bound on the mass of the lightest magnetic monopole.

3.2 Mass bounds from observed magnetic fields

Schwinger's results, given in Eqs. (**??**) and (**??**), are not directly applicable to monopoles due to the strong coupling $g \gg 1$. It is possible, however, to generalise Schwinger's result to

strongly coupled particles—in weak fields the result is [**?**]

$$\Gamma = \frac{g^2 B^2}{8\pi^3}(2s+1)\exp\left(-\frac{\pi m^2}{gB} + \frac{g^2}{4}\right), \tag{3.4}$$

where s denotes the spin of the particles (for a derivation of the exponent, see Section **??**). This is a modification to the $n = 1$ term in Eqs. (**??**) and (**??**), obtained by including, in addition to the diagrams in Fig. **??**, diagrams containing photon propagators internal to the loop.

Eq. (**??**) implies that the Schwinger limit for magnetic fields is parametrically different to Eq. (**??**) the equivalent limit:

$$B_{\text{Schwinger}} = \frac{4\pi m^2}{g^3}. \tag{3.5}$$

If a field of strength B is generated and no monopoles are observed, we can derive a lower bound on monopole masses:

$$m \gtrsim \sqrt{\frac{g^3 B}{4\pi}}. \tag{3.6}$$

It is worth considering typical orders of magnitude for magnetic field strengths and the monopole mass scales they correspond to. A typical fridge magnet has field strength $\mathcal{O}(10^{-3}$ T), so the fact that refrigerators are not sources of monopoles suggests a lower bound mass of $\mathcal{O}(10$ eV) for monopoles of unit Dirac charge. The strongest continuous magnetic fields created in a laboratory to date reach around 45 T [**?**], giving a bound of approximately 2.5 keV.

It is clear that more exotic phenomena are required to reach the GeV range and above. One possibility is neutron stars: those with the strongest fields—magnetars—can have surface field strengths of $\mathcal{O}(10^{11}$ T) [**?**]. A detailed consideration of monopole production from neutron stars was considered in Ref. [**?**], where the bound $m \gtrsim 0.31$ GeV for $g = g_{\text{D}}$ monopoles was obtained. It is possible that greater field strengths occur in neutron star cores or during neutron star mergers, but at present even the order of magnitude of such fields is not known.

A source of even greater magnetic field strengths occurs somewhat closer to home—in high-energy heavy ion collisions in particle accelerators. Simulations [**?**, **?**, **?**] show that TeV scale heavy ion collisions generate fields of $\mathcal{O}(10^{16}$ T). Eq. (**??**) suggests that this could produce monopoles of up to $\mathcal{O}(100$ GeV) for monopoles of unit Dirac charge, with higher masses for higher charges. Given the doubts cast on monopole production in few particle events such as proton-proton collisions (see Section **??**), it is quite possible that heavy ion collisions present the best terrestrial possibility of producing monopoles.

However, the magnetic Schwinger effect in heavy ion collisions is not as simple a picture as these naïve mass bounds suggest. This is because Eq. (**??**) is only valid in constant, spatially homogeneous fields. In heavy ion collisions, which have Lorentz factors of $\mathcal{O}(1000)$, these assumptions are far from justified (in Section **??**, the spacetime dependence of the fields in heavy ion collisions is examined in detail).

In order to make predictions about monopole production in heavy ion collisions, it is necessary to adapt Schwinger's results to take into account both the strong coupling of the monopoles and the spacetime dependence of the electromagnetic fields in which the monopoles are produced. This is the focus of Chapter **??**, which uses an approximate form of the fields in heavy ion collisions to compute the exponential dependence of the monopole pair production probability.

In fact, the calculations in Chapter **??** reveal a third complication: for ultrarelativistic collisions one must also take the internal structure of the monopoles into account. Combining the three complications—strong coupling, spacetime dependence of the fields, and monopole internal structure—has so far not been possible. However, in Chapter **??** we present a successful generalisation of the exponent in Eq. (**??**) to 't Hooft–Polyakov monopoles, laying the foundations for a full calculation in the future.

In the remainder of this chapter, we outline the theoretical frameworks used to overcome the complications described above, in preparation for presenting our main results in Chapters **??** and **??**.

3.3 Schwinger production via instantons

We wish to compute the Schwinger production rate for strongly coupled particles in an inhomogeneous field. One class of computational methods that are well suited to such calculations are the instanton methods described in Section **??**. These were first applied to the production of solitonic monopoles in weak fields in Ref. [**?**], and to more general strongly coupled particles in Ref. [**?**].

Following the general procedure outlined in Section **??**, we consider Schwinger production as a quantum tunnelling process. In this case, the false vacuum is the state with the external field present and no particles, which decays into a state containing a charged particle-antiparticle pair. As shown previously, the probability of such a decay occurring is

$$P \approx -2 \operatorname{Im} \log \int \mathcal{D}\phi \mathcal{D}A \, \mathrm{e}^{-S[\phi, A]}, \tag{3.7}$$

where $S[\phi, A]$ is the Euclidean action of the theory, which we have taken to consist of a

matter field ϕ and a gauge field A. For now, we will keep the theory general, as instanton methods can be applied to both elementary and solitonic monopoles.

In the semiclassical limit, the path integral may be approximated by

$$\int \mathcal{D}\phi\mathcal{D}A\, \mathrm{e}^{-S_\mathrm{E}} \approx \sum_n D_n \mathrm{e}^{-S[\phi_n, A_n]}, \tag{3.8}$$

where $\{\phi_n, A_n\}$ are the set of statinary points of S. As detailed in Section **??**, the relevant stationary points for tunnelling—those contributing and imaginary part—are saddle points with a single negative mode. If one saddle point $(\bar{\phi}, \bar{A})$ dominates the contribution to the action, in the dilute instanton gas approximation the pair production probability becomes

$$P \approx 2\,\mathrm{Im}\, D \exp(-S[\bar{\phi}, \bar{A}]). \tag{3.9}$$

The prefactor D can be obtained by considering fluctuations about the instanton solutions as described in Section **??**—note that in this Chapter we have absorbed a factor of -1 into D for notational convenience. The calculation of the exponential dependence of the pair production rate therefore reduces to the classical problem of extremising the action, subject to the boundary conditions

$$\begin{aligned} \phi(r \to \infty) &= \phi_0, \\ A(r \to \infty) &= A_\mathrm{ext}, \end{aligned} \tag{3.10}$$

where ϕ_0 is the vacuum value of the matter field and A_ext is the desired external field. Appropriate boundary conditions at the Euclidean spacetime origin must also be applied to ensure continuity and finite action, as well as fixing of any negative modes due to spacetime symmetries. The following sections outline techniques for finding such solutions.

3.4 The worldline instanton method

In general, the Euler-Lagrange equations arising from varying the Euclidean action are analytically intractable. However, if certain additional conditions are met, the worldline formalism of QFT [**?**] allows instanton solutions to be computed. These "worldline instantons" were first introduced in Ref. [**?**], and have been adapted to account for inhomogeneous fields [**?**, **?**] and to analyse the momentum distribution of the produced particles [**?**].

In this section, we assume that magnetic monopoles may be modelled as elementary particles. As we will rarely deal with electric charges, it is simplest to work in the dual formalism of electromagnetism, defining the dual electromagnetic field tensor $\tilde{F}^{\mu\nu} = \frac{1}{2}\varepsilon^{\mu\nu\rho\sigma}F_{\rho\sigma}$,

where $\varepsilon^{\mu\nu\rho\sigma}$ is the Levi-Civita symbol with $\varepsilon^{0123} = 1$; in Minkowski spacetime

$$\tilde{F}_{\mu\nu} = \begin{pmatrix} 0 & B_x & B_y & B_z \\ -B_x & 0 & E_z & -E_y \\ -B_y & -E_z & 0 & E_x \\ -B_z & E_y & -E_x & 0 \end{pmatrix}. \tag{3.11}$$

The dual gauge field, $\tilde{A}_\nu$, satisfies $\tilde{F}_{\mu\nu} = \partial_\mu \tilde{A}_\nu - \partial_\nu \tilde{A}_\mu$, and is simply a rearrangement of the usual two degrees of freedom of the photon field—it contains no extra degrees of freedom. We minimally couple the complex scalar monopole field ϕ to the dual gauge field, giving the Euclidean Lagrangian[1]

$$\mathcal{L} = \frac{1}{4} F_{\mu\nu} F_{\mu\nu} + (\tilde{D}_\mu \phi)^* (\tilde{D}_\mu \phi) + m^2 \phi^* \phi + \frac{\lambda}{4} (\phi^* \phi)^2. \tag{3.12}$$

A series of purely formal manipulations [**?**, **?**] can be carried out to transform the partition function from a path integral over fields to one over closed worldlines, parametrised by x^a_μ where a indexes the worldlines. In brief, the dual gauge field is split into a dynamical part and a background part, with the former being integrated out to leave only the external field $\tilde{A}^{\text{ext}}_\mu$. A series of integral "tricks" are then applied, adding the worldline parameters and integrating out the matter field. For full details of this calculation, readers are invited to consult the referenced articles (an introductory review for weakly coupled particles can also be found Ref. [**?**]). The overall result is

$$\begin{aligned} &\log \int \mathcal{D}\phi \mathcal{D}A \, \exp(-S[\phi, A]) = \\ &\log \left[1 + \sum_{n=1}^{\infty} \frac{1}{n!} \prod_{\alpha=1}^{n} \left(\int_0^\infty \frac{\mathrm{d}s_\alpha}{s_\alpha} \int \mathcal{D}x^\alpha_\mu \, \mathrm{e}^{-S[x^\alpha, s_\alpha; \tilde{A}_{\text{ext}}]} \, \mathrm{e}^{g^2 \sum_{\beta<\alpha} \oint \oint \mathrm{d}x^\alpha_\mu \mathrm{d}x^\beta_\nu G_{\mu\nu}(x^\alpha, x^\beta)} \right) \right]. \end{aligned} \tag{3.13}$$

Each term in the sum corresponds to the contribution from n closed worldlines in 4D Euclidean space. The s_j are often referred to as Schwinger parameters and $G_{\mu\nu}$ is the free photon propagator; the exponential containing $G_{\mu\nu}$ is the contribution from worldline interactions (self-interactions are absorbed into the effective action; see below) that cannot be ignored when g is nonperturbative.[2] Eq. (**??**) is an exact expression; as of yet, no approximations have been made.

[1] In this expression the kinetic term for the gauge field is given in terms of the standard (nondualised) gauge field, i.e. there are no tildes on the field tensors. It may be equivalently stated in terms of the dual field, but as the dynamical photon is to be integrated out the distinction is irrelevant.

[2] If $g \ll 1$, the worldline interaction terms may be dropped, and the integrals may be performed exactly, giving the magnetic dual of Schwinger's result (**??**).

Parametrising the worldline by u, the Euclidean worldline action is given by

$$\begin{aligned} S[x,s;\tilde{A}_{\rm ext}] = \frac{m^2 s}{2} + \frac{1}{2s}\int_0^1 {\rm d}u \dot{x}_\mu \dot{x}_\mu - ig\int_0^1 \tilde{A}^{\rm ext}_\mu \dot{x}_\mu {\rm d}u \\ + \frac{g^2}{8\pi^2}\int_0^1 {\rm d}u \int_0^1 {\rm d}u' \frac{\dot{x}_\mu(u)\dot{x}_\mu(u')}{|x(u)-x(u')|^2}, \end{aligned} \tag{3.14}$$

where in the last term we have inserted an explicit expression for $G_{\mu\nu}$ in a generic R_ξ gauge and noted that the gauge-dependent terms vanish for closed worldlines.

The last term in Eq. (**??**) is a double integral over the worldline, weighted with the photon propagator. It accounts for the self-interactions between different points on the worldline. For coincident points there is a UV divergence [**?**, **?**, **?**, **?**], proportional to the length of the worldline. This can be identified with the usual UV-divergent contribution to the charged particle self-energy, which is removed by adding a mass counterterm.[3] For worldlines without self intersections or kinks, this is the only divergence of this term. Various regularisation schemes exist, and, just as in the field representation, the powerlike divergence is absent in dimensionless regularisation schemes.

For spin 1/2 monopoles, Eqs. (**??**) and (**??**) are modified by the addition of spin-dependent terms in the action [**?**, **?**, **?**]. However, in the presence of weak external fields these terms are subdominant in powers of the weak field relative to the spin 0 part. For weak, constant, external fields, they contribute to the semiclassical prefactor, simply resulting in an overall factor of the number of degrees of freedom of the final state [**?**, **?**]. For spacetime-dependent fields, the spin-dependent corrections could be more complicated than this and are worth understanding, but they are nevertheless subdominant, so for all worldline calculations considered in this thesis the results are applicable to monopoles of any spin.

As previously discussed, for sufficiently slow rates of pair production this path integral may be approximated semiclassically by searching for instanton solutions. In addition, we make the dilute instanton gas approximation: as the terms in Eq. (**??**) with $n > 1$ are exponentially suppressed, for sufficiently weak external fields the pair production rate can be obtained by considering only the $n = 1$ term. This is a single, closed, connected worldline. This is equivalent to taking the leading term in a virial expansion [**?**].

Within the dilute instanton gas approximation, the sum over widely separated instanton configurations gives an second exponential that cancels the logarithm in Eq. (**??**) (see Section **??**). The pair production probability then becomes

$$P \approx D\exp(-S[x_\mu^{\rm inst}, s^{\rm inst}; \tilde{A}_{\rm ext}]), \tag{3.15}$$

[3] Details of the mass renormalisation can be found in Ref. [**?**].

where x^{inst} and s^{inst} are a saddle point solution of the worldline action (**??**), and D is a prefactor that can be calculated following the procedure outlined in Section **??**. This solution is known as a worldline instanton.

The arguments presented in this section have been made considering only elementary monopoles. If the worldline instanton is large compared to the length scales associated with the monopole, however, the worldline instanton method is equally applicable to solitonic monopoles. This is because if all relevant length scales are large compared to the monopole core size, only the long-ranged Abelian interactions need to be taken into account—solitonic monopoles may be described by an effective theory identical to that of elementary monopoles [**?**, **?**, **?**, **?**].

3.4.1 Example: monopole production from a constant external field

An instructive example of the worldline instanton method is the computation of the Schwinger production rate for monopoles in a constant magnetic field, first presented in Ref. [**?**]. We will denote the strength of the external field by B and choose the x_3 direction as the direction in which the field points, working in the gauge

$$\tilde{A}_\mu^{\text{ext}} = iBx_3\delta_{\mu 4}. \tag{3.16}$$

The factor of i in the gauge field accounts for the derivative with respect to imaginary time in the definition of the (dual) field tensor, and is generally accepted to produce the correct analytic continuation [**?**]. The worldline action (**??**) reduces to

$$S = \frac{m^2 s}{2} + \frac{1}{2s}\int_0^1 \mathrm{d}u \dot{x}_\mu \dot{x}_\mu - gB\int_0^1 \mathrm{d}u\, x_3 \dot{x}_4 + \frac{g^2}{8\pi^2}\int_0^1 \mathrm{d}u \int_0^1 \mathrm{d}u' \frac{\dot{x}_\mu(u)\dot{x}_\mu(u')}{|x(u)-x(u')|^2} \tag{3.17}$$

The first step is to stationarise with respect to the Schwinger parameter s: this gives the condition

$$s = \frac{1}{m}\sqrt{\int_0^1 \mathrm{d}u\, \dot{x}_\mu \dot{x}_\mu}. \tag{3.18}$$

Inserting this into the action gives

$$S = m\sqrt{\int_0^1 \mathrm{d}u\, \dot{x}_\mu \dot{x}_\mu} + gB\int_0^1 \mathrm{d}u\, x_3 \dot{x}_4 + \frac{g^2}{8\pi^2}\int_0^1 \mathrm{d}u \int_0^1 \mathrm{d}u' \frac{\dot{x}_\mu(u)\dot{x}_\mu(u')}{|x(u)-x(u')|^2}. \tag{3.19}$$

To proceed, Affleck, Alvarez and Manton [**?**] note that the action is symmetric under rotations in the x_3-x_4 plane. This implies two things: firstly, if a stationary point of the action exists,

there must be one which also obeys this symmetry (a circular worldline). Secondly, as the self-interaction term is scale invariant and does not break the symmetry, the solution may be obtained by considering the nonself-interacting case

$$S = m\sqrt{\int_0^1 \mathrm{d}u\, \dot{x}_\mu \dot{x_\mu}} + gB \int_0^1 \mathrm{d}u\, x_3 \dot{x}_4 \tag{3.20}$$

and computing the interaction terms separately. This is valid because all higher-order corrections to the solution arising from the interaction term vanish.

The circular worldline ansatz may be parametrised

$$x_\mu(u) = (0, 0, R\cos(2\pi u), R\sin(2\pi u)). \tag{3.21}$$

The only free parameter is the worldline radius R: the problem reduces to a one-dimensional optimisation. Substituting the circular worldline into the nonself-interacting action (**??**) gives

$$S = 2\pi m R + \pi g B R^2. \tag{3.22}$$

It is straightforward to show that the stationary value of the nonself-interacting action occurs when $R = m/gB$, and is given by

$$S_{\text{inst}} = \frac{\pi m^2}{gB}. \tag{3.23}$$

This is exactly the leading order contribution to the magnetic dual of Schwinger's result (**??**). Additional terms in Eq. (**??**) may be generated by considering multi-instantons, and the prefactor can be obtained by considering fluctuations about the instanton solution [**?**].

The remaining step in the calculation is to compute the contribution due to worldline self-interactions:

$$S_{\text{I}} = \frac{g^2}{8\pi^2} \int_0^1 \mathrm{d}u \int_0^1 \mathrm{d}u' \frac{\dot{x}_\mu(u)\dot{x}_\mu(u')}{|x(u) - x(u')|^2}. \tag{3.24}$$

Substituting the worldline instanton solution (**??**) gives (substituting $\theta = 2\pi u$ for brevity and simplifying)

$$S_I = \frac{g^2}{16\pi^2} \int_0^{2\pi} \mathrm{d}\theta \int_0^{2\pi} \mathrm{d}\theta' \frac{\cos(\theta - \theta')}{1 - \cos(\theta - \theta')}. \tag{3.25}$$

As previously mentioned, this integral diverges due to contributions from points where $\theta = \theta'$; this divergence may be removed by adding a mass counterterm. One way of evaluating the integral[4] is by using the substitution $u = \tan[(\theta - \theta')/2]$. Subtracting the aforementioned divergence yields

$$S_{\text{I}} = -\frac{g^2}{4} \tag{3.26}$$

[4]If a proof by Mathematica is not sufficient.

the action of the worldline instanton including worldline self-interactions is

$$S_{\text{inst}} = \frac{\pi m^2}{gB} - \frac{g^2}{4}. \tag{3.27}$$

It is important to note that even though the self-interactions have been treated in a similar manner to a perturbative expansion, this result is in fact accurate to all orders in g.

This gives the worldline approximation to the pair production rate for Schwinger production of monopoles in a constant magnetic field (c.f. Eq. (**??**)):

$$\Gamma = D \exp\left(-\frac{\pi m^2}{gB} + \frac{g^2}{4}\right). \tag{3.28}$$

The effect of the strong coupling is to significantly enhance the pair production rate; for a monopole carrying one unit of Dirac charge the enhancement is

$$\exp\left(\frac{g_{\text{D}}^2}{4}\right) \sim \mathrm{e}^{108} \sim 10^{47} \tag{3.29}$$

compared to Eq. (**??**). Of course, as monopoles are expected to be far more massive than electrons, there is a competing suppression from the first term in the exponent; as the estimates of Section **??** show, monopole production still requires a very strong magnetic field.

3.5 Instantons for solitonic monopoles

As will be seen in Chapter **??**, there are physically important circumstances in which the assumptions underlying the worldline approximation cease to be valid. In such situations, the size of the monopole becomes comparable to the length scales of the instanton, meaning that the internal structure of the monopole must be taken into account. For 't Hooft–Polyakov monopoles this can be achieved by computing instanton solutions in the full field theory describing the monopole of interest; this is achieved in Chapter **??**.

Though a worldline description of non-Abelian QFTs is possible, this description is not readily applicable to the production of 't Hooft–Polyakov monopoles. This is because the worldlines describe elementary particle excitations, rather than solitonic ones—it is not practical to describe a monopole in terms of worldlines of scalar and gauge bosons. Instead, it is necessary to compute the full field-theoretic instanton satisfying the boundary conditions (**??**).

In Ref. [**?**], the instanton in a weak, homogeneous external magnetic field was calculated in Georgi-Glashow SU(2) theory. This calculation was carried out in the regime where the

monopoles are small compared to the instanton, so the result is identical to the worldline result (**??**). The key result of Chapter **??** is the generalisation of this calculation to arbitrary field strengths.

The instanton equations for a non-Abelian gauge theory are not, in general, analytically tractable, so we instead choose to extremise the action numerically. The next chapter will detail the discretisation and numerical methods used to achieve this task.

Chapter 4

Numerical methods for optimisation in field theory

4.1 Basics of lattice field theory

A large part of the work presented in this thesis involves finding numerical solutions to the equations of motion of non-Abelian gauge theories. In order to make this problem computationally tractable, it is necessary to employ a discretisation scheme, restricting the infinite degrees of freedom in a field theory to a finite number. There are many possible discretisations, but the most appealing for gauge theories is lattice field theory, which maintains gauge invariance after discretisation, thereby avoiding unphysical artefacts. This section briefly reviews the key aspects of lattice field theory relevant to the calculations in Chapters **??** and **??**. It is by no means a complete introduction—most obviously the lattice field theory of fermions is totally omitted, as well as aspects of quantum lattice field theory such as Monte Carlo methods. More comprehensive introductions can be found in Refs. [**?**, **?**, **?**].

Throughout this chapter, and in future parts of this thesis involving lattice field theory, Einstein summation convention will *not* be used—repeated indices are only summed over if explicitly indicated.

4.1.1 Scalar fields

Lattice field theories are defined on a discretised Euclidean spacetime, normally a (hyper)cubic array of points with constant spacing a in each direction:[1] positions are indexed by a

[1] In future chapters it will be common to use units where $a = 1$, but in this section factors of a are kept explicit for clarity.

vector $x = \sum_\mu a n_\mu \hat{\mu}$, where n_μ are integers and $\hat{\mu}$ denotes a unit vector in the μ direction. A discretised scalar field $\Phi(x)$ is therefore a finite number of variables, one for each lattice point. Derivatives of scalar fields are replaced by finite differences:

$$\partial_\mu \Phi(x) \to \frac{1}{a}\left[\Phi(x + a\hat{\mu}) - \Phi(x)\right]. \tag{4.1}$$

The nonlocal nature of derivatives on the lattice requires boundary conditions to be imposed at the edges of the lattice. A common and simple choice are periodic boundary conditions:

$$\Phi(x + aN_\mu \hat{\mu}) = \Phi(x + L_\mu \hat{\mu}), \tag{4.2}$$

where N_μ denotes the maximum value of n_μ; $L_\mu = aN_\mu$ is the extent of the lattice in the μ direction. As we will see in later chapters, more complicated boundary conditions must be imposed to investigate some physical phenomena.

An integral over spacetime in the continuum theory is replaced by a sum over all lattice points:

$$\int \mathrm{d}^d x \to a^d \sum_x . \tag{4.3}$$

The action of a scalar field with canonical kinetic term and a potential $V(\Phi)$ on the lattice is therefore

$$S = a^d \sum_x \left\{ \frac{1}{2a^2} \sum_\mu \left[\Phi(x + a\hat{\mu}) - \Phi(x)\right]^2 + V(\Phi) \right\}. \tag{4.4}$$

This clearly reduces to the continuum result in the limit $a \to 0$. Note that the signature of the potential term is positive, as the lattice field theories we are interested in are defined in Euclidean spacetime.

4.1.2 Gauge fields

Now we consider a gauge field $A_\mu(x)$ taking values in the Lie algebra of some gauge group $\mathcal{G}$. Naïvely discretising gauge fields in the same manner as scalar fields does not preserve gauge invariance on the lattice. Instead, we introduce the link variable

$$U_\mu(x) = \mathrm{e}^{iea A_\mu(x)}, \tag{4.5}$$

where e is the coupling associated with the gauge group. The link variable is Lie group valued, and is defined on the link between a lattice point x and its neighbour $x + a\hat{\mu}$. Under a local gauge transformation $\Omega(x) \in \mathcal{G}$, the link variable transforms as

$$U_\mu(x) \to \Omega(x) U_\mu(x) \Omega^\dagger(x + a\hat{\mu}). \tag{4.6}$$

Link variables act as parallel transporters, allowing scalar fields at different points to be combined in a gauge invariant manner. Consider a scalar field $\phi(x)$ transforming under the fundamental representation of the gauge group:

$$\phi(x) \to \Omega(x)\phi(x). \tag{4.7}$$

The forward difference operator (**??**) is not gauge invariant, but using the link variable we can form a gauge covariant derivative operation on the lattice:

$$D_\mu\phi(x) = \frac{1}{a}\left[U_\mu(x)\phi(x + a\hat{\mu}) - \phi(x)\right]. \tag{4.8}$$

By expanding in small powers of a, it can be verified that in the continuum limit this reduces to $(\partial_\mu + ieaA_\mu)\phi$. The covariant derivative of an adjoint scalar $\Phi(x)$, transforming as

$$\Phi(x) \to \Omega(x)\Phi(x)\Omega^\dagger(x), \tag{4.9}$$

is

$$D_\mu\Phi(x) = \frac{1}{a}\left[U_\mu(x)\Phi(x + a\hat{\mu})U_\mu^\dagger(x) - \Phi(x)\right]. \tag{4.10}$$

It is also possible to construct gauge invariant objects from link variables alone. These are Wilson loops, the product of link variables along a closed path. The simplest Wilson loop is the plaquette variable, defined over an elementary square on the lattice:

$$U_{\mu\nu}(x) = U_\mu(x)U_\nu(x + a\hat{\mu})U_\mu^\dagger(x + a\hat{\nu})U_\nu^\dagger(x). \tag{4.11}$$

The plaquette can be used to define the Wilson action for an SU(N) gauge theory [**?**]:

$$S = \frac{2}{e^2}\sum_x\sum_{\mu<\nu}\left[N - \operatorname{Tr} U_{\mu\nu}(x)\right]. \tag{4.12}$$

This can be verified to retrieve the Yang-Mills action in the continuum limit by expanding in powers of a and utilising the Baker-Campbell-Hausdorff formula.

4.2 Gradient descent on the lattice

The motivation for our use of lattice field theory is to find instanton solutions in non-Abelian gauge theories. These are approximated by saddle points of the lattice action corresponding to the theory of interest. This saddle point finding is a nonlinear optimisation task: the action, which is a functional in the continuum, becomes a multivariate function when discretised. The optimisation variables are the scalar field and link variables, which, on a cubic lattice of

size N, number $\mathcal{O}(N^d)$. Typical lattice sizes used in this work are $N = 64$ or $N = 128$, with $d = 3$, so the optimisation is a computationally expensive task. The optimisation routines used in this thesis are all based on gradient descent; this section reviews the standard gradient descent algorithm (also known as gradient flow) applied to lattice field theory.

Consider an objective function f mapping a set of variables $\mathbf{x}$ to $\mathbb{R}$. Given a starting point $\mathbf{x}_0$, provided that the function is well defined and differentiable at $\mathbf{x}_0$, the direction of steepest descent is given by the negative gradient $-\nabla f(\mathbf{x}_0)$:

$$(\nabla f)_\alpha = \frac{\partial f}{\partial x_\alpha} \tag{4.13}$$

where α indexes the dimensions of the function domain. To locate a minimum of f, one can therefore perform the iterative procedure of gradient descent:

$$\mathbf{x}_{n+1} = \mathbf{x}_n - \gamma \nabla f(\mathbf{x}_n), \tag{4.14}$$

where γ is a real number, known as the step size or (in machine learning contexts) learning rate. If γ is sufficiently small, $f(\mathbf{x}_{n+1})$ is guaranteed to be smaller than $f(\mathbf{x}_n)$, so if $f(\mathbf{x})$ is bounded from below, the gradient descent will eventually converge on a minimum of the function. An alternative notation with identical meaning is to define a parameter τ known as flow time, denoting the step size $\delta\tau$:

$$\mathbf{x}(\tau + \delta\tau) = \mathbf{x}(\tau) - \nabla f(\mathbf{x})\delta\tau. \tag{4.15}$$

This evokes the metaphor of gradient flow as the progression of a physical system, with a diffusive evolution instead of the second-order evolution that would arise from dynamical equations of motion.

Gradient descent is advantageous because it only requires first-order gradient information, and is exceedingly simple to implement. However, in many cases it suffers from slow convergence and has a tendency to stick in unwanted local minima or saddle points.[2] In order to improve this, one can employ methods such as momentum [**?**], which includes previous values of the gradient in the update step, or step sizes that adapt for different parameters [**?**, **?**, **?**]. A practical overview of common gradient descent algorithms can be found in Ref. [**?**] and the references therein.

[2]For some purposes, as will be shown in later sections, getting stuck in saddle points is highly desirable.

4.2.1 Example: minimising the energy of Georgi-Glashow SU(2) theory

A example of optimisation in field theory is finding the vacuum of Georgi-Glashow SU(2) theory on the lattice. This is the field configuration that minimises the energy function

$$\begin{aligned} E(\Phi, U_i) = \sum_x \Bigg\{ & \frac{2}{e^2} \sum_{i<j} \left[2 - \operatorname{Tr} U_{ij}(\vec{x})\right] \\ & + 2 \sum_i \Big[\operatorname{Tr} \Phi(\vec{x})^2 - \operatorname{Tr} \Phi(\vec{x}) U_i(\vec{x}) \Phi(\vec{x} + \hat{\imath}) U_i^\dagger(\vec{x}) \Big] \\ & + \lambda \left(\operatorname{Tr} \Phi(\vec{x})^2 - v^2 \right)^2 \Bigg\}, \end{aligned} \tag{4.16}$$

where $i, j = 1, 2, 3$ indexes the three spatial dimensions, and we have chosen units where $a = 1$ for simplicity. Note that as the vacuum is a static solution, a gauge can always be chosen such that the timelike component of the gauge field vanishes; we have made this choice in order to reduce the number of optimisation variables.

Taking the gradient of the energy gives the (time-independent) equations of motion for the theory:

$$\begin{aligned} \frac{\partial E}{\partial \Phi(\vec{x})} &= 2 \sum_i \Big[2\Phi(\vec{x}) - U(\vec{x}) \Phi(\vec{x} + \hat{\imath}) U_i^\dagger(\vec{x}) - U_i^\dagger(\vec{x} - \hat{\imath}) \Phi(\vec{x} - \hat{\imath}) U_i(\vec{x} - \hat{\imath}) \Big] \\ &\quad + 4\lambda \left[\operatorname{Tr}(\Phi(\vec{x})^2 - v^2) \Phi(\vec{x}) \right], \\ \frac{\partial E}{\partial U_i(\vec{x})} &= \frac{2}{e^2} \sum_{j \neq i} \left[S_{ij}^+(\vec{x}) + S_{ij}^-(\vec{x}) \right] - 4\Phi(\vec{x}) U_i(\vec{x}) \Phi(\vec{x} + \hat{\imath}), \end{aligned} \tag{4.17}$$

where the "staple" variables are defined

$$S_{ij}^+(\vec{x}) = U_j(\vec{x}) U_i(\vec{x} + \hat{\jmath}) U_j^\dagger(\vec{x} + \hat{\imath}), \tag{4.18}$$

$$S_{ij}^-(\vec{x}) = U_j^\dagger(\vec{x} - \hat{\jmath}) U_i(\vec{x} - \hat{\jmath}) U_j(\vec{x} - \hat{\jmath} + \hat{\imath}). \tag{4.19}$$

These are matrix expressions: the notation $\partial E / \partial X$ implies

$$\left(\frac{\partial E}{\partial X} \right)_{\alpha\beta} = \frac{\partial E}{\partial X_{\alpha\beta}} \tag{4.20}$$

where $\alpha, \beta = 1, 2$ index the matrix components.

It is important to note that the (matrix) componentwise gradients of the gauge fields do not lie in the tangent space to SU(2). The gradient descent iteration (**??**) is therefore a nonunitary evolution, and using the bare gradient (**??**) will cause the link variables to move

away from the SU(2) manifold. This may be avoided by projecting the gradients to the SU(2) tangent space before performing the gradient descent iteration: the projection of a matrix $M \in \mathbb{C}^{2\times 2}$ to the tangent space to SU(2) at a point $U \in \mathrm{SU}(2)$ is

$$P_U(M) = M - \frac{1}{2}\operatorname{Tr}(MU^\dagger)U. \tag{4.21}$$

The gradient flow iteration to minimise the energy (**??**) is

$$\begin{aligned} \Phi(\vec{x}, \tau + \delta\tau) &= \Phi(\vec{x}, \tau) - \frac{\partial E}{\partial \Phi(\vec{x}, \tau)}\delta\tau, \\ U_i(\vec{x}, \tau + \delta\tau) &= U_i(\vec{x}, \tau) - P_{U_i(\vec{x},\tau)}\left(\frac{\partial E}{\partial U_i(\vec{x}, \tau)}\right)\delta\tau. \end{aligned} \tag{4.22}$$

In a numerical application, additional corrections must be applied to avoid the scalar and link variables deviating from their respective ranges due to floating point errors and the effects of finite step size.

4.3 Saddle point solutions in field theory

In Sections **??** and **??** we discussed the importance of sphaleron and instanton solutions to field equations: these are saddle points of the action or energy, as opposed to vacuum states, which are minima. To study such solutions on the lattice, one requires a numerical optimisation scheme that is capable of converging on saddle points as well as (or instead of) minima of the objective function. Standard gradient descent methods are unsuitable for this, as when converging correctly the overall effect is to decrease the objective function until a minimum is found. Indeed, many modern gradient flow algorithms are specifically designed to move through saddle points as quickly as possible [**?**].

One option for numerical saddle point finding is to use optimisation methods that involve calculating or approximate second-order gradient information. Examples of such algorithms include Newton's method or quasi-Newton methods [**?**]. Newton's method is used in Chapter **??** to compute worldline instantons numerically (see Appendix **??**), with $\mathcal{O}(1000)$ variables. However, for large lattice sizes these methods can be cumbersome and computationally expensive, and there are limited existing tools suitable for second-order optimisation methods of matrix valued fields. In this section we present two methods for saddle point optimisation that require only minor modifications to standard first-order gradient descent. While conceptually and computationally simple, we have used these methods effectively to compute sphaleron and instanton configurations in Georgi-Glashow SU(2) theory and electroweak theory [**?**, **?**, **?**]—in Sections **??** and **??** we present the results of these calculations in detail.

4.3.1 Chigusa-Moroi-Shoji gradient descent

The first saddle point finding method used in this thesis is derived from an algorithm first proposed by Chigusa, Moroi and Shoji (CMS) to numerically compute bounce configurations in cosmology [**?**]. The CMS gradient descent iteration is a modification of the standard gradient descent step (**??**): for an objective function $f(\mathbf{x})$

$$\mathbf{x}_{n+1} = \mathbf{x}_n - \gamma \left\{ \nabla f(\mathbf{x}) - k \left[\sum_\alpha (\nabla f)_\alpha G_\alpha \right] \mathbf{G} \right\}, \tag{4.23}$$

where $k > 1$ is a real parameter, $\mathbf{G}$ is a fixed vector in the same vector space as ∇f, normalised such that $\sum_\alpha |G_\alpha|^2 = 1$.

It can clearly be seen that if $\nabla f(\mathbf{x}) = 0$, $\mathbf{x}$ will be a fixed point of the CMS gradient flow (**??**). Following Ref. [**?**] we can prove the converse: that a fixed point of the CMS flow is a stationary point of f. A fixed point of the CMS flow satisfies

$$\nabla f(\mathbf{x}) - k \left[\sum_\alpha (\nabla f)_\alpha G_\alpha \right] \mathbf{G} = 0. \tag{4.24}$$

Contracting this with $\mathbf{G}$ (recalling that $\mathbf{G}$ is normalised) gives

$$(1-k) \sum_\alpha (\nabla f)_\alpha G_\alpha = 0. \tag{4.25}$$

For $k \neq 1$, if $\nabla f \neq 0$ this implies that ∇f and $\mathbf{G}$ are perpendicular. However, this means that Eq. (**??**) cannot be satisfied for $\nabla f \neq 0$; the two conditions are inconsistent and therefore a fixed point of Eq. (**??**) that is not a stationary point of f is a contradiction.

Now that we have confirmed that the CMS gradient flow indeed converges on a stationary point of f, the next step is to identify the correct choice of $\mathbf{G}$ to converge on the desired saddle point. Suppose we are in the vicinity of a saddle point $\bar{\mathbf{x}}$; the Hessian at $\bar{\mathbf{x}}$ is

$$H_{\alpha\beta} = \left. \frac{\partial^2 f}{\partial x_\alpha \partial x_\beta} \right|_{\mathbf{x}=\bar{\mathbf{x}}}. \tag{4.26}$$

Denote the normalised eigenvectors of H by $\mathbf{v}^{(a)}$, with corresponding eigenvalues $\lambda^{(a)}$:

$$H_{\alpha\beta} v_\beta^{(a)} = \lambda^{(a)} v_\alpha. \tag{4.27}$$

For a saddle point with a single negative mode,[3] the lowest lying eigenvalue $\lambda^{(-1)}$ is negative, with the rest $(\lambda^{(1)}, \lambda^{(2)}, \ldots)$ positive.

[3] All relevant saddle points in this thesis will take this form

Suppose that the starting point of the flow, $\mathbf{x}_0$, is in the vicinity of the saddle point: decomposing into the eigenbasis of the Hessian we can write

$$\mathbf{x}_0 = \bar{\mathbf{x}} + \sum_a c^{(a)} \mathbf{v}^{(a)}, \tag{4.28}$$

where the coefficients $c^{(a)}$ are small. To leading order, the gradient at $\mathbf{x}_0$ is

$$\nabla f \approx H(\mathbf{x}_0 - \bar{\mathbf{x}}) = \sum_a c^{(a)} \lambda^{(a)} \mathbf{v}^{(a)}. \tag{4.29}$$

The effect of standard gradient flow (**??**) on the coefficients $c^{(a)}$ is

$$c^{(a)}_{n+1} \approx c^{(a)}_n - \gamma c^{(a)}_n \lambda^{(a)}; \tag{4.30}$$

the coefficient of the negative mode eigenvector increases whilst the coefficients of the positive-mode eigenvectors decrease. This is the reason that standard gradient flow fails to converge on the saddle point. Now consider the CMS flow, decomposing the vector $\mathbf{G}$ as

$$\mathbf{G} = \sum_a g^{(a)} \mathbf{v}^{(a)}, \tag{4.31}$$

with $\sum_a g^{(a)} = 1$. The coefficients now evolve by

$$c^{(a)}_{n+1} \approx c^{(a)}_n - \gamma \left[c^{(a)}_n \lambda^{(a)} - k \left(\sum_b \lambda^{(b)} c^{(b)} g^{(b)} \right) g^{(a)} \right]. \tag{4.32}$$

One clear choice that results in $c^{(a)}_n$ decreasing for all a is

$$\mathbf{G} = \mathbf{v}^{(-1)}; \tag{4.33}$$

we choose $\mathbf{G}$ to be a unit vector pointing in the direction of the negative mode. Then for all $k > 1$, the CMS flow descends along the positive mode and climbs along the negative mode, ultimately converging on the saddle point.

Of course, without already having knowledge of the saddle point of interest, it is highly unlikely that one has knowledge of the negative mode in any nontrivial case. Thankfully, the CMS flow will still converge to the saddle point provided that $\mathbf{G}$ is sufficiently close to the negative mode. Explicitly, the condition is that the matrix

$$(1 - k\mathbf{G}\mathbf{G}^\top) \operatorname{diag}(\lambda^{(-1)}, \lambda^{(1)}, \lambda^{(2)}, \dots) \tag{4.34}$$

has eigenvalues with positive definite real parts [**?**].

In the case of finding sphaleron solutions in lattice field theory, we have identified a heuristic prescription for choosing $\mathbf{G}$ that requires minimal knowledge of the function being optimised. The prescription exploits the fact that standard gradient flow moves slowly through saddle points—a feature that makes standard gradient descent unsuitable for many optimisation tasks. If the initial conditions are chosen suitably close to the saddle point of interest, Eq. (**??**) shows that over time ∇f will become more aligned with the negative mode. At the point of closest approach where $|\nabla f| = \sqrt{\sum_\alpha (\partial_\alpha f)^2}$ is smallest, we find that ∇f is close enough to the negative mode to be used to define a vector $\mathbf{G}$ that allows the CMS algorithm to converge on the saddle point. The algorithm used in this thesis is as follows:

1. Choose an initial point $\mathbf{x}_0$ that is as close as possible to the saddle point. This can be achieved by using an analytic approximation, or a previously found saddle point solution with incrementally different parameter values.

2. Perform standard gradient descent (**??**) iterations until the norm of the gradients $|\nabla f|$ reaches its minimum value, $\nabla f_{\min}$.

3. Perform CMS gradient descent iterations (**??**) using $\mathbf{G} = \nabla f_{\min}/|\nabla f_{\min}|$ until convergence on the saddle point is achieved to the required tolerance.

The hyperparameters γ and k in Eqs. (**??**) and (**??**) are generally chosen via trial and error.

The main advantage of CMS gradient descent is that it is computationally inexpensive. Implementing the CMS gradient descent iteration requires only marginally more computational cost than a standard gradient descent step; the cost is comparable to, for example, gradient descent with a momentum term. The disadvantage is the fact that the convergence is nonmonotonic—the objective function and gradient often oscillate while converging, which can make it difficult to determine whether the algorithm is converging or diverging. Furthermore, the convergence of the algorithm is often rather sensitive to the choice of k and the initial conditions, meaning that ensuring convergence can be fiddly. Nonetheless, if a solution is found, it is guaranteed to be a true stationary point of the action, and the fact that it is a saddle point rather than a minimum can be easily verified by showing that the solution is unstable under standard gradient descent.

4.3.2 Gradient squared descent

The second saddle point optimisation method that is used in this thesis is gradient squared descent (GSD).[4] Rather than optimising the objective function f directly, GSD minimises

[4]Not to be confused with stochastic gradient descent, often abbreviated to SGD.

the sum of squares of the gradients of f: the objective function is

$$\mathcal{G}^2(\mathbf{x}) = \sum_\alpha \left| \frac{\partial f}{\partial x_\alpha} \right|^2 . \tag{4.35}$$

$\mathcal{G}^2$ is a positive semidefinite function, with global minima $\mathcal{G}^2 = 0$ at all stationary points of f regardless of their signature. If suitable initial conditions are chosen, minimising $\mathcal{G}^2$ using a standard gradient descent algorithm will yield the desired saddle point of f. The idea of optimising a squared gradient function on the lattice is well known (see, for example, Refs. [**?**, **?**, **?**]), but in the past has been severely limited by computational demands. By taking advantage of modern technologies developed for optimisation in contexts such as machine learning, we have overcome these difficulties and computed saddle point solutions on large lattices to a high degree of accuracy.

To illustrate the practical difficulties in GSD, we consider the example of lattice energy function of Georgi-Glashow SU(2) theory, $E(\Phi, U_i)$, defined in Eq. (**??**). The squared gradient of this function is

$$\mathcal{G}^2(\Phi, U_i) = \sum_{\vec{x}} \left\{ \mathrm{Tr} \left(\frac{\partial E}{\partial \Phi(\vec{x})} \right)^2 + \sum_j \mathrm{Tr} \left[i P_{U_j(\vec{x})} \left(\frac{\partial E}{\partial U_j(\vec{x})} \right) \right]^2 \right\} . \tag{4.36}$$

From the form of the gradients (**??**) it is clear that this is a long and cumbersome expression; its derivatives even more so. Manually differentiating the squared gradients and implementing the gradient descent is expensive both in terms of human time spent coding and debugging, and computation time on large lattices.

To overcome these difficulties, one can compute derivatives algorithmically using automatic differentiation. This involves decomposing an arbitrarily complicated function into elementary operations and computing the overall derivative using the chain rule. However, it differs from symbolic differentiation in that rather than storing the symbolic expressions for the elementary function derivatives, only the numeric values are stored. Using memoisation, this enables redundant repeated calculations to be omitted, greatly improving the computational efficiency: the computational cost of evaluating the automatic derivative of a function is linearly related to the cost of evaluating the function itself [**?**], with a constant of proportionality of less than 10 [**?**]. Automatic differentiation also retains far greater accuracy than numerical differentiation using, for example, finite differences, as there are no errors resulting from discretisation.

A review of the use and implementation of automatic differentiation can be found in Ref. [**?**]. As automatic differentiation is not (yet) a common tool in computational physics,

it is illustrative to provide a very simple example, adapted from Ref. [?], of how automatic differentiation improves upon symbolic differentiation. Consider a function of one variable

$$f(x) = u(x)v(x), \tag{4.37}$$

that is differentiable at the point x_0. Using elementary calculus,

$$f'(x_0) = u'(x_0)v(x_0) + u(x_0)v'(x_0). \tag{4.38}$$

If we have evaluated $f(x_0)$, we must have evaluated $u(x_0)$ and $v(x_0)$ already. This means that computing Eq. (??) requires us to evaluate $u(x_0)$ and $v(x_0)$ again, which, if the functions are expensive, is undesirable.[5] In automatic differentiation, $u(x_0)$ and $v(x_0)$ can be stored upon their first computation, removing this redundancy. While this example is almost trivial, in functions that are complicated or heavily nested, using symbolic calculus can result in exponentially large expressions; automatic differentiation reduces the computational complexity to linear in the time taken to evaluate the original function [?].

Another problem that can arise from GSD is that the squared gradient function may have spurious local minima with $\mathcal{G}^2 > 0$; these do not correspond to stationary points of the original objective function but can trap a gradient descent algorithm. One method of mitigating this issue is to add a biasing term to $\mathcal{G}^2$ to destabilise these local minima [?]. However, we find that for our purposes it is sufficient to choose a good initial condition, and make use of more sophisticated gradient descent algorithms such as momentum [?]. From personal experience, gradient descent algorithms that are common in machine learning contexts such as RMSprop [?] and Adam [?] seem to perform less well than gradient descent with momentum when optimising observables in lattice field theory. This may be due to the sparsity of the objective function, or the fact that a closer convergence to the absolute minimum is sought than in many machine learning applications.

Both automatic differentiation and advanced gradient descent algorithms are common features of software packages designed for use in machine learning. These packages can be adapted to perform optimisation tasks in field theory—this thesis is accompanied by the `tfmonopoles` Python package [?], which makes use of tools from the TensorFlow library [?].

[5] There may be situations in which only $f'(x_0)$ is required, without needing evaluation of $f(x_0)$. However, note that, for example, $u(x_0)$ and $u'(x_0)$ are both required to evaluate $f'(x_0)$; with sufficiently complicated functions, redundancy will always occur.

Chapter 5

Monopole production in heavy ion collisions

5.1 Electromagnetic fields in heavy ion collisions

In a heavy ion collision, nuclei with a large number of constituent nucleons—commonly gold, lead, or uranium—are accelerated to relativistic speeds and fired at each other. This generates extreme conditions, including temperatures of $\mathcal{O}(10^{12}\text{ K})$ [**?**] and the strongest electromagnetic fields in the known Universe [**?**]. The latter property makes heavy ion collisions one of the most promising terrestrial sources of magnetic monopoles. This chapter presents the advances we have made towards a theoretical understanding of monopole production in the fields of heavy ion collisions.

Before applying the methods discussed in Chapter **??** to heavy ion collisions, it is necessary to determine the form of the electromagnetic fields that are present. In this section, we review the mechanism by which the fields are generated and present an approximate analytic expression, which we use to calculate the Schwinger production rate in Section **??**, and the monopole momentum distribution in Section **??**.

Throughout this chapter, we will use the geometry defined in Fig. **??**: the beam axis, along which the ions move, will be aligned with the z axis of our coordinate system, with the impact parameter b pointing in the x direction.[1] The spatial origin will be the centre of mass of the system, and the temporal origin will be the time of collision, when the distance

[1] We have also chosen the convention that the words "transverse" and "longitudinal" are taken with respect to a given magnetic field, *not* with respect to the ion beam. This resolves an unfortunate inconsistency between Refs. [**?**] and [**?**] that should be kept in mind when reading these papers.

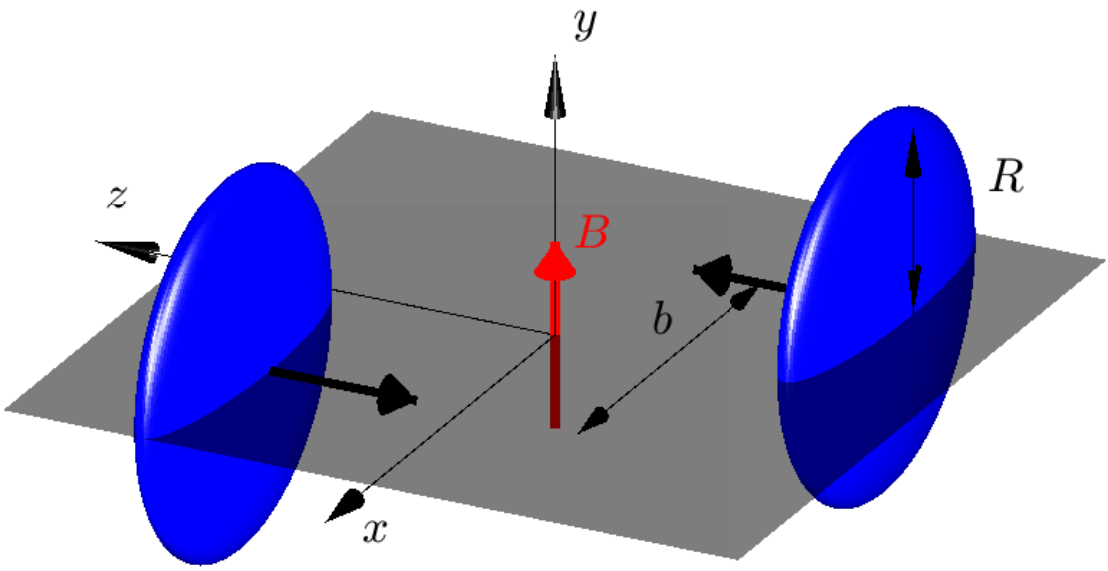

Figure 5.1: Heavy ion collision geometry defining the coordinate system used in this work.

Symbol	Parameter	Approximate value
R	Ion radius	35 GeV^{-1}
Z	Proton number	82
b	Impact parameter	0-70 GeV^{-1}
$\sqrt{s_{\mathrm{NN}}}$	Centre of mass energy per nucleon	5020 GeV
γ	Collision Lorentz factor	2675

Table 5.1: Table of common heavy ion parameters in natural units. All values are for Pb-Pb collisions at 5.02 TeV.

between the ion centres is minimal. Due to the effects of Lorentz contraction, when viewed in the centre of mass frame the ions are highly flattened along the beam direction: if the rest-frame radius of an ion is R, its extent along the z direction is R/γ, where γ is the Lorentz factor of the collision.

Modern heavy ion collisions reach ultrarelativistic centre of mass energies $\sqrt{s_{\mathrm{NN}}}$, with RHIC reaching approximately 200 GeV per nucleon [**?**] and LHC energies at 5.02 TeV per nucleon [**?**]. The Lorentz factor of these collisions is given by

$$\gamma \approx \frac{\sqrt{s_{\mathrm{NN}}}}{2m_{\mathrm{p}}}, \tag{5.1}$$

where m_{p} is the mass of a proton: this gives a value of $\gamma \approx 213$ for RHIC and $\gamma \approx 2675$ for LHC.[2] Unless otherwise stated, numerical values in this and the following sections will be computed at energies of 5.02 TeV, and often we will make use of the assumption $\gamma \gg 1$. Table **??** summarises the heavy ion parameters used in this chapter, and their typical values in lead-lead collisions at 5.02 TeV.

The electromagnetic fields in ultrarelativistic heavy ion collisions have been studied by many authors and are reviewed in Ref. [**?**]. In the rest frame of an ion, the electromagnetic field is the purely electric Coulomb field. When boosted to a moving frame, the electric field of the ion is Lorentz contracted, and the ion gains a magnetic field perpendicular to both the electric field and the direction of motion. For $\gamma \gg 1$, this magnetic field is of the same magnitude as the electric field.[3]

Ref. [**?**] presents the results of a detailed numerical study of the electromagnetic fields in

[2]Because the proton mass is approximately 1 GeV, a "back of the envelope" estimate of γ can be obtained by halving the centre of mass energy in GeV.

[3]Note that a single ion cannot induce pair production due to the vanishing of the electromagnetic invariant $\sqrt{B^2 - E^2}$.

heavy ion collisions at different impact parameters and energies, including their spacetime dependence and event-by-event fluctuations. The peak event-averaged magnetic fields occur at $b \approx 2R$, when the colliding ions barely touch (or even miss) each other. When considering monopole production via the Schwinger effec, these peripheral collisions are therefore of most interest.

Whilst the results of Ref. [**?**] provide a sophisticated and detailed computation of the electromagnetic fields, for our purposes of calculating the Schwinger production rate of monopoles, it is useful to have an approximate analytical form for the electromagnetic fields in a heavy ion collision. In Ref. [**?**], an independent simulation was carried out with this goal in mind. The following assumptions were used:

1. All nucleons were treated as spectator nucleons, i.e. no momentum exchange between particles. As only peripheral collisions are relevant, the spectator nucleons are expected to dominate up to $\mathcal{O}(Z^{-1})$ corrections to the values of the field components [**?**].

2. The conductivity of the ions was neglected, as this does not affect the fields at early times when the magnetic fields are strongest.

3. Quantum corrections to the fields were neglected, as these are expected to be small [**?**].

The ions (in their rest frame) were modelled in a mean field approximation as classical Woods-Saxon electric charge distributions

$$\rho_{\mathrm{SW}}(r, R, a) = \frac{A}{1 + \mathrm{e}^{(r-R)/a}}, \tag{5.2}$$

where r is the distance from the centre of the nucleus, R and a are experimentally determined parameters, and A is a normalisation constant. Numerical evaluations took values of $R = 6.62 \pm 0.06$ fm and $a = 0.546 \pm 0.010$ fm for lead ions, based on data from low-energy electron-nucleus scattering experiments [**?**, **?**].

Under the above assumptions, the approximate fields in a heavy ion collision can be computed by solving the Liénard-Wiechert potentials for the charge distribution (**??**). There are a number of qualitative observations that can be made to motivate the eventual parametrisation we present. Firstly, we note that the maximum value of the magnetic field is in the neighbourhood of the spacetime origin. At this point, one can see from the symmetry of the system (see Fig. **??**) that the electric field must vanish, while the magnetic field points solely in the y direction. By scaling the integrals of the Lorentz-boosted Coulomb field over the

distribution (**??**), one can obtain the parametric relations

$$\begin{aligned}\frac{\partial F_{\mu\nu}}{\partial x} &\sim \frac{\partial F_{\mu\nu}}{\partial y} \sim \frac{F_{\mu\nu}}{R},\\ \frac{\partial F_{\mu\nu}}{\partial z} &\sim \frac{\partial F_{\mu\nu}}{\partial t} \sim \frac{F_{\mu\nu}}{R/\gamma},\end{aligned} \tag{5.3}$$

where $F_{\mu\nu}$ is any component of the electromagnetic field, and we have taken $R \sim b \sim a$, which holds at the order of magnitude level. For very large γ, this means that the electromagnetic fields are localised to a region of size $\mathcal{O}(R/\gamma)$ in the z and t directions and of size $\mathcal{O}(R)$ in the x and y directions. This separation of scales permits us to drop the x and y dependence of the fields and focus only on the z and t dependence.[4]

In this case, only two components of the electromagnetic field are nonzero: B_y and E_x. Recalling from Chapter **??** that for analysing monopole production it is simplest to work in the dual formalism of electromagnetism, we note that the electromagnetic dual of this field configuration is given by $\tilde{E}_y = B_y$ and $\tilde{B}_x = -E_x$. The results of performing the integrals of the Liénard-Wiechert potentials over the Woods-Saxon distributions are shown in Fig. **??** and Fig. **??**. Inspired by the field configurations for pointlike charges, we find that the results can be well approximated by

$$\begin{aligned}B_y &= \frac{B}{2}\left(\frac{1}{(1+\omega^2(t-z)^2)^{3/2}} + \frac{1}{(1+\omega^2(t+z)^2)^{3/2}}\right),\\ E_x &= \frac{B}{2}\left(\frac{1}{(1+\omega^2(t-z)^2)^{3/2}} - \frac{1}{(1+\omega^2(t+z)^2)^{3/2}}\right),\end{aligned} \tag{5.4}$$

where B is the value of the magnetic field at the spacetime origin and ω is the inverse decay time of the magnetic field magnitude. Both depend on the particular heavy ion collision considered through b and γ, and are fitted numerically using least squares.

In Fig. **??** we show the magnetic field along with our fit at $z = 0$. Relative deviations from our fit are only a few percent, so we do not complicate our fit function to account for them.

Recall that our goal is to approximate the cross section for monopole production from these magnetic fields. The differential cross section as a function of impact parameter is expected to take the form

$$\frac{\mathrm{d}\sigma}{\mathrm{d}b} \sim \mathrm{e}^{-f[F_{\mu\nu}(b)]} \tag{5.5}$$

for some currently unknown function f. The total cross section can be found by integrating this, and as we are only interested at present in the exponential dependence of the cross

[4] In Section **??** it will be shown that the extent of the worldline instanton justifies this approximation.

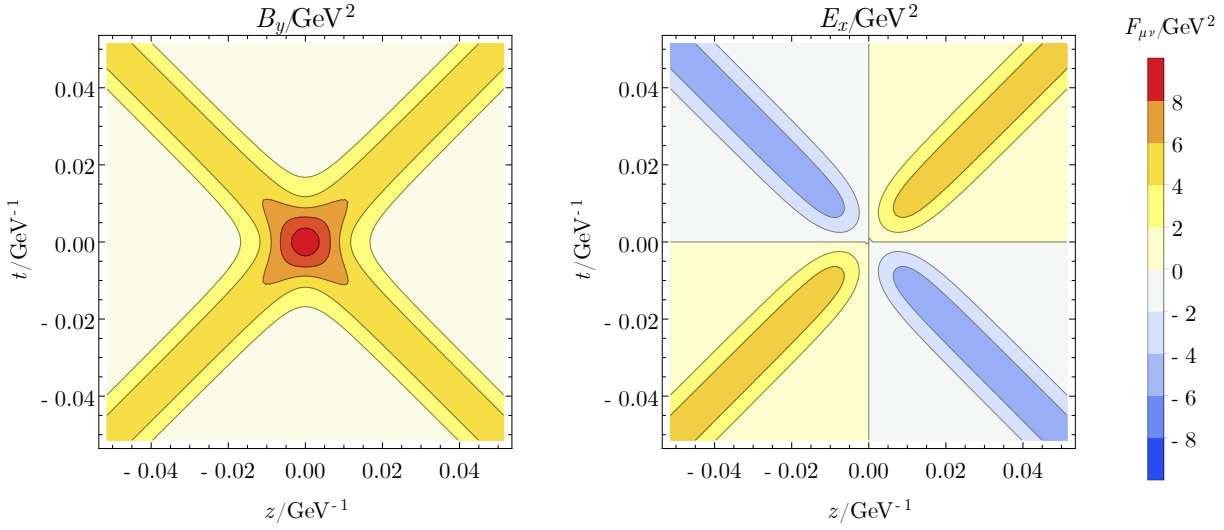

Figure 5.2: Magnetic field component, B_y and electric field component, E_x, near origin of coordinate system for a collision of two lead ions with centre of mass energy per nucleon equal to 5.02TeV and impact parameter $2R$. Note that $x = y = 0$ here.

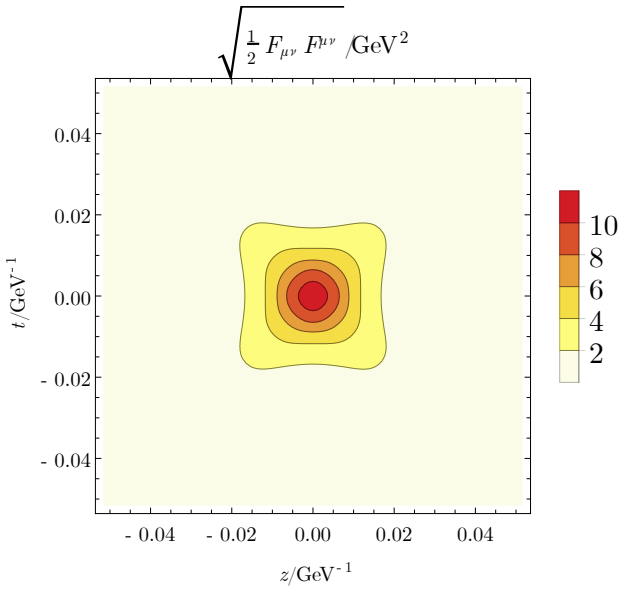

Figure 5.3: Plot of the nonzero scalar invariant of the electromagnetic field, $\frac{1}{2}F_{\mu\nu}F^{\mu\nu} = |\vec{B}|^2 - |\vec{E}|^2$. In this plane, the other scalar invariant, $\frac{1}{4}F_{\mu\nu}\tilde{F}^{\mu\nu} = \vec{E} \cdot \vec{B}$ is zero and away from this plane it is suppressed relatively by γ.

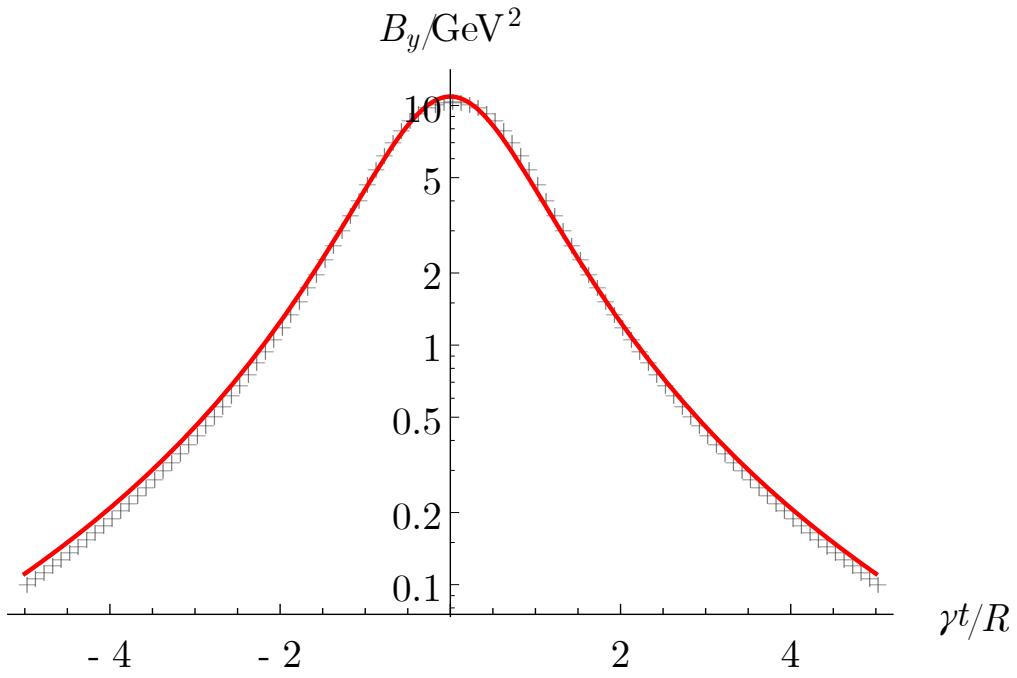

Figure 5.4: Plot of the magnetic field, B_y, at the spatial origin of the coordinates for a collision of two lead ions with centre of mass energy per nucleon equal to 5.02TeV and impact parameter $2R$. Note that $x = y = z = 0$ here. Our fit, Eq. (**??**), is shown as a continuous red line alongside the results of performing the numerical integrals, as black crosses.

section, a steepest descent approximation is sufficient. In this case

$$\sigma \sim \mathrm{e}^{-f[F_{\mu\nu}(b_{\max})]}, \tag{5.6}$$

where $b_{\max}$ is the value of the impact parameter that minimises f (maximising the cross section). It is reasonable to assume that this is also the value of b that maximises B, the peak magnetic field strength. Our numerical calculations found that for $b \lesssim 2R$, B increases linearly with b, peaking at $b_{\max} \approx 1.94R$ before decreasing again. This agrees with the event-averaged results from Ref. [**?**]. The b dependence can be rationalised by considering the fact that for small impact parameters, most nucleons collide with each other, whilst for large impact parameters (compared to the ion radius), the nucleons can be considered to be point particles. The value of $b_{\max}$ can be shown to be independent of γ. About this maximum, we find

$$B(b,\gamma) = B(b_{\max},\gamma)\left(1 - \frac{1}{2}\frac{c_{B2}}{R^2}(b-b_{\max})^2 + \mathcal{O}(b-b_{\max})^3\right), \tag{5.7}$$

where the numerical coefficient $c_{B2} \approx 1.37$ is found by a quadratic fit to the numerical data and, like $b_{\max}$, is independent of γ.

For fixed b, the magnetic field is a linearly increasing function of γ. For $b = b_{\max}$, we find

$$B(b_{\max},\gamma) \approx c_B \frac{Zev\gamma}{2\pi R^2}, \tag{5.8}$$

where we have written the result in terms of that for pointlike ions, v is the ion speed, and the numerical coefficient $c_B \approx 0.78$ is independent of γ.

The second parameter of the fit, ω, is of order γ/R, as is clear from Eqs. (**??**). We find

$$\omega(b_{\max},\gamma) \approx c_\omega \frac{v\gamma}{R}, \tag{5.9}$$

where the numerical coefficient $c_\omega \approx 0.92$ is independent of γ. For $b \lesssim b_{\max}$ we find that ω is approximately independent of b, whereas for $b \gtrsim b_{\max}$ it decreases approximately linearly,

$$\omega(b,\gamma) \approx \omega(b_{\max},\gamma)\left(1 - \frac{c_{\omega 1}}{R}\theta(b-b_{\max})(b-b_{\max})\right), \tag{5.10}$$

where $c_{\omega 1} \approx 0.25$ and is independent of γ for $\gamma \gtrsim 5$. Of course, the transition is not as sharp as the step function suggests, but is smoothed over a region of size a (see Eq. (**??**)). The fact that ω is smaller for $b \gtrsim b_{\max}$ than for $b \lesssim b_{\max}$ will lead to a reduction of the production cross section for near misses with respect to peripheral collisions.

In our calculations of the fields, we have not included event-by-event fluctuations in nucleon positions, which cause deviations from our mean field results [**?**]. However, including

these effects would not change the scaling relations outlined above: in the directions perpendicular to the beam, the field varies over a larger distance (by a factor of $\sim \gamma$) than in the beam direction, and the approximate analytic expression for the time dependence still holds. Furthermore, at the spacetime origin, the component of the magnetic field parallel to the beam, and the components of the electric field, remain at least an of magnitude smaller than the magnetic field perpendicular to the beam direction.

5.2 Worldline instantons for monopole production in heavy ion collisions

In this section we compute the worldline instanton solution for fields of the form (**??**) and calculate the corresponding exponential dependence of the pair production probability using the method outlined in Section **??**. This is given by

$$P \approx D\, \mathrm{e}^{-S_{\mathrm{inst}}}, \tag{5.11}$$

where S_{inst} is the classical action (**??**) evaluated at its saddle point, and D is the semiclassical prefactor, which can be calculated from the functional determinant given in Section **??**.

The fields of interest are those given in (**??**). To find instantons we perform a Wick rotation $t \to i\tau$, yielding the Euclidean fields

$$\begin{aligned} B_y^E &= -\frac{iB}{2}\left(\frac{1}{\left(1+\omega^2(i\tau-z)^2\right)^{3/2}} + \frac{1}{\left(1+\omega^2(i\tau+z)^2\right)^{3/2}}\right), \\ E_x^E &= \quad \frac{B}{2}\left(\frac{1}{\left(1+\omega^2(i\tau-z)^2\right)^{3/2}} - \frac{1}{\left(1+\omega^2(i\tau+z)^2\right)^{3/2}}\right). \end{aligned} \tag{5.12}$$

The extra factor of $-i$ in the magnetic field is a conventional choice accounting for the derivative with respect to imaginary time in the definition of the (dual) field tensor [**?**]. For these specific fields, it makes both E^E and B^E purely imaginary. This means that the Euclidean worldline instanton equations are purely real:

$$\ddot{x}_\mu = -igs\tilde{F}^E_{\mu\nu}\dot{x}_\nu, \tag{5.13}$$

where

$$\tilde{F}^E_{\mu\nu} = \begin{pmatrix} 0 & 0 & 0 & 0 \\ 0 & 0 & -E_x^E & B_y^E \\ 0 & E_x^E & 0 & 0 \\ 0 & -B_y^E & 0 & 0 \end{pmatrix} \tag{5.14}$$

and the indices μ and ν run over 1,2,3,4, with the 4 component last.

Worldline instantons are closed solutions to the Euclidean worldline equations of motion. From the symmetry of the field it is clear that such a solution exists in the plane $x = z = 0$, where the fields reduce to

$$\begin{aligned} B_y^E(x, z = 0) &= \frac{-iB}{(1 - (\omega\tau)^2)^{3/2}}, \\ E_x^E(x, z = 0) &= 0. \end{aligned} \tag{5.15}$$

The instanton equations then reduce to those in a purely time-dependent magnetic field: because the interaction between the worldline and the electromagnetic field is local, if the worldline does not leave the y-τ plane it is insensitive to the spatial inhomogeneity in the field. This feature of instantons in fields where the spatial variation is perpendicular to the direction of the field has been noted previously in Ref. [**?**]. As the exponential dependence of the pair production probability is determined completely by the action of the worldline instanton, the effects of the inhomogeneity in the transverse spatial directions will only contribute to the production probability at the level of the prefactor. This considerably simplifies the problem of computing the pair production probability: Schwinger production in fields that vary along a single spacetime dimension have been widely studied [**?**, **?**, **?**, **?**, **?**].

Henceforth, for notational convenience, all fields will be implicitly Euclidean unless otherwise indicated.

Following Ref. [**?**] (reviewed in Section **??**) we treat the worldline self-interaction term separately, writing the action (**??**) as

$$S[x_\mu, s] = S_0[x_\mu, s] + \Delta S[x_\mu] \tag{5.16}$$

where

$$S_0[x_\mu, s] = \frac{m^2 s}{2} + \frac{1}{2s}\int_0^1 \mathrm{d}u \dot{x}_\mu \dot{x}_\mu - ig\int_0^1 \mathrm{d}u\, \tilde{A}_\mu^{\mathrm{ext}} \dot{x}_\mu, \tag{5.17}$$

$$\Delta S[x_\mu] = \frac{g^2}{8\pi^2}\int_0^1 \mathrm{d}u \int_0^1 \mathrm{d}u' \frac{\dot{x}_\mu(u)\dot{x}_\mu(u')}{|x(u) - x(u')|^2}. \tag{5.18}$$

In Sections **??** and **??** we assume that $|\Delta S| \ll |S_0|$ when evaluated at the saddle point. Note that this is not a perturbative expansion in g; the precise conditions for this relation to hold will be examined at the end of Section **??**. In Section **??** we perform a full calculation treating ΔS to all orders, numerically.

5.2.1 Worldline instanton without self-interactions

It is convenient to choose a gauge such that the dual electromagnetic potential is

$$\tilde{A}_\mu^{\text{ext}} = \frac{iB\tau}{\sqrt{1-(\omega\tau)^2}}\delta_{\mu 2}. \tag{5.19}$$

Ignoring the self-interaction term, the worldline instanton stationarises

$$\begin{aligned} S_0[x_\mu, s] = \frac{m^2 s}{2} + \frac{1}{2s}\int_0^1 \mathrm{d}u \dot{x}_\mu \dot{x}_\mu \\ + gB\int_0^1 \mathrm{d}u \frac{\dot{y}\tau}{\sqrt{1-(\omega\tau)^2}}. \end{aligned} \tag{5.20}$$

Worldline actions of this form have been extensively studied by Dunne *et al.* [**?**, **?**]. In order to follow the general prescription outlined in Ref. [**?**] (motivated by the work of Keldysh on ionisation in inhomogeneous fields [**?**]) we define the dimensionless *Keldysh parameter*

$$\xi = \frac{m\omega}{gB}. \tag{5.21}$$

We choose to use ξ instead of the more conventional γ in order to avoid confusion with the Lorentz factor. The physical interpretation of ξ when considering monopole production in heavy ion collisions is discussed in Section **??**.

It was shown in Refs. [**?**, **?**] (in the context of electron-positron pair production) that, at the saddle point, the nonself-interacting action (**??**) evaluates to

$$\begin{aligned} S_0[x_\mu^{(0)}] &= \frac{2m^2}{gB}\int_{-1}^1 \mathrm{d}\zeta \frac{\sqrt{1-\zeta^2}}{(1+\xi^2\zeta^2)^{\frac{3}{2}}} \\ &= \frac{4m^2}{gB\xi^2}[\mathbf{E}(-\xi^2) - \mathbf{K}(-\xi^2)], \end{aligned} \tag{5.22}$$

where $\mathbf{E}$ and $\mathbf{K}$ are elliptic integrals, and $x_\mu^{(0)}$ denotes the worldline instanton for the nonself-interacting action (detailed below). This result is shown as the red curve in Fig. **??**. In the above expression, ζ is a dummy variable introduced to simplify the calculation; for more details, see Ref. [**?**].

As $\xi \to 0$,

$$S_0[x_\mu^{(0)}] \to \frac{\pi m^2}{gB}; \tag{5.23}$$

the constant field result is obtained. For a rapidly varying field ($\xi \gg 1$),

$$S_0[x_\mu^{(0)}] \to \frac{4m^2}{gB\xi} = \frac{4m}{\omega}. \tag{5.24}$$

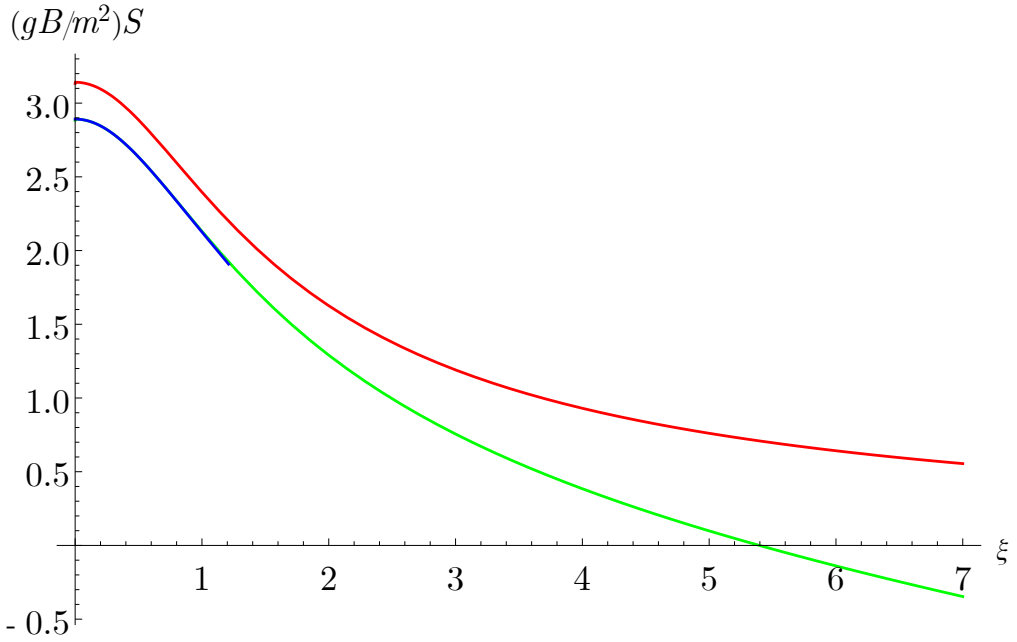

Figure 5.5: Plot of the worldline instanton action as a function of the Keldysh parameter in various levels of approximation. The red line is the result without self-interactions, Eq. (**??**), the green line includes the leading correction from self-interactions, Eq. (**??**), and the blue line gives the numerical results (to all orders) of Section **??**, for $g^3B/m^2 = 1$.

The functional form of the pair production probability—notably the mass dependence—changes in the limit of strongly time-dependent fields. This has important implications for the production of high-mass monopoles in heavy ion collisions, discussed in Section **??**.

In Refs. [**?**, **?**] the fluctuation prefactor D (see Eq. (**??**)) for fields of the form (**??**) is also calculated, and is given approximately by

$$D \approx (2s+1)V_3 \left(\frac{\sqrt{2\pi}(gB)^{3/2}}{32\pi^2}\right) \frac{(1+\xi^2)^{3/4}}{\mathbf{E}(-\xi^2)\sqrt{(1+\xi^2)\mathbf{K}(-\xi^2)-(1-\xi^2)\mathbf{E}(-\xi^2)}}, \tag{5.25}$$

where s is the monopole spin and V_3 is the spatial volume factor. However, for our case, the z dependence of the field will modify the prefactor to leading order in γ. This is because the prefactor involves the determinant of fluctuations about the instanton, and fluctuations in the z direction will feel this dependence (unlike the worldline, which is local, and so is not sensitive to the z dependence of the fields).

However, for the purpose of obtaining order of magnitude estimates, we note that the ξ-dependent part of the prefactor is equal to $1/\xi$ to within an $\mathcal{O}(1)$ factor for all ξ: the prefactor is of the same order as that in the locally constant field approximation (LCFA) regardless of the magnitude of the Keldysh parameter. Noting this, we propose using the LCFA to approximate the prefactor also in the spatial directions (see Appendix **??** for details). In this approximation, the curvature of the field at its maximum determines the prefactor. Denoting the much slower decay rate of the field in the x_1 and y directions as $\Omega \ll \omega$, we therefore expect

$$D \sim \frac{(2s+1)(gB)^4}{18\pi^3 m^4 \omega^2 \Omega^2}, \tag{5.26}$$

to provide a reasonable estimate of the prefactor, up to an $\mathcal{O}(1)$ multiplicative factor.

The shape of the worldline can be determined using a method closely related to that used in Ref. [**?**]. Contracting the Euclidean equations of motion (**??**) with $\dot{x}_\mu$ shows that $\dot{x}_\mu \dot{x}_\mu$ is a constant of motion, and varying the action with respect to the Schwinger parameter s shows that its saddle point value satisfies

$$s^2 = \dot{x}_\mu \dot{x}_\mu. \tag{5.27}$$

Using the symmetry properties of the field, Eq. (**??**) simplifies significantly; the nontrivial relations remaining are

$$\ddot{y} = \frac{gB}{m}\frac{s\dot{\tau}}{[1-(\xi\tau)^2]^{3/2}}, \tag{5.28}$$

$$\ddot{\tau} = -\frac{gB}{m}\frac{s\dot{y}}{[1-(\xi\tau)^2]^{3/2}}, \tag{5.29}$$

$$s^2 = (\dot{y})^2 + (\dot{\tau})^2. \tag{5.30}$$

Integrating Eq. (**??**) gives

$$\dot{y} = \frac{gB}{m}\frac{s\tau}{\sqrt{1-(\omega\tau)^2}}, \tag{5.31}$$

and combining this with Eq. (**??**) gives

$$(\dot{\tau})^2 = s^2\left(1 - \frac{\tau}{\sqrt{1-(\omega\tau)^2}}\right). \tag{5.32}$$

This can be integrated directly to give an explicit proper time parametrisation of $\tau(u)$ and $y(u)$ in terms of Jacobi elliptic functions. However, the shape of the worldline in the y-τ plane can be seen more clearly from the implicit expression

$$\left(\frac{\mathrm{d}\tau}{\mathrm{d}y}\right)^2 = \frac{s^2-(\dot{y})^2}{(\dot{y})^2} = \frac{s^2}{(\dot{y})^2} - 1. \tag{5.33}$$

Substituting Eq. (**??**) gives

$$\left(\frac{\mathrm{d}\tau}{\mathrm{d}y}\right)^2 = \left(\frac{m}{gB}\right)^2\frac{1}{(\tau)^2} - (\xi^2+1). \tag{5.34}$$

This can be readily checked to describe an ellipse: comparison with standard expressions gives the semimajor axis aligned along τ:

$$a_\tau = \frac{m}{gB}\frac{1}{\sqrt{1+\xi^2}}, \tag{5.35}$$

and the semiminor axis aligned along y:

$$a_y = \frac{m}{gB}\frac{1}{1+\xi^2}. \tag{5.36}$$

In corroboration with results from previous analyses [**?**, **?**], the time dependence of the magnetic field contracts the worldline instanton and increases its departure from the circular constant field result. The time dependence of the field can be parametrised by the Keldysh parameter ξ, and the constant field result is obtained smoothly in the limit $\xi \to 0$. Plots of the nonself-interacting worldline instanton for different values of the Keldysh parameter are shown in Figure **??**.

5.2.2 Self interactions to leading order

Section **??** was largely a reproduction of known results for Schwinger production in time-dependent fields. In this and the following section, we extend the calculation to account for

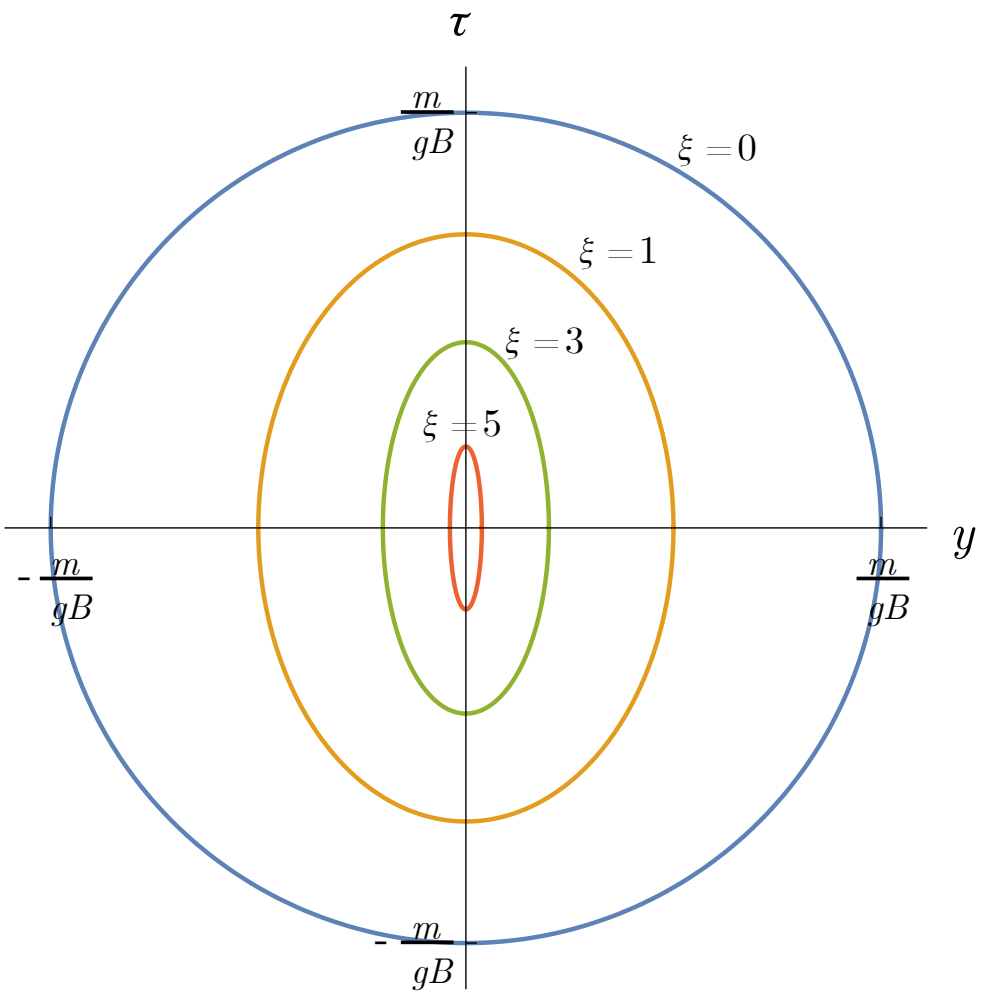

Figure 5.6: Elliptical worldlines stationarising the nonself-interacting action (**??**) for different values of the Keldysh parameter, ξ.

worldline self-interactions. We start by considering just the leading order corrections from worldline self-interactions, which give a contribution to the action

$$\Delta S[x_\mu] = \frac{g^2}{8\pi^2}\int_0^1 \mathrm{d}u \int_0^1 \mathrm{d}u' \frac{\dot{x}_\mu(u)\dot{x}_\mu(u')}{|x(u)-x(u')|^2}. \tag{5.37}$$

This self-interaction term was originally studied in a similar context in Ref. [**?**], where they considered a constant external field. As the nonself-interacting worldline instanton (**??**) stationarises Eq. (**??**), the leading order correction can be computed by evaluating ΔS over the elliptical worldline described by Eq. (**??**).

The self-interaction term is independent of the choice of worldline parametrisation, so we may choose to parametrise the nonself-interacting worldline instanton $x_\mu^{(0)}$ in terms of the cylindrical polar angle $\theta = \tan^{-1}(\tau/y)$:

$$x_\mu^{(0)}(\theta) = \frac{m}{gB(1+\xi^2)}(0, \cos\theta, 0, \sqrt{1+\xi^2}\sin\theta). \tag{5.38}$$

With this parametrisation the leading order correction may be expressed by

$$\Delta S[x_\mu^{(0)}] = \frac{g^2}{8\pi^2}\int_0^{2\pi} \mathrm{d}\theta \int_0^{2\pi} \mathrm{d}\theta' \frac{(1+\xi^2)\cos\theta\cos\theta' + \sin\theta\sin\theta'}{[\cos\theta-\cos\theta']^2 + (1+\xi^2)[\sin\theta-\sin\theta']^2}. \tag{5.39}$$

This integral may be expressed as a double contour integral in the complex plane by performing the substitutions $w = \mathrm{e}^{i\theta}$, $w' = \mathrm{e}^{i\theta'}$:

$$\Delta S[x_\mu^{(0)}] = \frac{g^2}{8\pi^2}\oint_{|w|=1} \mathrm{d}w \oint_{|w'|=1} \mathrm{d}w' \frac{(1+\xi^2)(w^2+1)(w'^2+1) - (w^2-1)(w'^2-1)}{(w-w')^2[2+\xi^2(ww'-1)][2+\xi^2(ww'+1)]}. \tag{5.40}$$

The integral can now be performed using the residue theorem. As the integrand is explicitly symmetric under $w \leftrightarrow w'$ the order of integration is unimportant. The pole at $w = w'$ corresponds to the expected divergence from coincident points [**?**,**?**,**?**], which may be removed by adding a mass counterterm as previously discussed in Section **??**. After subtracting this divergence, and noting that $\xi > 0$ for all physical cases, we find

$$\Delta S[x_\mu^{(0)}] = -\frac{g^2}{8}\left(\sqrt{1+\xi^2} + \frac{1}{\sqrt{1+\xi^2}}\right). \tag{5.41}$$

This tends to the known result for the circular worldline [**?**], in the constant-field limit $\xi \to 0$,

$$\lim_{\xi\to 0}\Delta S[x_\mu^{(0)}] = -\frac{g^2}{4}. \tag{5.42}$$

We have also verified its agreement with a numerical evaluation of the integral with an explicit short distance regularisation and counterterm following Ref. [**?**]. It qualitatively matches a

numerical evaluation of the correction for fields with a similar time dependence presented in [**?**], universally enhancing production probability, with a stationary point at $\xi = 0$ and linear ξ dependence in the large ξ limit. As in the constant-field case, the leading order self-interaction term is scale invariant; it is only a function of worldline shape.

The exponential dependence of the monopole pair production probability in a high-energy heavy ion collision is thus, to first order in the worldline self-interaction,

$$\ln P \approx -\frac{\pi m^2}{gB}\frac{4[\mathbf{E}(-\xi^2)-\mathbf{K}(-\xi^2)]}{\pi\xi^2}+\frac{g^2}{8}\left(\sqrt{1+\xi^2}+\frac{1}{\sqrt{1+\xi^2}}\right). \tag{5.43}$$

This is shown as the green curve in Fig. **??**.

Examining the limits of this expression highlights the conditions under which the assumption $|\Delta S| \ll |S_0|$ is valid: as $\xi \to 0$ we retain the constant-field case, where the condition is

$$\frac{g^3 B}{4\pi m^2} \ll 1. \tag{5.44}$$

However, for strictly constant fields, all higher order corrections vanish due to symmetry [**?**], and hence this condition is in fact not necessary. For $\xi \gg 1$, the condition becomes

$$\frac{g^3 B\xi^2}{32m^2} = \frac{g\omega^2}{32B} \ll 1. \tag{5.45}$$

Note that both of these conditions may be achieved for any value of the monopole charge, g; the application of perturbation theory in the self-interactions does not require weak coupling. On the other hand, condition (**??**) always fails at high enough ξ, indicating that the leading order self-interaction correction is then no longer sufficient.

5.2.3 Self interactions to all orders

Going beyond treating the self-interactions perturbatively, in this section we present our calculation of the worldline instantons taking self-interactions into account to all orders. In this case the equations of motion are integrodifferential due to the nonlocal nature of the self-interactions. Due to the lack of symmetries, these equations are rather hard to solve and hence we resort to a numerical approach, following Ref. [**?**] (see also Ref. [**?**]). We discretise the worldline, approximating it by a finite but large number of points, $N \gg 1$. The equations of motion are then simply N nonlinear algebraic equations which we solve iteratively, using the Newton-Raphson method.

The self-interaction is singular at short distances, and hence needs regularisation. We follow the approach of Ref. [**?**] and introduce an explicit cutoff scale, a. However, for numerical

stability we modify the counterterm following Ref. [**?**] (see Appendix **??** for details). By solving the equations of motion for a range of cutoff scales, we can then extrapolate to the $a \to 0$ limit, which we do following Ref. [**?**]. The explicit formulation of the worldline discretisation is given in Appendix **??**.

The number N must be chosen such that the distance between neighbouring points, $|dx^i| = |x^{i+1} - x^i|$, is much smaller than the smallest scale in the problem, the cutoff, a. Note that for a continuous worldline, the global reparametrisation symmetry $u \to u + c$ means that $\dot{x}_\mu \dot{x}_\mu$ is constant. Thus, to leading order in $1/N$, $|dx^i|$ is independent of i and hence equal to $L[x_\mu]/N$, where $L[x_\mu]$ is the length of the loop. Further, the cutoff a must be chosen to be much smaller than any other scale in the problem. In summary, we require

$$\frac{L[x_\mu]}{N} \ll a \ll \mathrm{Min}\left[\kappa, R_{\mathrm{C}}(x;i)\right], \tag{5.46}$$

where $R_{\mathrm{C}}(x_\mu;i)$ is the radius of curvature of the worldline at the point i. We mostly used $N = 2^{12}$ points to describe the worldlines, though we also compared this to other values of N in checking the $N \to \infty$ behaviour.

The blue curve in Fig. **??** shows the resulting instanton action for $g^3B/m^2 = 1$. One can see that the agreement with the leading order corrected result (**??**) is good, and the full action appears to be slightly lower. We were not able to reach higher ξ, where the higher order corrections are expected to become more important, as for large ξ the worldlines become highly curved, and it was not possible to maintain the necessary hierarchy of scales, Eq. (**??**).

Fig. **??** shows the full action in the parameter region $(g^3B/m^2, \xi) \in ([0,1],[0,2.5])$. For the reasons discussed above, we were not able to obtain results for the top right corner of the plot. We leave the numerical investigation of larger g^3B/m^2 and ξ for future work.

Our numerical results show remarkably good agreement with Eq. (**??**). Thus, at least in the regime we have considered, higher order terms in g^3B/m^2 are small. This might have been expected, given that all higher order terms in g^3B/m^2 vanish at $\xi = 0$ [**?**]. However, extrapolating the $\mathcal{O}(g^3B/m^2)$ corrections to large ξ, one sees that they eventually dominate over the leading order term, making the action negative. This may indicate the breakdown of the semiclassical approximation, though higher order corrections at large ξ may temper this breakdown. Note, however, that the constant field action also becomes negative at sufficiently large values of g^3B/m^2.

In Fig. **??** we also show the effect of interactions on the shape of the worldline instanton. In the region of parameter space we have been able to explore numerically, interactions lead to a modest increase in the curvature of the worldline instanton. As we will discuss in Section

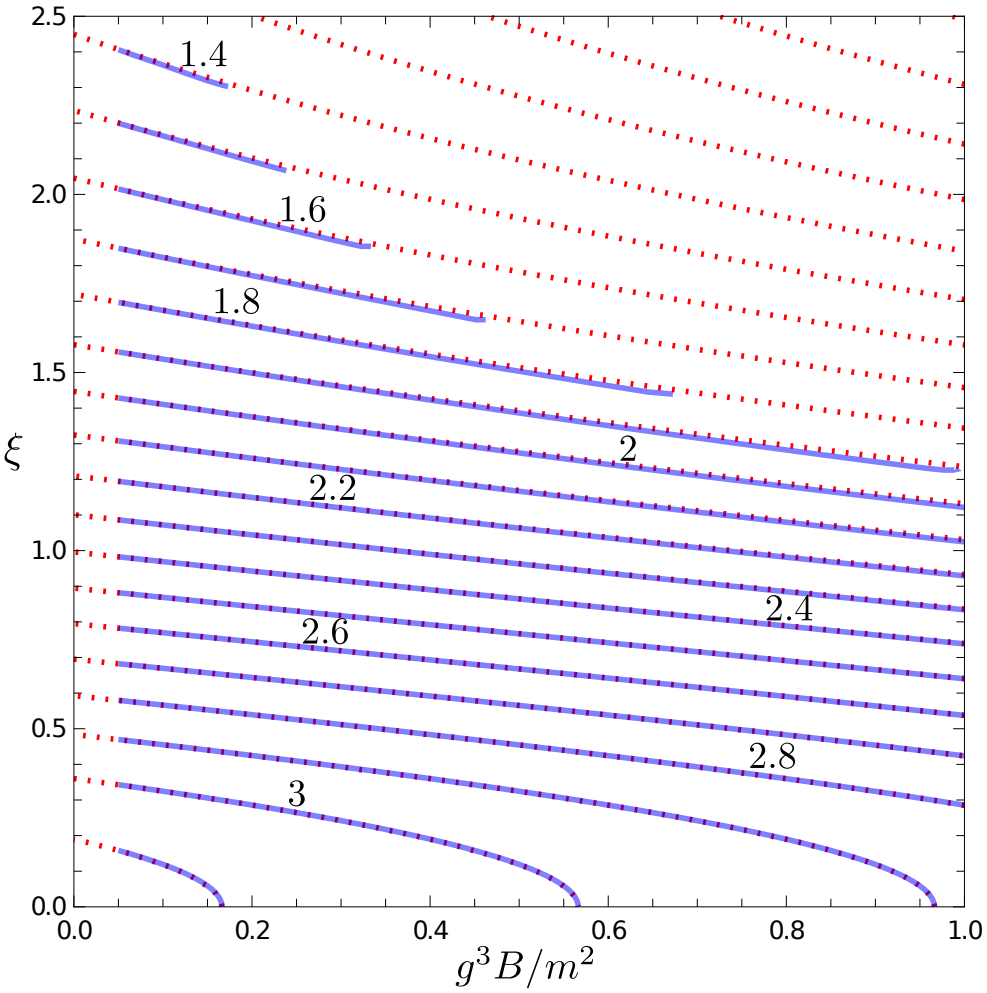

Figure 5.7: The worldline instanton action, S, scaled by gB/m^2. The contour plot shows the action is largest at the origin, for constant, weak fields, and decreases away from that, faster in the direction of ξ than g^3B/m^2. Here the numerical results (to all orders) are shown in blue alongside, in dashed red, the analytic approximation containing only the leading order correction due to self-interactions, Eq. (**??**). Their close agreements shows that higher order corrections are small in this region of parameter space. In the top right, where the numerical results are absent, we were unable to obtain numerical solutions to the instanton equations due to the breakdown of Eq. (**??**).

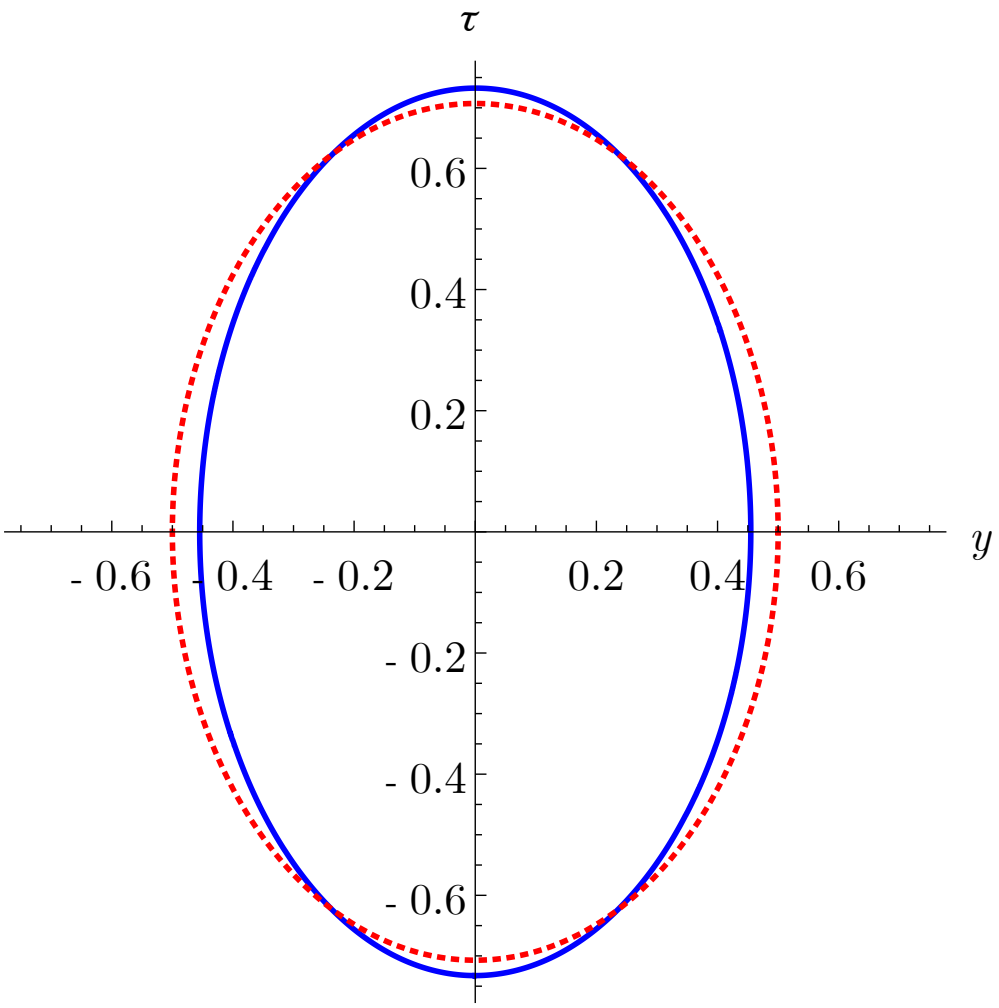

Figure 5.8: The worldline instanton to all orders in the self-interactions at $(g^3B/m^2, \xi) = (1, 1)$, shown in blue. This is compared to the analytic result without self-interactions, i.e. at $(g^3B/m^2, \xi) = (0, 1)$, in dashed red. Self interactions give a modest increase to the maximum curvature of the worldline instanton.

??, this suggests that self-interactions do not prevent the breakdown of the small-monopole approximation at large ξ.

5.3 Limitations of the worldline instanton method

The key result from Section **??** is Eq. (**??**), the exponential dependence of the monopole pair production probability. The time dependence of the field of the heavy ion collision enters the rate, and the corresponding worldline instanton, through a single dimensionless parameter ξ, defined in Eq. (**??**) in terms of the peak value B of the magnetic field and the decay constant ω of the field's time dependence. As discussed in Section **??**, for peripheral collisions (the type most likely to produce monopoles), Eqs. (**??**) and (**??**) give

$$B \approx c_B \frac{Zev\gamma}{2\pi R^2}, \tag{5.47}$$

$$\omega \approx c_\omega \frac{v\gamma}{R}, \tag{5.48}$$

where Ze is the heavy ion charge, R is the heavy ion radius (in its rest frame), v is the ion speed, $\gamma = 1/\sqrt{1-v^2}$ is the Lorentz factor of the collision, and c_B and c_ω are $\mathcal{O}(1)$ dimensionless constants. It follows then that the temporal inhomogeneity of the magnetic field in a peripheral heavy ion collision is parametrised by

$$\xi \approx \frac{c_\omega}{c_B} \frac{2\pi m R}{Zeg}. \tag{5.49}$$

The most striking consequence of this observation is that the temporal inhomogeneity of the field is *independent* of the energy of the collision. This may be understood by considering that, while the temporal extent of the field decreases proportionally to γ, the increase in peak field strength causes a contraction of the worldline instanton that precisely cancels this effect. If the field "looks constant"—i.e. does not vary significantly over the worldline instanton—at any given relativistic energy, this holds for all relativistic energies.

The Keldysh parameter (**??**) for heavy ion collisions can be expressed in an alternate form by utilising the Dirac quantisation condition (**??**). This gives

$$\xi \approx \frac{c_\omega}{c_B} \frac{mR}{Zn}, \tag{5.50}$$

where n is the Dirac charge of the monopole. The values of R and Z are specific to the colliding species, so for a given heavy ion collision, ξ is proportional to the ratio of the monopole mass to the Dirac charge. Using the commonly accepted values for lead-lead

collisions at the LHC of $R = 6.62\,\text{fm}$, $Z = 82$ [?], and the numerical fits $c_\omega = 0.78$ and $c_B = 0.92$ obtained in Section ??,

$$\xi \sim \frac{m}{2.4n\,\text{GeV}}. \tag{5.51}$$

This suggests that, when considering production of monopoles with mass greater than about 2.4 GeV,[5] the time dependence of the magnetic field cannot be neglected at any relativistic energy. The current best theoretical mass bounds [?] are close to this scale, and many theoretical models (e.g. [?, ?]) predict masses far greater. As a result, we conclude that the effects of time dependence are crucial to our understanding of potential magnetic monopole production in heavy ion collisions.

For heavy monopoles (such that $\xi \gg 1$), the pair production probability has exponential dependence (to leading order in $(mR)^{-1}$)

$$\log P \sim -\frac{4mR}{v\gamma} + \frac{\pi^2 nmR}{2Ze^2}, \tag{5.52}$$

where we have dropped the dependence on the $\mathcal{O}(1)$ constants, c_B and c_ω, for simplicity. Combining this with Eq. (??) for an approximation to the prefactor gives, for production of high-mass monopoles in peripheral heavy ion collisions,

$$\left.\frac{d\sigma}{db}\right|_{b=2R} \sim \frac{2(2s+1)v^3\gamma^2 n^4 Z^4}{9\pi^2 m^4 R^3} \exp\left(-\frac{4mR}{v\gamma} + \frac{\pi^2 nmR}{2Ze^2}\right) \tag{5.53}$$

up to an $\mathcal{O}(1)$ multiplicative factor. The total cross section can be obtained by including the impact parameter dependence of the fields (see Section ??) and then integrating over all values of the impact parameter.

The properties of heavy ions and the form of the magnetic fields in peripheral collisions are fixed, and, along with the Dirac quantisation condition, strongly constrain the parameter space in which our results could be applied. The only free parameters are the monopole mass, m, its Dirac charge n, and the collision Lorentz factor γ, which for the LHC heavy ions is approximately 2675. In this section we examine the assumptions made in Section ?? and show that there is unfortunately no region in the experimental parameter space where all our approximations are valid.

[5] This mass corresponds to a classical radius of around 3 fm, which is smaller than the ion radius, though perhaps not small enough to justify a "$\ll$" symbol. Note, however, that most models given serious theoretical consideration predict masses orders of magnitude higher.

5.3.1 The semiclassical approximation

The results of Section **??** are valid under two main assumptions. The first is the semiclassical limit, required to justify the use of instanton methods:

$$S[x_\mu^{\rm inst}, s^{\rm inst}; \tilde{A}_{\rm ext}] \gg 1 \tag{5.54}$$

For high-mass monopoles, $m \gg 2.4n\,\mathrm{GeV}$, the next-to-leading order action (**??**) is proportional to $mR \gg 1$, so the semiclassical approximation is satisfied as long as the action is positive (ignoring a very narrow region of parameter space where the action is between zero and one). As a result, the semiclassicality condition is

$$nv\gamma \lesssim \frac{8Ze^2}{\pi^2}, \tag{5.55}$$

or, taking $Z = 82$ for lead,

$$nv\gamma \lesssim 6. \tag{5.56}$$

This condition is not satisfied in LHC heavy ion collisions because of their high Lorentz factor.

The breakdown of the semiclassical approximation usually indicates unsuppressed particle production, as long as all other approximations are under control at this point. However, in our case (**??**) it happens because the self-interaction correction becomes comparable to the tree level action and cancels it. It therefore merely shows that one needs to include the self-interaction to all orders, as was done in Section **??**. However, in that section we were not able to explore the relevant regime, due to the difficulty of resolving the large hierarchy of scales that arises in this case.

While our current work focuses on magnetic monopoles, the need to include all orders in worldline self-interactions at high inhomogeneities is also relevant when considering Schwinger production of electrons. For high values of the Keldysh parameter, the curvature of the worldline instanton (scaled to its size) is so large that self-interactions cannot be ignored even for weak coupling. This explains the apparent "weak-field" divergence of the results in Ref. [**?**]: it in fact corresponds to a departure from the small self-interaction regime. Under such conditions, the nonself-interacting worldline solution is no longer a good approximation to the true saddle point solution of the full action. Increasing curvature with increasing temporal inhomogeneity appears to be a general feature of time-dependent fields [**?**], so our current calculations and planned numerical work are relevant to a wider class of Schwinger production scenarios.

5.3.2 The small-monopole approximation

The second approximation our calculation relies upon is the dilute instanton gas approximation (discussed in Section **??**). This requires that all scales of the worldline instanton are large compared with the scale on which small, virtual monopole-antimonopole pairs become important:

$$\mathrm{Min}\left[R_{\mathrm{C}}(x_{\mu}^{\mathrm{inst}}(u))\right] \gg \frac{r_{\mathrm{cl}}}{2}, \tag{5.57}$$

where $R_{\mathrm{C}}(x_{\mu}^{\mathrm{inst}}(u))$ is the radius of curvature of the worldline instanton at a point u. The size of virtual monopole-antimonopole pairs, r, can be estimated by equating the rest mass of a monopole-antimonopole pair, $2m$, to their Coulomb attraction, $g^2/(4\pi r)$, resulting in $r = r_{\mathrm{cl}}/2$. Equation (**??**) is important to ensure that the effects of virtual monopole-antimonopole pairs can be factored out of the instanton calculation, affecting only the running of couplings [**?**]. Alternatively, in the case that the monopoles are actually solitonic excitations being described by an effective field theory, Eq. (**??**) is the condition under which the effective field theory description is valid. This is because the core size of a solitonic monopole is the same as the classical monopole radius.

Using the radius of curvature of the ellipse (**??**), Eq. (**??**) becomes

$$\frac{2mRv\gamma}{\pi Z^2 e^2} \ll 1. \tag{5.58}$$

Assuming that the monopole mass is high, this is the most stringent constraint, requiring (for lead-lead collisions)

$$mv\gamma \ll 10\,\mathrm{GeV}. \tag{5.59}$$

This limit prevents application of our results to any energies relevant to modern heavy ion collisions, and for the energies at which the small-monopole approximation does apply, the Lorentz factor is too low to justify the assumptions (from the fits in Section **??**) that the electromagnetic field varies more slowly in the directions perpendicular to the beam. As a result, we are unable at present to provide a reliable monopole production cross section.

For 't Hooft-Polyakov monopoles, one can overcome the limitations of the small-monopole approximation by performing an instanton calculation in the full field theory describing the monopole of interest. The results of this calculation for constant fields are given in Chapter **??** of this thesis. Extending these results to the inhomogeneous fields (**??**) is an important task for future research.

The inapplicability of our results to realistic heavy ion collisions at present is shown clearly in Fig. **??**. This shows the regions in the γ-m plane in which the small monopole

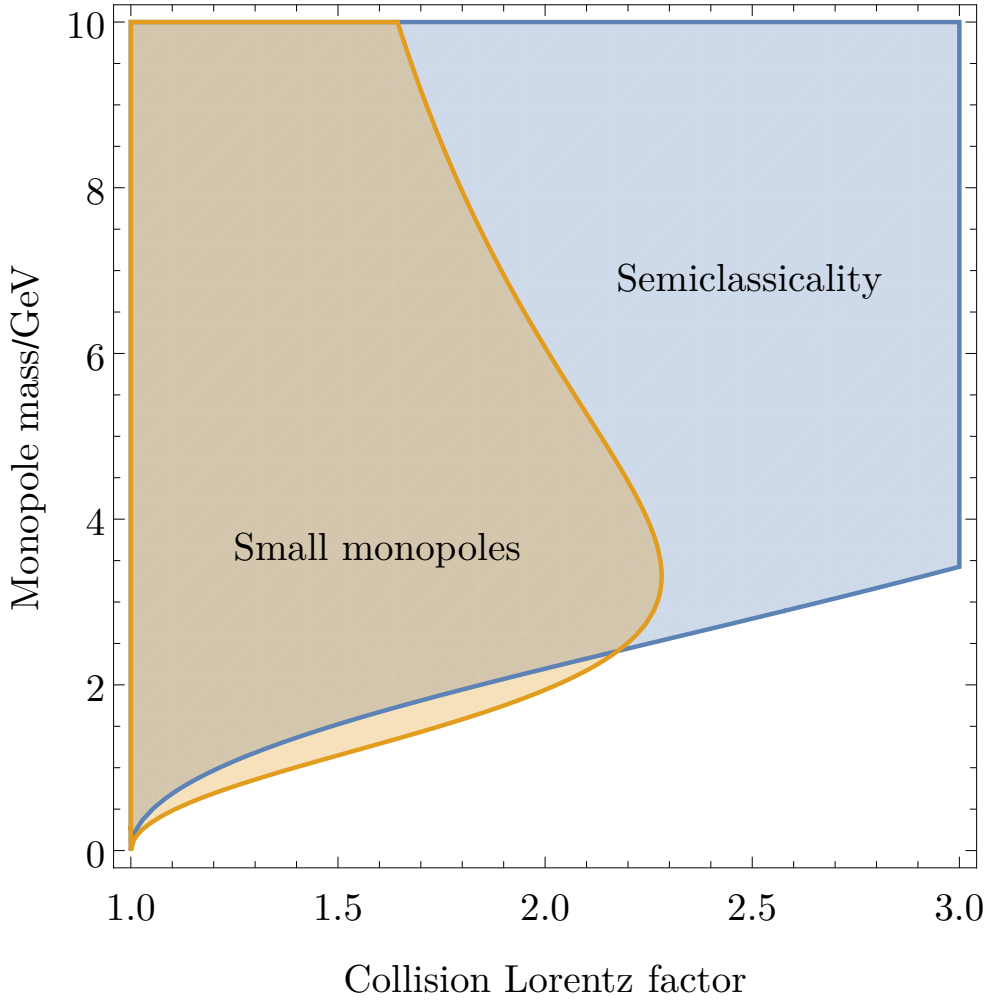

Figure 5.9: Plot showing the regions in the γ-m plane in which the approximations of semiclassicality (blue) and small monopoles (orange) are valid (assuming the Dirac charge $n = 1$). Note that there is a turning point in the region of applicability of the small-monopole approximation, preventing us from going to large Lorentz factors.

and small self-interaction approximations respectively hold, assuming monopoles with Dirac charge $n = 1$. The boundary of the region in which the small monopole assumption is valid has a turning point meaning that to probe $\gamma \gtrsim 2$ (which is necessary if we are to apply the fits from Section **??**) we must move beyond the worldline method.

Fig. **??** shows that the region in which the small-monopole approximation applies lies almost entirely within the region where the effect of worldline self-interactions are small. This suggests that moving beyond the small-monopole approximation is of the highest priority. The results of Section **??** showed that, at least in the region of parameter space we were able to study, self-interactions yield worldline instantons with somewhat higher curvature. This implies that the small-monopole approximation breaks down slightly earlier than suggested in Fig. **??**.

5.4 Lower bounds on monopole cross sections

The outcome of Section **??** may seem somewhat disheartening: the assumptions used to obtain the main results of this chapter are not valid in any relativistic heavy ion collision. However, in this section we will argue that there is sufficient evidence to justify a lower-bound cross section that can in turn be used to place lower bounds on the mass of monopoles, assuming that none are found in future heavy ion collisions.

There are three effects that must be taken into account in order to give a reliable estimate of the probability of producing monopoles in ultrarelativstic heavy ion collisions: strong coupling of the monopoles, spacetime dependence of the electromagnetic fields, and the internal structure of the monopoles. The previous sections combine the first and second of these, but ultimately fails due to the fact that there is no region of parameter space where the third condition does not apply. Chapter **??** will deal with the strong coupling and internal structure of the monopole whilst neglecting the spacetime dependence; combining all three complications has not yet proved possible.

A key observation from our investigations so far is that all the effects considered appear to enhance the pair production probability when compared to the constant-field case:

- Including strong coupling effects to all orders in the worldline approximation lowers the instanton action (see Fig. **??**), giving an exponential enhancement.
- The geometry of the fields mean that time dependence is the dominant effect in the worldline approximation, again giving an exponential enhancement as seen in Refs. [**?**, **?**].

- Considering the internal structure of the monopole in a constant field lowers the instanton action (see Chapter **??**).

This suggests that an analysis that omits one or more of the complicating factors is likely to underestimate the pair production probability, so such an estimation may be suitable for placing lower bounds on monopole masses. Eq. (**??**) is unfortunately unsuitable, as semiclassicality breaks down at relevant Lorentz factors (see Eq. (**??**)). Two approximations that may be used to give conservative estimates of the monopole production probability are the locally constant field approximation (LCFA) and the free particle approximation (FPA).

The LCFA is widely used in the study of the electric Schwinger effect; for a recent discussion see Refs. [**?**, **?**, **?**]. It approximates the overall production probability by assuming that at each spacetime point the local rate of pair production is given by the constant field result evaluated at that spacetime point. For the case of monopoles, the relevant constant field result is Eq. (**??**), so the LCFA production probability is [**?**, **?**]

$$P_{\text{LCFA}} = \frac{2s+1}{8\pi}\int \mathrm{d}^4x\, \exp\left(-\frac{\pi m^2}{g\sqrt{|\vec{B}(x)|^2 - |\vec{E}(x)|^2}} + \frac{g^2}{4}\right), \tag{5.60}$$

where the electromagnetic fields as a function of spacetime are given by Eq. (**??**). This approximation accounts for the strong coupling of the monopole but treats the spacetime inhomogeneity perturbatively. This integral can be performed using a stationary phase approximation to yield

$$P_{\text{LCFA}} \approx \frac{(2s+1)(gB)^4}{18\pi^3 m^4 \omega^2 \Omega^2}\exp\left(-\frac{\pi m^2}{gB} + \frac{g^2}{4}\right), \tag{5.61}$$

where $\Omega \approx R^{-1}$ is the decay width of the field in the x and y directions, defined in Section **??**.

In the FPA, the spacetime dependence is addressed fully in the same manner as Section **??**, but the monopoles are modelled as nonself-interacting. In this case the nonself-interacting worldline action (**??**) is relevant, and the corresponding pair probability is

$$P_{\text{FPA}} \approx \frac{(2s+1)(gB)^4}{18\pi^3 m^4 \omega^2 \Omega^2}\exp\left(-\frac{gB}{\omega^2}\left[\mathbf{E}(-\xi^2) - \mathbf{K}(-\xi^2)\right]\right). \tag{5.62}$$

Assuming $m \gg 2.4n$ GeV this simplifies to

$$P_{\text{FPA}} \approx \frac{(2s+1)(gB)^4}{18\pi^3 m^4 \omega^2 \Omega^2}\exp\left(-\frac{4m}{\omega}\right). \tag{5.63}$$

Both the FPA and the LCFA omit vital features, meaning neither are likely to give an accurate monopole production probability. However, the omitted effects in both cases are

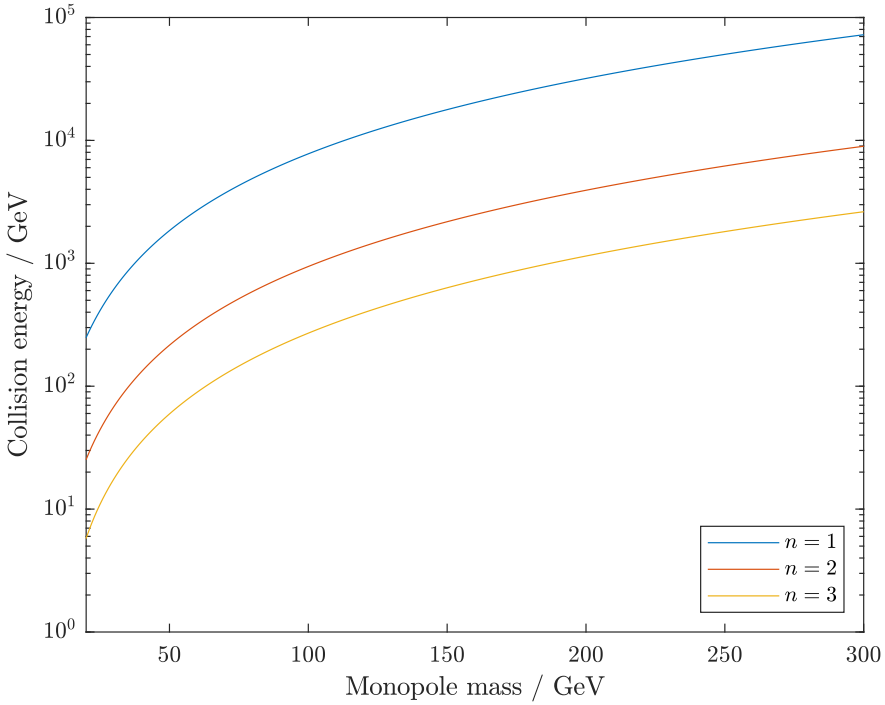

Figure 5.10: Lines in parameter space where Eqs. (**??**) and (**??**) are equal for lead-lead collisions: to the left of the lines the FPA is more conservative whilst to the right the LCFA is more conservative. Different lines indicate different values of n, the number of Dirac charge quanta the monopole carries. The origin of the x axis in this plot is at 20 GeV.

expected to enhance monopole production, meaning that Eqs. (**??**) and (**??**) are likely to be underestimates. A conservative method of obtaining lower bounds on monopole masses would be to take whichever of Eqs. (**??**) and (**??**) gives the smaller bound. This depends on the collision energy as well as the mass and charge of the monopoles. Fig. **??** shows the regions in which each approximation gives a more conservative estimate.

5.5 Momentum distribution of monopoles produced in heavy ion collisions

In addition to a lower bound calculation of the monopole cross section, it is also possible to use the FPA to approximate the momentum distribution of monopoles that are produced in a heavy ion collision. This distribution is a vitally important ingredient for experimental monopole searches, as in order to determine the acceptance of a given experimental setup,

the trajectories of the produced particles must be computed. In this section, we will outline the calculation of this distribution in the FPA, and present its approximate analytical form. Though, as discussed in Section **??**, the FPA is not designed to be a faithful model for monopole production, in Section **??** we will present general arguments as to why the momentum distribution given here is likely to be accurate to within an $\mathcal{O}(1)$ factor.

In the FPA, the coupling between the monopoles and the external electromagnetic field is considered in full, but the interactions between the monopoles themselves are dropped. Making this approximation allows us to draw on the advances made in the study of Schwinger production in QED. Several methods have been used for computing the momentum distribution of Schwinger-produced electrons, including quantum kinetic equations [**?**, **?**, **?**], the Wigner formalism [**?**, **?**, **?**] and WKB methods [**?**, **?**, **?**]. However, we choose to continue with worldline instanton methods, adapting the approach of Ref. [**?**], which utilises "complex worldline instantons" to obtain the momentum distribution of Schwinger-produced particles from inhomogeneous fields. The reason for choosing worldline methods is the fact that, though in this work we remain in the FPA, in the future it may be possible to incorporate an arbitrary coupling constant using a similar approach to Section **??**.

We continue to use the geometry of Fig. **??** and focus on the fields (**??**). A dual electromagnetic potential which leads to the electromagnetic fields of Eq. (**??**) in this limit is

$$\tilde{A}_2 = \frac{(B/2)\,(t-z)}{\sqrt{1+\omega^2\,(t-z)^2}} + \frac{(B/2)\,(t+z)}{\sqrt{1+\omega^2\,(t+z)^2}}\,, \tag{5.64}$$

with all other components zero. In the context of QED, the momentum spectrum of electron-positron pairs produced by similarly spacetime-dependent fields as Eq. (**??**) has been studied in Refs. [**?**, **?**, **?**, **?**, **?**, **?**]. Within the FPA, the methods used in these references are directly applicable to monopole production, and their application would be valuable.

In section **??** we noted that due to the symmetry of the fields under $z \to -z$, the exponential dependence of the total monopole pair production probability is the same as that for the much simpler field with only spacetime dependence through the time coordinate:

$$B_y^{\text{ext}} = \frac{B}{[1+(\omega t)^2]^{3/2}}, \tag{5.65}$$

where B and ω are the same constants as above and all other components of $\vec{E}$ and $\vec{B}$ vanish. In the following, we will continue to use Eq. (**??**) to compute the momentum distribution of Schwinger-produced monopoles in the FPA. We expect this to provide an accurate distribution for the momenta in the x and y direction, but the true momentum distribution in the

z direction may differ from the result presented here by up to an $\mathcal{O}(1)$ factor (discussed in Section **??**).

The relation of the dual potential to the magnetic field is $B^i_{\text{ext}} = \partial^i A_0 - \partial_0 A^i$. For the magnetic field of Eq. (**??**), without z dependence, the dual gauge field reduces to

$$\tilde{A}_y = \frac{Bt}{\sqrt{1+(\omega t)^2}}. \tag{5.66}$$

The worldline instanton method with imaginary t coordinate (i.e. a Wick rotation) was used in Section **??** to compute the overall production probability of monopole-antimonopole pairs in the field given by Eq. (**??**). In this section, we instead follow the approach of Ref. [**?**]: rather than Wick rotating, we promote the spacetime coordinates to complex numbers and search for periodic solutions to the equations of motion with imaginary proper time.

These equations are simply the Lorentz force law for magnetically charged particles:

$$\begin{aligned} m\ddot{t} &= \frac{gB\dot{y}}{[1+(\omega t)^2]^{3/2}}, \\ m\ddot{y} &= \frac{gB\dot{t}}{[1+(\omega t)^2]^{3/2}}, \\ m\ddot{x} &= m\ddot{z} = 0. \end{aligned} \tag{5.67}$$

Here a dot denotes a derivative with respect to proper time $\mathscr{t}$ along the particle worldline,[6] and g is the magnetic charge of the particle. The first integral of these equations provides the constraint

$$\dot{t}^2 - \dot{x}^2 - \dot{y}^2 - \dot{z}^2 = 1, \tag{5.68}$$

motivating the description of $\mathscr{t}$ as proper time even when it takes an imaginary value. From the three spatial translation symmetries, Noether's theorem gives the conserved charges

$$\begin{aligned} p_x &= m\dot{x}, \\ p_y &= m\dot{y} - gA_y, \\ p_z &= m\dot{z}, \end{aligned} \tag{5.69}$$

which may be interpreted as the canonical momenta of the produced particles. Eq. (**??**) can therefore be rewritten as

$$\dot{t}^2 - \frac{1}{m^2}\left[p_x^2 + (p_y + gA_y(t))^2 + p_z^2\right] = 1. \tag{5.70}$$

[6]Not to be confused with Euclidean time τ used in earlier sections.

In order to determine the worldline trajectory, we must specify the initial values $x_\mu(\ell = 0)$ and $\dot{x}_\mu(\ell = 0)$. Due to the translational symmetry of the magnetic field, we are free to fix the spatial position of the worldline, and without loss of generality we can choose

$$x(0) = y(0) = z(0) = 0. \tag{5.71}$$

The initial conditions on the proper time derivatives of the spatial coordinates are equivalent to specifying canonical momenta:

$$\begin{aligned} m\dot{x}(0) &= p_x, \\ m\dot{y}(0) &= p_y + gA_y(t(0)), \\ m\dot{z}(0) &= p_z. \end{aligned} \tag{5.72}$$

For fields of the form (**??**), the final kinetic momentum[7] is related to the canonical momentum by

$$k_2 = p_y + gA_y(t \to \infty) = p_y + \frac{gB}{\omega} \approx p_y + 2.4n \text{ GeV}, \tag{5.73}$$

with the canonical and kinetic momenta being equal in other directions. Here n denotes the number of Dirac charge quanta the monopole carries. For the approximate numerical value of gB/ω, we have assumed ultrarelativistic lead ion collisions, as relevant to the LHC.

The remaining initial conditions to be chosen are $t(0)$ and $\dot{t}(0)$. These are specified by stipulating [**?**] that the classical worldline trajectories pass through WKB turning points, defined by

$$m^2 + p_x^2 + (p_y + gA_y(t_{\text{wkb}}))^2 + p_z^2 = 0. \tag{5.74}$$

Note that because t, and thus A_y, is complex, this does not imply that $p_x = p_z = 0$. Solving this equation gives a complex conjugate pair of turning points in the complex t plane; the worldline solution interpolates between them. We thus choose the initial condition

$$t(0) = t_{\text{wkb}}. \tag{5.75}$$

The condition (**??**) requires the final boundary condition

$$\dot{t}(0) = 0. \tag{5.76}$$

The fact that Eq. (**??**) is satisfied at $\ell = 0$ allows a simplification of the $\dot{y}$ initial condition: substituting Eq. (**??**) into Eq. (**??**) gives

$$m\dot{y}(0) = \pm i m_\perp, \tag{5.77}$$

[7]This is the quantity that would be measured by a detector.

where the "transverse mass" is defined

$$m_\perp^2 = m^2 + p_x^2 + p_z^2. \tag{5.78}$$

The sign indicates the direction in which the worldline is traversed and does not affect the value of the action.

The probability of producing particles with a given canonical momentum p_y is given by the imaginary part of the effective action of the worldline solving Eqs. (**??**) for imaginary proper time.

$$n(m, \vec{p}) \sim \exp\left(-\mathrm{Im}(S_{\mathrm{eff}}[t])\right), \tag{5.79}$$

where [**?**]

$$\begin{aligned} S_{\mathrm{eff}}[t] =& \frac{1}{2}\int_0^T \Big\{ m + m\dot{t}^2 \\ &+ \frac{1}{m}\left[p_x^2 + \left(p_y + gA_y(t)\right)^2 + p_z^2\right] \Big\} \mathrm{d}\ell, \end{aligned} \tag{5.80}$$

T being the worldline period. Using Eq. (**??**) and the relation $m\dot{y}(0) = p_y + gA_y$, one can show that on shell,

$$S_{\mathrm{eff}}[t] = m\int_0^T \dot{t}^2\, \mathrm{d}\ell. \tag{5.81}$$

As a final observation, note that the physical mass m factors out of the equations of motion and can be removed entirely by rescaling $\ell \to \ell/m$. The only mass dependence in the action originates from the transverse mass term in the initial condition for $\dot{y}$, Eq. (**??**). This means that the action at arbitrary transverse momentum can be obtained by solving the equations of motion for $p_x = p_z = 0$, and substituting $m \to m_\perp$. In the following, we drop the transverse momentum terms for brevity.

For $p_y = 0$ the equations of motion (**??**) are analytically solvable: the solution has t purely imaginary and takes the form of an ellipse in the Im(t)-Re(y) plane [**?**]. The ellipse has semimajor and semiminor axes

$$a_t = \frac{m}{gB}\frac{1}{\sqrt{1+\xi^2}}, \tag{5.82}$$

$$a_y = \frac{m}{gB}\frac{1}{1+\xi^2}, \tag{5.83}$$

where $\xi = m\omega/(gB)$ is the Keldysh parameter, and the imaginary part of the action is [**?**]

$$\mathrm{Im}(S[x_\mu]) = \frac{\pi m^2}{gB}\frac{4[\mathbf{E}(-\xi^2) - \mathbf{K}(-\xi^2)]}{\pi\xi^2}. \tag{5.84}$$

Here **E** and **K** denote elliptic integrals. As previously discussed, for ultrarelativistic heavy ion collisions the $\xi \gg 1$ limit is relevant: in this case

$$a_t \approx \frac{m}{gB\xi} = \frac{1}{\omega}, \tag{5.85}$$

$$a_y \approx \frac{m}{gB\xi^2} = \frac{1}{\xi\omega}, \tag{5.86}$$

$$\mathrm{Im}(S[x_\mu]) \approx \frac{4m^2}{gB\xi} = \frac{4m}{\omega}. \tag{5.87}$$

The elliptical worldline solution becomes increasingly prolate with increasing ξ; for very large values of ξ the worldline barely deviates from the imaginary t axis.

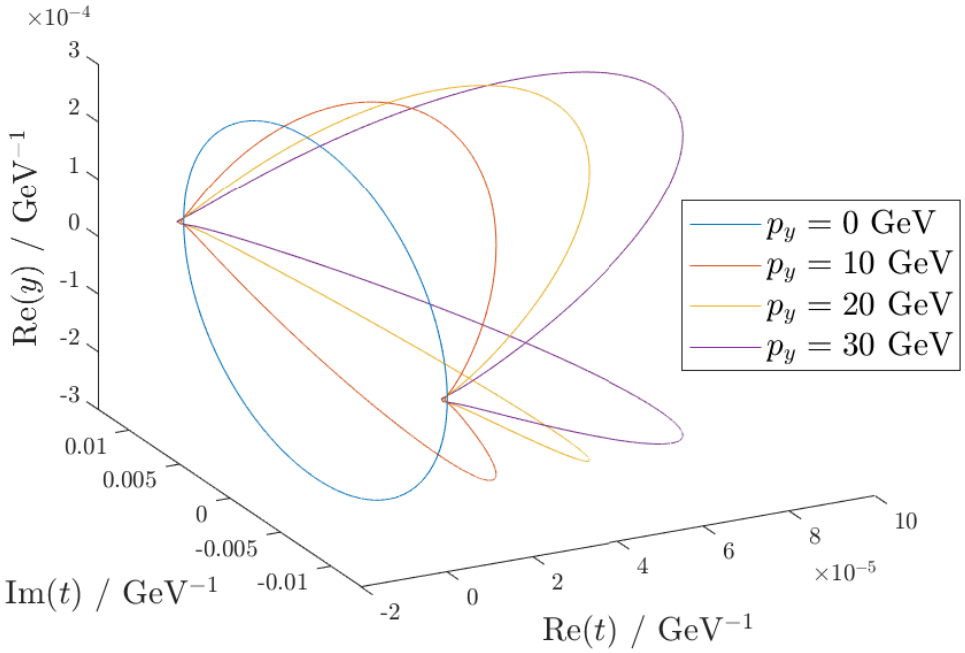

Figure 5.11: 3D plots of complex worldline instantons in the field given by Eq. (**??**), for monopoles of mass 100 GeV and a collision energy of 5.02 TeV per nucleon.

For $p_y \neq 0$, the initial condition (**??**) means that t is no longer purely imaginary; in Ref. [**?**] the solutions were termed "complex worldline instantons". These solutions are not obtainable analytically, but can be determined using a numerical prescription outlined in Ref. [**?**]; we have carried out this calculation for monopoles produced in collisions at LHC energies of 5.02 TeV per nucleon. The effect of nonzero longitudinal momentum is to bend the worldline away from the imaginary t axis: this is illustrated in Fig. **??**. Note that

these worldlines are not symmetric about the real t axis; worldlines with negative values of longitudinal momentum would bend in the other direction.

The momentum distribution resulting from our numerical calculation is plotted in Fig. **??**. It can be seen that the probability distribution is well approximated by the expression

$$n(m, p_y) \sim \exp\left(-\frac{4}{\omega}\sqrt{p_y^2 + m^2}\right), \tag{5.88}$$

which can be obtained by substituting $m \to \sqrt{m^2 + p_y^2}$ into the zero momentum result (**??**) and taking the high-inhomogeneity limit. It therefore reproduces the known analytic result at zero momentum. Note that this is not a numerical fit, as there are no free parameters. We conjecture that this relationship is valid for any field of the form (**??**), provided that the Keldysh parameter

$$\frac{m\omega}{gB} \approx \frac{m}{2.4n \text{ GeV}} \gg 1, \tag{5.89}$$

where n is the number of Dirac charge quanta the monopole carries. Comparing the computed and approximated values for monopole production at LHC energies with momenta $p_y \in [-m/2, m/2]$ we find that Eq. (**??**) is accurate to within around 1% for $m = 30$ GeV, and the error is even smaller for higher masses. Excluding a narrow window not yet excluded by existing mass bounds [**?**] realistic monopole models will satisfy inequality (**??**).

As the transverse momentum affects the final result only via a modification of the effective mass, the relative momentum distribution is thus the isotropic distribution

$$n_{\text{rel}}(m, \vec{p}) \equiv \frac{n(m, \vec{p})}{n(m, 0)} = \exp\left[-\frac{4}{\omega}\left(\sqrt{m^2 + |\vec{p}|^2} - m\right)\right]. \tag{5.90}$$

The surprising fact that the field direction does not seem to affect the angular distribution is discussed in the next section.

The kinetic momentum $\mathbf{k}$ measured by a detector is related to the canonical momentum $\vec{p}$ by Eq. (**??**). This means that a plot of the kinetic momentum spectrum would be shifted by approximately $2.4n$ GeV compared to Fig. **??**. As the widths of the peaks shown are much greater than this, the approximation of an isotropic kinetic momentum distribution is also justified.

A similar analysis with, for example, the Sauter pulse

$$B_\mu^{\text{ext}} = B \operatorname{sech}^2\left(\frac{\pi}{2}\omega t\right) \delta_{\mu 2}, \tag{5.91}$$

shows a similar momentum distribution, differing only by an $\mathcal{O}(1)$ factor. This suggests that the general structure of the momentum distribution may be a consequence of the localisation of the magnetic field to a time interval of order $1/\omega$, and not of its specific functional form.

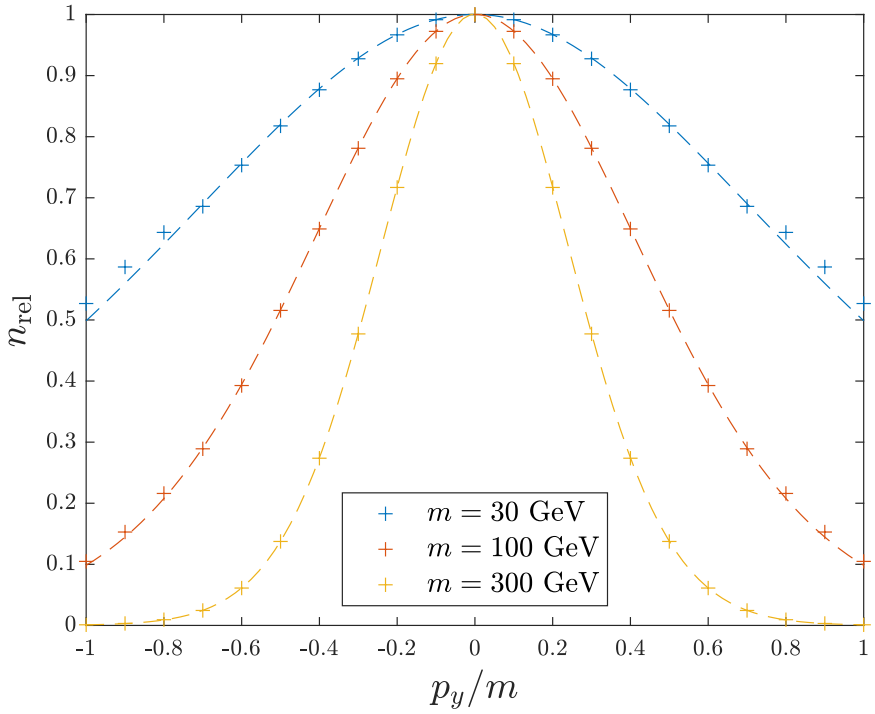

Figure 5.12: Relative momentum distribution of monopole-antimonopole pairs produced from the field (**??**), for collision energies of 5.02 TeV at various monopole masses. Dashed lines show Eq. (**??**) for comparison.

5.6 Limitations of the free particle approximation for Schwinger momenta

Some of the limitations of the FPA have already been discussed in Section **??**, where we argued that the omission of monopole self-interactions and internal structure in FPA worldline calculations results in a conservative estimate of the overall production rate, allowing lower bounds on monopole mass to be computed if no monopoles are found in future heavy ion searches. In this section we discuss the extent to which the momentum distribution given in Eq. (**??**) is likely to give an accurate prediction.

One complication that is currently not resolved by any known calculation of monopole production in heavy ion collisions is the issue of whether the monopole "fits" in the magnetic field. While the magnetic field is extended over a region of order R in the x and y directions, in the z direction it is much narrower due to Lorentz contraction along the beam axis with a width of order R/γ. Taking the classical radius of the monopole $r_{\mathrm{cl}} = g^2/4\pi m$, this suggests that monopoles with $m < \gamma g^2/4\pi R$ are large compared to the extent of the magnetic field in

the z direction. In principle, a lattice calculation generalising the work of Chapter **??** would be able to solve this problem, though it is expected to be computationally difficult due to the large separation of scales.

The limited spatial extent of the field in the z direction also has consequences for our computation of the distribution of the p_z component of the monopole momentum. Our calculation in Section **??** was performed in the background of the spatially homogeneous field (**??**), which means that the dual potential may be written as a function of time only, and the real part of the z coordinate along the worldline instanton remains constant. In general, the instanton solutions in the background of the full fields (**??**) are not known, though due to the $z \to -z$ symmetry of the system the $p_z = 0$ family of solutions must be identical to the corresponding solutions we have found. The p_x and p_y dependence of Eq. (**??**) is therefore expected to be accurate. For $p_z \neq 0$, however, we expect the instanton solutions in the background of the full field to deviate along the real z axis. This suggests that the p_z dependence of the true momentum distribution may differ from our result (**??**), though the difference can be, at most, of order $\mathcal{O}(1)$, as no new scales enter the problem.

An interesting feature of the distribution that we have calculated is that it saturates the time-energy uncertainty principle [**?**, **?**]. This suggests that the relative momentum distribution may be valid more generally, at least as a lower bound on the momentum variance. As time is not represented by an operator in quantum mechanics, the time-energy uncertainty principle does not have the same rigorous basis as uncertainty principles for conjugate observables: the general statement of the principle,

$$\Delta t \Delta E \geq \frac{\hbar}{2}, \tag{5.92}$$

has many interpretations. It is most commonly discussed as representing uncertainty of measurement outcomes, but the most relevant interpretation in the context of our work is preparation time-energy uncertainty, which has a more solid theoretical footing than many other interpretations [**?**].

The preparation time-energy uncertainty principle concerns the preparation of a quantum state with definite energy E, assumed to be drawn from a continuous spectrum of energies. The principle states that if the state is prepared in a finite time Δt, the final energy cannot be chosen with absolute precision, and instead has an uncertainty of at least ΔE satisfying the relation (**??**). This is exactly the situation in our setup, where a state containing a monopole-antimonopole pair is prepared from the vacuum state in a time $\Delta t \approx 1/\omega$. The energy of the pair is

$$E = 2\sqrt{m^2 + |\vec{p}|^2} = 2(m + E_{\text{kin}}), \tag{5.93}$$

where $E_{\text{kin}} = \sqrt{m^2 + |\vec{p}|^2} - m$ is the kinetic energy of a single monopole.

In order for the monopoles to be produced at rest, we would require $E = 2m$. However, the uncertainty principle means that $\Delta E \geq \omega/2$, meaning that the typical kinetic energy must satisfy the relation

$$\langle E_{\text{kin}} \rangle \gtrsim \frac{\omega}{4}. \tag{5.94}$$

Our predicted momentum distribution (**??**) may be written

$$n_{\text{rel}} = \exp\left(-\frac{4E_{\text{kin}}}{\omega}\right), \tag{5.95}$$

saturating this bound. This suggests that even though the specific assumptions of the FPA are not valid for monopole production in heavy ion collisions, the final result should be a good approximation: the momentum distribution cannot be any narrower without violating the uncertainty principle, and if preparation time is the dominant factor (indicated by the fact that ω is the only parameter of the collision that appears in the final result), we do not expect it to be any wider. This observation may also explain why Eq. (**??**) is isotropic despite the fact that the direction of the magnetic field defines a preferred direction in space.

The position-momentum uncertainty principle also applies to our result, as particle production occurs at a significant rate only in a finite region of space. This means that we expect the width of the momentum distribution in the x and y directions to be at least $\Delta p_x, \Delta p_y \gtrsim 1/R$. For ultrarelativistic collisions this is a much weaker condition than Eq. (**??**). The contraction of the field in the z direction, however, means that we expect $\Delta p_z \approx \omega$. This constraint is satisfied by Eq. (**??**) at the level of orders of magnitude, though as discussed earlier there may be an $\mathcal{O}(1)$ correction to the shape of the momentum distribution in the z direction.

5.7 Summary

In this section, we have presented the current state of the art in the analysis of magnetic monopole production from heavy ion collisions via the Schwinger effect. While there is still much more to be done with regard to obtaining theoretical results that account for all the complications of ultrarelativistic heavy ion collisions, there is significant evidence to suggest the results of this chapter are suitable for imposing lower bounds on the overall cross section of monopoles, and an approximation to the monopoles' momentum distribution.

The first key result of the chapter is the lower bound for the monopole pair production

probability in the free particle approximation:

$$P \gtrsim \exp\left(-\frac{4m}{\omega}\right) = \exp\left(-\frac{4m\gamma}{R}\right), \tag{5.96}$$

As discussed in Section **??**, this should be compared to the locally constant field approximation

$$P \gtrsim \exp\left(-\frac{\pi m^2}{gB} + \frac{g^2}{4}\right) = \exp\left(-\frac{2\pi m^2 R^2}{Zeg} + \frac{g^2}{4}\right), \tag{5.97}$$

with the lower result giving the more conservative estimate of the overall cross section. In the above expressions, the exponential prefactor has been dropped, as well as $\mathcal{O}(1)$ constants in the exponentials in terms of ion parameters (see Eqs. (**??**) and (**??**)).

The second key result is the approximate relative momentum distribution of the Schwinger-produced monopoles:

$$n_{\text{rel}} \approx \exp\left[-\frac{4}{\omega}\left(\sqrt{m^2 + |\vec{p}|^2} - m\right)\right]. \tag{5.98}$$

As discussed in Section **??**, this is expected to be accurate to within an $\mathcal{O}(1)$ factor in the exponent.

These approximations have recently been used by the MoEDAL collaboration in Ref. [**?**], which gives the results of the first dedicated experimental search for production of magnetic monopoles via the Schwinger mechanism, in heavy ion collisions at the LHC. Monopoles with an overall production probability given by Eqs. (**??**) and (**??**), and a momentum distribution given by Eq. (**??**), were simulated using the GEANT4 [**?**] software package. The modelled interaction with the detection apparatus was used to determine the acceptance of the MoEDAL detectors, which, as no magnetic monopoles were detected, enabled a lower bound of 70-75 GeV (depending on monopole charge) to be placed on the monopole mass. While these are less restrictive than some bounds from other experiments (see Section **??** for details), they improve the bounds of Ref. [**?**] by almost two orders of magnitude, and are not subject to the limitations of other monopole production calculations due to the nonperturbative nature of the Schwinger effect.

Chapter 6

Production of 't Hooft–Polyakov monopoles from magnetic fields

6.1 Moving beyond the worldline method

The previous chapter, and the vast majority of the existing literature on monopole production from magnetic fields, considers Schwinger production in cases where the worldline approximation is valid. This is equivalent to requiring that the length scale associated with the monopole is small compared to all other length scales in the problem. The relevant scale for both Dirac and solitonic monopoles is the classical monopole radius

$$r_{\mathrm{M}} = \frac{g^2}{4\pi m}. \tag{6.1}$$

When the monopoles in question are solitonic field configurations, this represents the size of the monopole core, where the non-Abelian nature of the fields become important. If the monopoles appear as elementary particles with their own source term in the Lagrangian, this is the radius at which nonlinear QED effects "dress" the monopole, effectively delocalising the photon-monopole interactions [**?**, **?**].

When the length scales in the system are large compared to r_{M}, the worldline methods used in Chapter **??** can be utilised effectively—for solitonic monopoles one can employ an effective field theory identical to one describing elementary monopoles [**?**, **?**, **?**, **?**]. However, there is both theoretical and experimental interest in situations where the worldline approximation breaks down. For monopole production in constant magnetic fields, the relevant condition for the worldline approximation to be valid is

$$\frac{g^3 B}{4\pi m^2} \ll 1. \tag{6.2}$$

This ceases to hold when the field becomes strong in units defined by the monopole mass and charge. For the inhomogeneous fields of heavy ion collisions, investigated in Chapter **??**, the relevant condition (at high monopole masses) can be expressed using the radius of curvature of the ellipse (**??**) as

$$\frac{m\omega^3}{4\pi B^2} \ll 1, \tag{6.3}$$

where B is the peak value of the magnetic field and ω is the field's decay time. Using the parameter values for lead-lead collisions given in Section **??**, this can be converted to a constraint on the energy of a collision to which worldline methods can be reliably applied: dropping $\mathcal{O}(1)$ constants, we get

$$mv\gamma \ll 10 \text{ GeV}, \tag{6.4}$$

where v is the ion velocity and γ is the ion Lorentz factor in the lab frame. As $\gamma \gg 1$ for modern heavy ion collisions, and monopole masses below $\mathcal{O}(1 \text{ GeV})$ have been conclusively ruled out [**?**], it is clear that resolving distances below r_{M} is crucial for the theoretical understanding of monopole production in particle colliders.

This chapter details the efforts made to move beyond the worldline approximation and take the internal structure of monopoles into account when computing Schwinger production rates. In order to do this, one must specify the monopole model in question. Throughout this chapter, we use the canonical 't Hooft–Polyakov monopole [**?**, **?**], which may be embedded in any Grand Unified Theory encompassing the Standard Model of particle physics. The results of this chapter are therefore generalisable to many theories admitting solitonic monopoles, though do not address the "dressing" of elementary monopoles described in Refs. [**?**, **?**]. We note, however, that in some theories the existence of dualities [**?**] allows point particles to be described as solitons and vice versa—in such theories, our results may also be applicable to point particles.

We continue to make use of semiclassical instanton methods, but instead of working within the worldline approximation, we move to a non-Abelian gauge theory—specifically Georgi-Glashow SU(2) theory [**?**]. This has the continuum Lagrangian

$$\mathcal{L} = -\frac{1}{2}\operatorname{Tr} F_{\mu\nu}F^{\mu\nu} + \operatorname{Tr} D_\mu \Phi D^\mu \Phi - \lambda(\operatorname{Tr}\Phi^2 - v^2)^2. \tag{6.5}$$

and admits 't Hooft–Polyakov monopole solutions (see Section **??** for details, where the meaning of the terms in Eq. (**??**) are also discussed). Because we consider all the field-theoretic degrees of freedom of the problem, our results take into account both the monopole internal structure and its strong coupling at all orders. In order to solve the equations of motion of the theory, we use the lattice techniques and numerical methods outlined in

Chapter **??**. This has enabled us to generalise the worldline results of Refs. [**?**, **?**] to full field-theoretic results, explicitly computing new sphaleron and instanton solutions for the first time.

6.2 The Ambjørn-Olesen instability

Before we begin the process of finding sphalerons and instantons in the background of an external magnetic field, it is instructive to consider the range of field strengths that are relevant. In classical electrodynamics, a constant, spatially homogeneous magnetic field is a minimum of the Maxwell Lagrangian at all field strengths. In non-Abelian gauge theories, however, this is not generally the case [**?**]. If the theory contains charged vector bosons, the interaction between the external field and the magnetic moment of the charged vector bosons can destabilise the homogeneous vacuum: this was first studied by Ambjørn and Olesen in the context of Georgi-Glashow theory in Ref. [**?**], and in electroweak theory by the same authors in Refs. [**?**, **?**]. In Georgi-Glashow theory, the theory studied in the chapter, the magnetic field strength at which the instability occurs is

$$B_{\text{crit}} = \frac{m_{\text{v}}^2}{e}, \tag{6.6}$$

where m_{v} is the vector boson mass, and e is the electric gauge coupling. Following Ref. [**?**] we can demonstrate this by fixing the scalar field

$$\Phi = \frac{v}{\sqrt{2}}\sigma_3, \tag{6.7}$$

and (for now) ignoring its dynamics. The dynamical part of the Lagrangian (**??**) is thus

$$\mathcal{L} = -\frac{1}{2}\operatorname{Tr} F_{\mu\nu}F^{\mu\nu} - 2e^2v^2\left[(A_\mu^1)^2 + (A_\mu^2)^2\right]. \tag{6.8}$$

We then perform a field redefinition

$$W_\mu = \frac{1}{\sqrt{2}}(A_\mu^1 + iA_\mu^2), \qquad A_\mu = A_\mu^3, \tag{6.9}$$

defining the U(1) field strength tensor

$$f_{\mu\nu} = \partial_\mu A_\nu - \partial_\nu A_\mu. \tag{6.10}$$

This allows us to rewrite the Lagrangian (**??**) as

$$\begin{aligned}\mathcal{L} = &-\frac{1}{4}f_{\mu\nu}f^{\mu\nu} - \frac{1}{2}|D_\mu W_\nu - D_\nu W_\mu|^2 \\ &-\frac{1}{2}m_{\text{v}}^2 W_\mu^\dagger W^\mu - ief_{\mu\nu}W^{\mu\dagger}W^\nu \\ &+\frac{1}{2}e^2\left[W_\mu^\dagger W^{\mu\dagger}W_\nu W^\nu - (W_\mu^\dagger W^\mu)^2\right].\end{aligned} \tag{6.11}$$

We now linearise about a constant magnetic field, choosing without loss of generality $f_{12} = -f_{21} = B$ with all other components vanishing. The effective mass term for the vector bosons (the second line of the above equation) is then

$$\begin{pmatrix} W_1^\dagger & W_2^\dagger \end{pmatrix} \begin{pmatrix} m_\mathrm{v}^2 & ieB \\ -ieB & m_\mathrm{v}^2 \end{pmatrix} \begin{pmatrix} W_1 \\ W_2 \end{pmatrix}. \tag{6.12}$$

The determinant $m_\mathrm{v}^4 - e^2B^2$ becomes negative precisely when $B = B_\mathrm{crit}$, indicating the presence of a tachyonic mode. A field with strength greater than B_crit can lower its energy by forming a condensate of vector bosons, so the homogeneous vacuum becomes unstable.

In Ref. [**?**], Ambjørn and Olesen find the vacuum of the Lagrangian (**??**) in a field with $B > B_\mathrm{crit}$, which takes the form of a lattice of vortices. However, this treatment neglects the dynamics of the scalar field, which prove to be crucial in understanding the vacuum structure of Georgi-Glashow theory at high magnetic field strengths. In the rest of this chapter, we will show that in fact the Ambjørn-Olesen instability leads to the classical production of 't Hooft–Polyakov monopoles. B_crit therefore indicates the maximum possible field strength in classical Georgi-Glashow theory before monopoles are produced spontaneously from the vacuum.

6.3 Schwinger sphaleron for 't Hooft–Polyakov monopoles

When an external magnetic field is present, the vacuum structure of non-Abelian gauge theories becomes richer, with new solutions to the equations of motion arising that are not present when the field is absent. The first solution that we will examine is what we have termed the Schwinger sphaleron. This is a static, unstable solution to the equations of motion corresponding to the peak of the barrier between the uniform field state and a state containing a monopole-antimonopole pair, of the type described in Section **??**.

The Schwinger sphaleron is most relevant when considering production of monopoles from magnetic fields at high temperatures. In this case, it is possible to thermally excite the fields so that monopoles cross the potential barrier classically; the rate of thermal Schwinger production is

$$\Gamma = D \exp\left(-\frac{E_\mathrm{sph}}{T}\right), \tag{6.13}$$

where E_sph is the sphaleron energy. This rate, including the prefactor D, was calculated in weak fields in the worldline approximation in Refs. [**?**, **?**]. In this section we perform

the equivalent calculation for the exponential factor in Georgi-Glashow SU(2) theory, at all relevant field strengths.

The Schwinger sphaleron connects two physically different states: the state consisting of only a magnetic field, and a state containing a monopole-antimonopole pair. This means that the Schwinger sphaleron is physically different to the Taubes sphaleron [**?**], which is a topological sphaleron mediating a change in Chern-Simons number.

In the limit where the monopole core size is small compared to the other scales in the problem, the Schwinger sphaleron can be found using classical magnetostatics: it consists of a monopole-antimonopole pair separated along the field at precisely the separation where the Coulomb attraction balances the repulsive force from the external field. The total energy of the system as a function of pole separation r is

$$E(r) = 2m - gBr - \frac{g^2}{4\pi r}, \tag{6.14}$$

where m is the monopole mass, g is the monopole charge and B is the strength of the external field. This can be solved straightforwardly to give the equilibrium separation

$$r_{\mathrm{sph}} = \sqrt{\frac{g}{4\pi B}} \tag{6.15}$$

and the sphaleron energy

$$E_{\mathrm{sph}} = 2m - \sqrt{\frac{g^3 B}{\pi}}. \tag{6.16}$$

For 't Hooft–Polyakov monopoles this approximation may be improved upon while still remaining in the pointlike limit. If the monopoles are aligned in isospace, the monopole-antimonopole potential can be modified to take into account short-ranged interactions mediated by the scalar and massive vector bosons [**?**]:

$$V_{\mathrm{m\bar{m}}}(r) = -\frac{1}{4\pi r}\left[1 + 2\mathrm{e}^{-m_{\mathrm{v}}r} + \mathrm{e}^{-m_{\mathrm{s}}r}\left(1 - \mathrm{e}^{-m_{\mathrm{v}}r}\right)\right], \tag{6.17}$$

where m_{s} and m_{v} are the scalar and charged vector boson masses respectively. The sphaleron energy E_{sph} is then the maximum of the function

$$E(r) = 2m - gBr + V_{\mathrm{m\bar{m}}}(r), \tag{6.18}$$

which is straightforward to compute numerically. This solution offers a useful comparison to our results; it is expected to break down when $r_{\mathrm{sph}} \sim r_{\mathrm{M}}$, the monopole core size.

6.3.1 Setup

We work in Georgi-Glashow SU(2) theory, discussed in Section **??**: the continuum Lagrangian (in Minkowski space) is given by Eq. (**??**). As we are focusing on a static solution to the field equations, we are free to work in the three-dimensional theory where all time derivatives, along with the timelike components of the gauge field, vanish. The quantity to be extremised is then the energy

$$E = \int \mathrm{d}^3x \left[\frac{1}{2} \operatorname{Tr} F_{ij} F^{ij} + \operatorname{Tr} D_i \Phi D^i \Phi + \lambda (\operatorname{Tr} \Phi^2 - v^2)^2 \right], \tag{6.19}$$

where $i, j = 1, 2, 3$ index the spatial dimensions. To perform numerical calculations we discretise this to give the lattice energy, which in units defined by the lattice spacing a is

$$\begin{aligned} E_{\mathrm{lat}}(\Phi, U_i) = \sum_x \Bigg\{ & \frac{2}{e^2} \sum_{i<j} \left[2 - \operatorname{Tr} U_{ij}(\vec{x}) \right] \\ & + 2 \sum_i \left[\operatorname{Tr} \Phi(\vec{x})^2 - \operatorname{Tr} \Phi(\vec{x}) U_i(\vec{x}) \Phi(\vec{x} + \hat{\imath}) U_i^\dagger(\vec{x}) \right] \\ & + \lambda \left(\operatorname{Tr} \Phi(\vec{x})^2 - v^2 \right)^2 \Bigg\}, \end{aligned} \tag{6.20}$$

where $U_i(\vec{x})$ are link variables and $U_{ij}(\vec{x})$ denotes the Wilson plaquette (for more details see Sections **??** and **??**). This is the quantity we are extremise in this section.

As we are interested in saddle points of E_{lat} in the presence of a background magnetic field, it is necessary to define the magnetic field in terms of lattice variables. This can be achieved using the lattice projection operator [**?**]

$$\Pi_+ = \frac{1}{2} \left(\mathbf{1} + \frac{\Phi}{|\Phi|} \right). \tag{6.21}$$

This projects out the component of a link variable parallel to the unbroken $U(1)$ generator: the projected link variable is

$$u_i(\vec{x}) = \Pi_+(\vec{x}) U_i(\vec{x}) \Pi_+(\vec{x} + \hat{\imath}). \tag{6.22}$$

This can be used to define an Abelian field strength tensor

$$f_{ij}(\vec{x}) = \frac{2}{e} \arg \operatorname{Tr} u_i(\vec{x}) u_j(\vec{x} + \hat{\imath}) u_i^\dagger(\vec{x} + \hat{\jmath}) u_j^\dagger(\vec{x}). \tag{6.23}$$

The magnetic field is then given by

$$B_i(\vec{x}) = \frac{1}{2a^2} \varepsilon_{ijk} f_{jk}(\vec{x}) \tag{6.24}$$

In the Higgs vacuum, this is an unambiguous definition of the magnetic field. Away from the Higgs vacuum, different definitions are equally valid [**?**], but Eq. (**??**) is useful because it is defined modulo $B_{\max} = 2\pi/ea^2$. This means that the magnetic charge, defined by the magnetic field's divergence, is quantised in units of $4\pi/e$.

We are looking for saddle points of the lattice energy (**??**) with an external magnetic field present. This poses the challenge of how to impose the external field on our solutions. One possibility would be to treat this as a constrained optimisation problem, with the external field as a constraint, adding a Lagrange multiplier to the energy. This would be equivalent to adding a source current term to the Lagrangian, which is undesirable as we are interested in pure vacuum solutions to the equations of motion. Another possibility would be to impose Dirichlet boundary conditions, fixing the values of the links at the boundary such that the field at the edge of the lattice is a pure magnetic field. This is also undesirable, as it will inevitably introduce unphysical finite-size effects, which are likely to require very large lattice sizes to tame.

Boundary conditions, however, do hold the key to solving this problem. The most desirable boundary conditions are those that preserve the symmetries of the action, such as periodic boundary conditions: on a cubic lattice of side length N these may be expressed

$$\begin{aligned} \Phi(\vec{x} + N\hat{\jmath}) &= \Phi(\vec{x}), \\ U_i(\vec{x} + N\hat{\jmath}) &= U_i(\vec{x}). \end{aligned} \tag{6.25}$$

Periodic boundary conditions reduce finite-size effects by ensuring that the solutions found are valid, albeit repeating, solutions on an infinite lattice (though finite-size effects can still be present; see Ref. [**?**] for an example involving monopoles). They also impose the constraint that the magnetic flux through any face of the lattice is an integer multiple of $4\pi/e$. This results in an advantageous effect: when performing gradient descent on the lattice, provided the step size is sufficiently small, the flow is unable to change the flux through the boundary (without creating or annihilating a monopole-antimonopole pair). This means that if initial conditions are chosen with an external flux, this external flux will be present in the solution. It is therefore possible to find extrema of the energy with an external magnetic field present, without requiring unphysical modifications to the Lagrangian or boundary conditions.

The saddle point solutions presented here were obtained by extremising the energy (**??**) on a 64^3 lattice using the Chigusa-Moroi-Shoji gradient descent algorithm [**?**] detailed in Section **??**. A Barzilai-Borwein adaptive step size [**?**] was used to speed convergence, and the LATField2 C++ library [**?**] was utilised to aid parallelisation. An external field of total flux $48\pi/e$ was imposed as described above, giving a uniform magnetic field strength $B \approx$

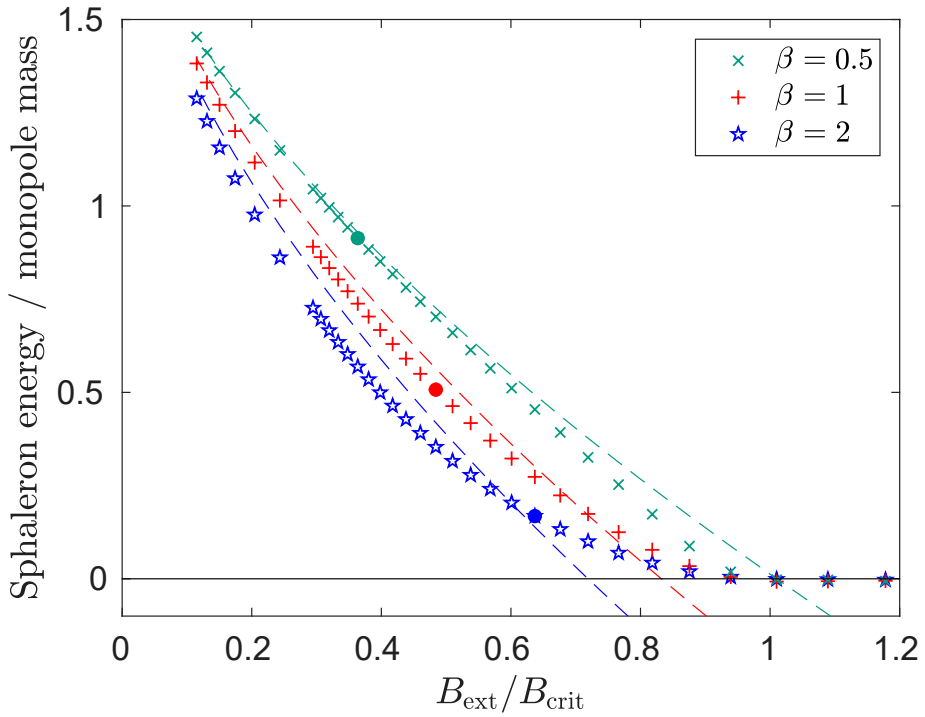

Figure 6.1: Plot of sphaleron energy against field strength for different values of $\beta = m_{\text{s}}/m_{\text{v}}$. The dashed lines indicate the predicted sphaleron energy assuming pointlike monopoles (Eq. (**??**)). The solid circles indicate the field strength at which the sphaleron ceases to contain separated magnetic charges.

$0.037/ea^2$. The field was varied incrementally by changing the scalar field VEV, keeping the mass ratio $\beta = m_{\text{s}}/m_{\text{v}}$ constant. Three different values of β were investigated: $\beta = 0.5$, $\beta = 1$ and $\beta = 2$.

6.3.2 Results

In weak magnetic fields, the sphaleron bears a clear resemblance to the pointlike approximation of a monopole and an antimonopole separated along the direction of the external field. The magnetic charge is nonzero in two cubes lying on a line parallel to the field axis, and the magnitude of the scalar field has two minima, at the same points (due to discretisation effects the scalar field does not vanish). An example of a sphaleron solution with separated magnetic charges is shown in Fig. **??**(a).

Fig. **??** shows the dependence of sphaleron energy on external field strength. As the field strength increases, the energy barrier to monopole production lowers. For fields well below

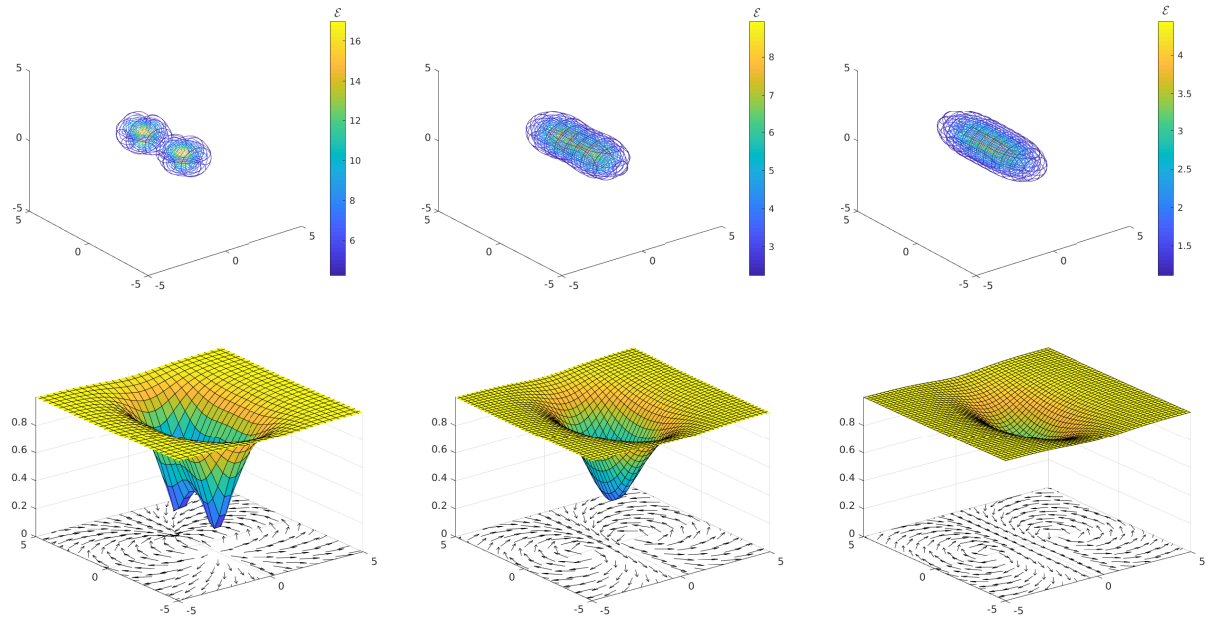

(a) $B/B_{\text{crit}} = 0.29$ (b) $B/B_{\text{crit}} = 0.60$ (c) $B/B_{\text{crit}} = 0.82$

Figure 6.2: Visualisations of sphaleron solutions for (a) subannihilating and (b, c) superannihilating magnetic field strengths. Top plots show energy density contours in units of m_{v}^4 in 3D space. Bottom plots show slices in a plane parallel to the magnetic field intersecting the sphaleron at its centre: the surface gives the scalar field magnitude in units of its VEV, whilst the vector plots give the direction of the magnetic field (with the background subtracted) through the same slice. All plots shown have $m_{\text{v}} = m_{\text{s}}$. Spatial axes have units of m_{v}^{-1}.

the critical field strength, this fits well to the sphaleron energy for pointlike charges (**??**). As the field increases, the calculated sphaleron energy dips below the point particle prediction. This is likely due to the effects of partial cancellation between the overlapping monopole cores (as observed in Ref. [**?**]).

As the field increases further, the distance between the positive and negative magnetic charges decreases, and eventually they cancel each other. We refer to this phenomenon as 'annihilation', though it is not a dynamical process. The higher the value of β, the stronger the field required to annihilate the monopoles (see Fig. **??**). There is no visible discontinuity in energy at annihilation.

Above the annihilation threshold, the scalar field has only one minimum, and the magnetic charge is zero everywhere. The sphaleron still has a nonzero magnetic dipole moment, originating from an axisymmetric ring of electric current density centred about the minimum of the scalar field (see Figs. **??**(b) and **??**(c)). In fields slightly stronger than the annihilation

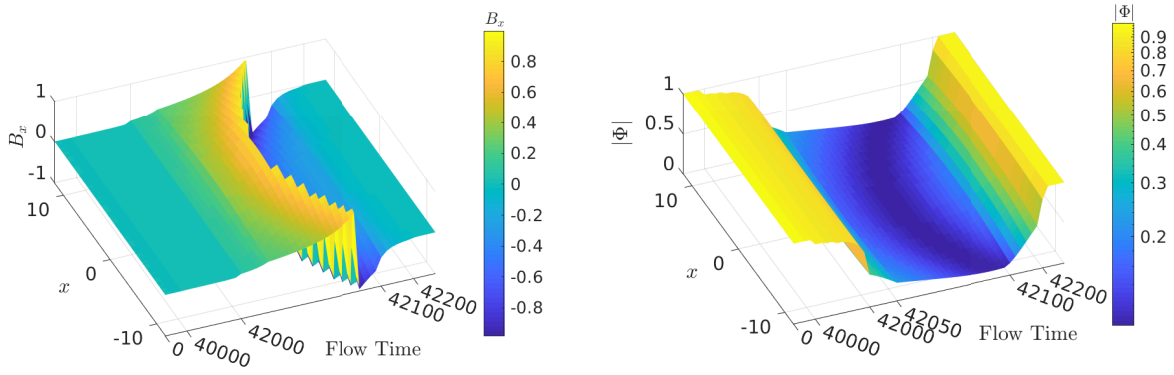

Figure 6.3: Standard gradient flow evolution of the magnetic field component in the direction of the external field B_x (left panel) and the scalar field magnitude $|\Phi|$ (right panel), starting from a supercritical homogeneous magnetic field with a stochastic perturbation and leading to the production of a monopole-antimonopole pair at flow time 42050. Values are taken along a line parallel to the field axis, passing through the cores of the produced monopoles. The magnetic field is given in units of B_{max} the scalar field magnitude in units of its VEV, and spatial distance in units of m_{v}^{-1}. The colours indicate the magnitude of the quantity plotted as shown in the colour bar. Note the uneven scale on the flow time axis. The plot shows the magnetic field strength B_x increasing exponentially due to the instability until it reaches B_{max}, at which time the monopoles (seen as discontinuities in the magnetic field) form. Once formed, the monopoles rapidly move to the boundary where they annihilate, allowing the system to settle in the new equilibrium state with lower magnetic field.

field strength, the energy density contours of the sphaleron continue to define a peanutlike shape with two separate maxima (Fig. **??**(b)). In very high magnetic fields, energy contours are pill shaped (Fig. **??**(c)).

The sphaleron energy decreases monotonically with increasing B until it reaches zero, where it plateaus (see Fig. **??**). At this point the saddle point configuration transitions to the vacuum configuration with only the homogeneous background magnetic field present. From Fig. **??** it can be seen that the field strength where this happens is independent of $\beta = m_{\text{s}}/m_{\text{v}}$, and appears to coincide with the Ambjørn-Olesen critical field [**?**] described in Section **??**: $B = B_{\text{crit}} = m_{\text{v}}^2/e$.

Above B_{crit} there is no energy barrier to the creation of monopole-antimonopole pairs, which suggests that monopole-antimonopole pairs are produced by a classical instability.

We investigated this hypothesis by performing standard gradient flow from a uniform

supercritical background field with small random white noise perturbations in the gauge fields. The results are summarised in Fig. **??**. A clear instability is seen, as predicted in Ref. [**?**], but rather than stabilising to the Ambjørn-Olesen vortex lattice solution presented in Ref. [**?**], the magnetic field continues to become increasingly more localised. The local field strength at the centre of the vortex grows exponentially until it reaches $B_{\max}$, which is the maximum value allowed on the lattice. At this time (≈ 42050 flow time units in Fig. **??**), a monopole-antimonopole pair is produced. This may be interpreted as the breaking of the vortex.

At the time of the pair production, both the magnetic field and the energy density are highly localised in a vortex line aligned with the external field. Inside the vortex line, the scalar field vanishes (see Fig. **??**), which restores the SU(2) symmetry locally, and therefore the energy density remains finite $\sim V(0) = \lambda v^4$, in spite of the local magnetic field reaching nominally cutoff scale values. When the local magnetic field crosses $B_{\max}$ it flips sign, and the vortex line breaks, forming monopoles, which quickly move to the edges of the lattice and annihilate, lowering the magnetic flux by $4\pi/e$.

6.4 Schwinger instanton for 't Hooft–Polyakov monopoles

In the previous section, we computed the Schwinger sphaleron, a static solution to the equation of motion that mediates high-temperature Schwinger production of monopoles from magnetic fields,[1] when the fields are thermally excited and pass classically over the sphaleron barrier. At zero temperature, Schwinger production is a purely quantum process, mediated by a four-dimensional instanton solution to the field equations. This solution was first analysed in the worldline limit in Refs. [**?**, **?**]—this calculation was reviewed in Section **??**. In this section we extend this calculation beyond the worldline limit, computing the full field-theoretic saddle point solution in Georgi-Glashow SU(2) theory.

We will consider pair production in a constant external magnetic field of strength B. Without loss of generality we choose the x_3 direction as the field axis; the U(1) field strength tensor is

$$f^{\text{ext}}_{\mu\nu} = (\delta_{\mu 1}\delta_{\nu 2} - \delta_{\mu 2}\delta_{\nu 1})B. \tag{6.26}$$

[1] At such high temperatures, one can employ a Euclidean-time formalism where the extent of the compact time direction is so small that the problem reduces to three-dimensional case investigated in the previous section.

As we have previously seen, the worldline instanton in this field is a circle in the x_3-x_4 plane (where x_4 denotes the Euclidean time direction) of radius

$$r_{\text{inst}} = \frac{m}{gB}, \tag{6.27}$$

where m is the monopole mass and g is its charge. The corresponding action is

$$S_{\text{inst}} = \frac{\pi m^2}{gB} - \frac{g^2}{4}; \tag{6.28}$$

this provides a useful comparison for our results.

6.4.1 Setup

The instanton is a four-dimensional object, extremising the Euclidean Georgi-Glashow action

$$S = \int \mathrm{d}^4x \left[\frac{1}{2}\operatorname{Tr} F_{\mu\nu}F^{\mu\nu} + \operatorname{Tr} D_\mu\Phi D^\mu\Phi + \lambda(\operatorname{Tr}\Phi^2 - v^2)^2\right], \tag{6.29}$$

where $\mu, \nu = 1, 2, 3, 4$. One way to compute the instanton would be to numerically search for saddle points of the discretised form of this action. However, optimisation on a four-dimensional lattice with a reasonable resolution would require a large amount of computational resources. Instead, we can exploit some of the symmetries of the solution to reduce the dimensionality of the problem.

It is clear that this is invariant under rotations in the x_3-x_4 plane (Euclidean boosts). As a consequence, if instanton solutions exist at all, there must be an instanton solution to the field equations that obeys this symmetry. In weak fields this is the circular worldline instanton identified in Ref. [**?**] and described in Section **??**. We proceed by exploiting this symmetry, changing to "cylindrical" coordinates

$$\begin{aligned} x &= x_1, \\ y &= x_2, \\ \rho &= \sqrt{x_3^2 + x_4^2}, \\ \chi &= \arctan(x_4/x_3). \end{aligned} \tag{6.30}$$

As noted in Ref. [**?**], the symmetry of the system means that one may choose a gauge such that all fields are independent of χ, and the gauge field component A_χ vanishes. Such a field configuration has the action

$$S = 2\pi \int \rho\,\mathrm{d}x\,\mathrm{d}y\,\mathrm{d}\rho \left[\frac{1}{2}\operatorname{Tr} F_{ij}F^{ij} + \operatorname{Tr} D_i\Phi D^i\Phi + \lambda(\operatorname{Tr}\Phi^2 - v^2)^2\right], \tag{6.31}$$

where i, j represent x, y, ρ. This action is similar to the three-dimensional energy density used in Section **??** to study static field configurations, differing only in the Jacobian. We are therefore able to use similar methods to compute the desired instanton solutions, working on a three-dimensional lattice with three gauge field components.[2]

In order to solve the equations of motion that arise from varying (**??**), we must discretise the action. The symmetry of the problem means that we only need to consider a three-dimensional grid of points $\vec{x} = (n_x, n_y, n_\rho)a$, where (n_x, n_y, n_ρ) are integers and a is a fixed lattice spacing. Because the coordinate curves of x, y, and ρ form a Cartesian lattice, the nontrivialities that usually occur when performing a lattice discretisation in curvilinear coordinates are circumvented.

The discretised form of Eq. (**??**) is the lattice action

$$\begin{aligned} S_{\text{lat}} = 2\pi \sum_{\vec{x}} \Bigg\{ & \sum_{i<j} \rho_{ij}^{\square}(\vec{x}) \left[2 - \operatorname{Tr} U_{ij}(\vec{x})\right] \\ & + 2 \sum_{i} \bar{\rho}_i(\vec{x}) \operatorname{Tr} \left[U_i(\vec{x}) \Phi(\vec{x} + \hat{\imath}) U_i^\dagger(\vec{x}) - \Phi(\vec{x})\right]^2 \\ & + \rho(\vec{x}) \lambda (\operatorname{Tr} \Phi(\vec{x})^2 - v^2)^2 \Bigg\}. \end{aligned} \tag{6.32}$$

In this expression and in the rest of this section we use units such that $a = 1$. We also define appropriately averaged Jacobian factors:

$$\begin{aligned} \rho_{ij}^{\square}(\vec{x}) &= \frac{1}{4} \left[\rho(\vec{x}) + \rho(\vec{x} + \hat{\imath}) + \rho(\vec{x} + \hat{\imath} + \hat{\jmath}) + \rho(\vec{x} + \hat{\jmath})\right], \\ \bar{\rho}_i(\vec{x}) &= \frac{1}{2} \left[\rho(\vec{x}) + \rho(\vec{x} + \hat{\imath})\right]. \end{aligned} \tag{6.33}$$

In order to perform calculations it is necessary to impose boundary conditions at $\rho = 0$ and $\rho \to \infty$. This is complicated slightly by the fact that the $U_\rho(\vec{x})$ links are located between lattice points: in our notation the link $U_\rho(n_x, n_y, n_\rho)$ is located at $(n_x, n_y, n_\rho + \frac{1}{2})$. We choose a discretisation such that n_ρ takes half-integer values in $[-\frac{1}{2}, R - \frac{1}{2}]$, where $R \in \mathbb{Z}$ is the number of lattice points in the ρ direction. We then impose boundary conditions at the origin that are compatible with the instanton solution:

$$\begin{aligned} \Phi(x, y, -\tfrac{1}{2}) &= \Phi(x, y, \tfrac{1}{2}), \\ U_{x,y}(x, y, -\tfrac{1}{2}) &= U_{x,y}(x, y, \tfrac{1}{2}), \\ U_\rho(x, y, -\tfrac{1}{2}) &= \mathbb{I}_2; \end{aligned} \tag{6.34}$$

[2]Note that the field also has a symmetry in the x_1-x_2 plane, which we do not take advantage of here. This is because of complications when performing a lattice discretisation in the resulting bicylindrical coordinates.

In the continuum limit this is equivalent to imposing symmetry about the origin on Φ and $A_{x,y}$, and imposing antisymmetry about the origin on A_ρ.

At $n_\rho = R$ the choice of boundary conditions is not important, as our solutions are in the vacuum at this point. For computational simplicity we impose reflecting boundary conditions

$$\begin{aligned}\Phi(x, y, R + \tfrac{1}{2}) &= \Phi(x, y, R - \tfrac{1}{2}),\\ U_{x,y,\rho}(x, y, R + \tfrac{1}{2}) &= U_{x,y,\rho}(x, y, R - \tfrac{1}{2}).\end{aligned} \tag{6.35}$$

In the x and y directions we impose periodic boundary conditions: for n_x and n_y taking integer values in $[0, L]$, where L is the lattice size,

$$\begin{aligned}\Phi(L + 1, y, \rho) &= \Phi(0, y, \rho),\\ U_{x,y,\rho}(L + 1, y, \rho) &= U_{x,y,\rho}(0, y, \rho),\\ \Phi(x, L + 1, \rho) &= \Phi(x, 0, \rho),\\ U_{x,y,\rho}(x, L + 1, \rho) &= U_{x,y,\rho}(x, 0, \rho).\end{aligned} \tag{6.36}$$

As in the three-dimensional case, one can define an Abelian field strength tensor f_{ij} using lattice projection operators (**??**). In our cylindrical coordinates, speaking of the magnetic field (B_1, B_2, B_3) can cause confusion; we will work directly with the field strength tensor to avoid this. The periodic boundary conditions in the x and y directions quantise the magnetic flux $\sum_x \sum_y f_{xy}(x, y, \rho)$, meaning that the same trick described in Section **??** can be used to include the external magnetic field.

The results in this section were obtained using the gradient squared descent (GSD) algorithm described in Section **??**. The gradient squared function minimised to yield the instanton solutions was

$$\mathcal{G}^2[\Phi, U_i] = \sum_{\vec{x}} \left\{ \mathrm{Tr}\left(\frac{1}{\rho(\vec{x})} \frac{\partial S_{\mathrm{lat}}}{\partial \Phi(\vec{x})} \right)^2 + \sum_j \mathrm{Tr}\left(\frac{i}{\rho(\vec{x})} P_{U_j}\left[\frac{\partial S_{\mathrm{lat}}}{\partial U_j(\vec{x})} \right] \right)^2 \right\}, \tag{6.37}$$

where the SU(2) tangent space projection operator P_{U_i} is defined in Section **??**. This was minimised numerically using a gradient descent algorithm with momentum [**?**]. To further speed convergence in regions where the gradients are shallow, the gradients of the scalar field and link variables were normalised at each step; the gradient descent update was (omitting the momentum term for brevity)

$$\begin{aligned}\Phi(\vec{x}, \tau + \Delta\tau) &= \Phi(\vec{x}, \tau) - \frac{\Delta\tau}{\sqrt{\sum_{\vec{x}'} [\frac{1}{\rho(\vec{x}')} \partial_\Phi \mathcal{G}^2)]^2 + \epsilon}} \frac{1}{\rho(\vec{x})} \partial_\Phi(\mathcal{G}^2),\\ U_i(\vec{x}, \tau + \Delta\tau) &= U_i(\vec{x}, \tau) - \frac{\Delta\tau}{\sqrt{\sum_{\vec{x}', j} [\frac{i}{\rho(\vec{x}')} \partial_{U_j}(\mathcal{G}^2)]^2 + \epsilon}} \frac{1}{\rho(\vec{x})} \partial_{U_i}(\mathcal{G}^2),\end{aligned} \tag{6.38}$$

where ϵ is a small, positive parameter to avoid divide-by-zero errors and

$$\begin{aligned} \partial_\Phi(\mathcal{G}^2) &= \frac{\partial(\mathcal{G}^2)}{\partial\Phi(\vec{x})}, \\ \partial_{U_i}(\mathcal{G}^2) &= P_{U_i}\left[\frac{\partial(\mathcal{G}^2)}{\partial U_i(\vec{x})}\right]. \end{aligned} \tag{6.39}$$

The first instanton configurations, in weak fields, were generated using single monopole configurations as initial conditions. Subsequent instanton solutions in stronger fields were generated incrementally by varying the VEV and lattice spacing in the theory.

The full code used to find the instanton solutions is publicly available as part of the `tfmonopoles` Python package [**?**]. This uses automatic differentiation and other optimisation tools in the TensorFlow package [**?**] to perform the gradient descent, leveraging tools originally designed for machine learning.

6.4.2 Results

We computed the instanton solution relevant to Schwinger production at magnetic field strengths up to the critical value, for three values of the boson mass ratio: $\beta = 0.5$, $\beta = 1$, and $\beta = 2$. Our calculations were performed on a 64^3 lattice, and an external magnetic flux was fixed by the periodic boundary conditions in the x and y direction as described in Section **??**. The field strength in units of m_v^2 was varied by incrementally changing the scalar field VEV, while keeping β constant.

In weak fields, the instanton solutions strongly resemble the pointlike approximation; the solution is a circular ring of magnetic charge with localised energy density. An example can be seen in Fig. **??**(a) and Fig. **??**(a); the energy contours trace a "doughnut" shape. The scalar field drops to a minimum on a ring of roughly the worldline instanton radius (**??**) (in the continuum the scalar field magnitude would vanish), and returns to near the vacuum in the centre of the instanton.

As the field strength increases, the overall extent of the instanton initially stays close to the worldline instanton radius (**??**), but the instanton becomes less localised: the hole of the doughnut begins to fill in (see Figs. **??**(b) and **??**(b)). At high external field strengths, the instanton size is significantly larger than the worldline radius (see Figs. **??**(c) and **??**(c)). The minima of the scalar field move closer to the centre of the instanton, until eventually there is a single minimum instead of a ring. At this point, the instanton contains no separated magnetic charges.

As the external field approaches the critical value B_crit, the scalar field magnitude continuously approaches the VEV and the instanton action continuously approaches zero. At the

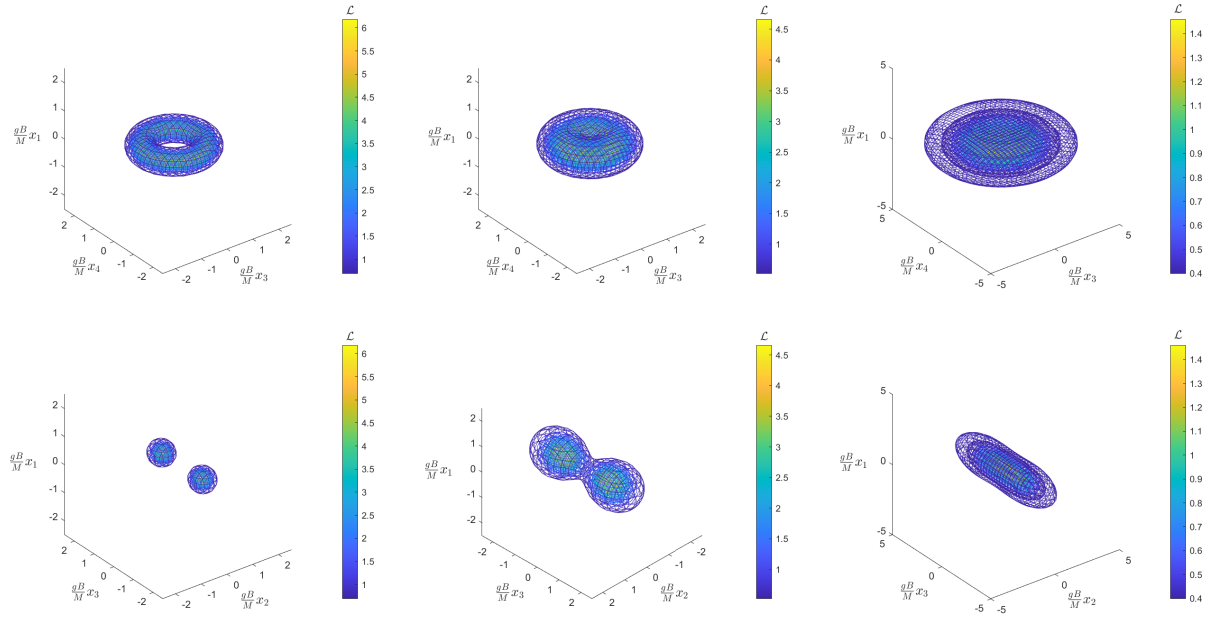

(a) $B/B_{\text{crit}} = 0.3$ (b) $B/B_{\text{crit}} = 0.6$ (c) $B/B_{\text{crit}} = 0.9$

Figure 6.4: Lagrangian density contours for instanton solutions for $\beta = 1$ ($m_{\text{s}} = m_{\text{v}}$), with the background field subtracted, at different external field strengths. In the upper plots, the x_2 dimension is suppressed; in the lower plots, the x_4 dimension is suppressed. Note the difference in scale between the (a), (b) plots and the (c) plots.. Lagrangian density values in units of m_{v}^{-4} are shown in the colourbars.

critical field and above, the saddle point solution and the vacuum coincide for all investigated values of β.

To compare the instanton actions it is useful to rewrite the worldline instanton action (**??**) in terms of dimensionless parameters: defining

$$\kappa = \frac{g^3 B}{4\pi m^2}, \tag{6.40}$$

the action in the worldline approximation is

$$S_{\text{inst}} = \frac{g^2}{4}\left(\frac{1}{\kappa} - 1\right). \tag{6.41}$$

The instanton action as a function of κ is plotted in Fig. **??**. For all values of β investigated, the instanton action agrees well with the worldline prediction when κ is small, and plateaus at $S_{\text{inst}} = 0$ when $B = B_{\text{crit}}$. Note that for different values of β, $B = B_{\text{crit}}$ corresponds to a different value of κ:

$$\kappa(B_{\text{crit}}) = \frac{1}{f(\beta)^2}, \tag{6.42}$$

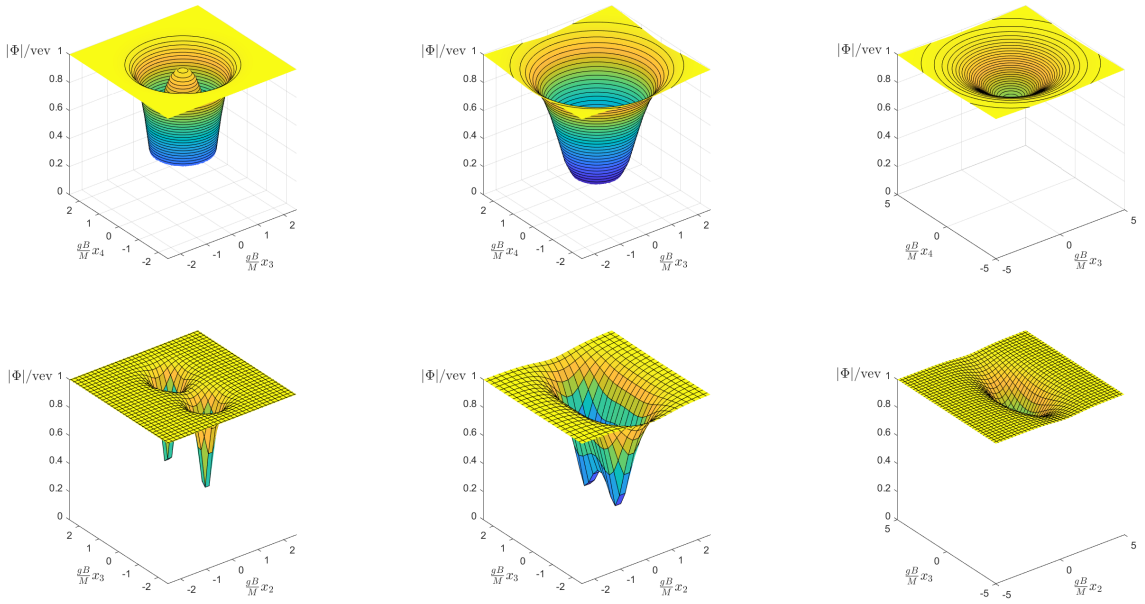

(a) $B/B_{\text{crit}} = 0.3$ (b) $B/B_{\text{crit}} = 0.6$ (c) $B/B_{\text{crit}} = 0.9$

Figure 6.5: Surface plots of scalar field magnitude on slices through the instanton centre for different external field strengths, with $\beta = 1$ ($m_{\text{s}} = m_{\text{v}}$). Upper plots show the x_3-x_4 plane, while lower plots show the x_2-x_3 plane. Note the difference in scale between the (a), (b) plots and the (c) plots.

where $f(\beta)$ is the monopole mass function given in Eq. (**??**). Using the results of the high-precision calculations in Ref. [**?**], this gives $\kappa(B_{\text{crit}}) \approx 0.313$ in the limit $\beta \to \infty$. In the $\beta \to 0$ limit, $\kappa(B_{\text{crit}}) = 1$. Though computing the instanton in these limits is beyond the reach of our current methods, there may be simplifications that render the calculation more tractable in future work, particularly in the BPS limit $\beta \to 0$, where the 't Hooft–Polyakov monopole solution can be found analytically.

It is interesting to note that the calculated action deviates from the worldline prediction at $\kappa \approx 0.3$ for all three values of β, but the curves for different values of β remain consistent until $\kappa \approx 0.5$. This could be because the worldline prediction only accounts for the Coulomb interaction, while 't Hooft–Polyakov monopoles also participate in short-ranged interactions mediated by the scalar and massive vector bosons. Accounting for these forces could result in a worldline prediction that is accurate at higher values of κ (the instanton equivalent of Eq. (**??**)), though such a calculation is nontrivial due to nonlocal worldline self-interactions.

Another important property shown in Fig. **??** is the fact that the instanton action for 't Hooft–Polyakov monopoles is lower than that for point particles for all values of β. This suggests that the effects of finite monopole size solely enhance monopole pair production rate when compared to the pointlike approximation. This observation may be surprising, considering the fact that in elementary particle collisions, solitonic monopole production is generally expected to be heavily suppressed compared to Dirac monopole production [**?**, **?**]. However, it is important to remember that the external magnetic field selects a preferred direction in field configuration space, increasing the likelihood of processes that separate magnetic charges. This means that entropic arguments, assuming a uniform distribution of final microstates, do not apply to Schwinger production.

The instanton action against $1 - B/B_{\text{crit}}$ is plotted on a logarithmic scale in Fig. **??**. For all three values of β, there appears to be power-law scaling as the external field approaches its critical value. From the plot, the exponents appear to be similar for all three values of β, though a numerical fit shows a slight decrease in exponent with increasing β. The fitted exponents are given in Table **??**.

6.5 Summary

In this chapter, we have explicitly computed two novel solutions to the equations of motion of Georgi-Glashow SU(2) theory: the Schwinger sphaleron and the Schwinger instanton. These are physically relevant as mediators of the production of solitonic monopoles from

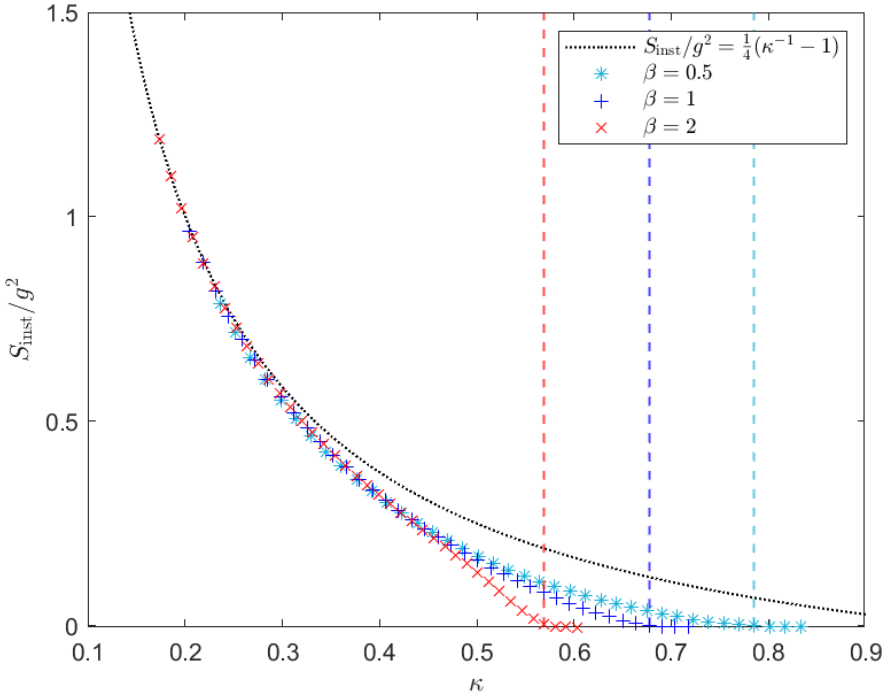

Figure 6.6: Scaled instanton action plotted against the dimensionless parameter $\kappa = g^3 B/(4\pi M^2)$ for different values of β. The dotted black curve gives the worldline approximation, and vertical dashed lines indicate the values of κ at which $B = B_{\text{crit}}$.

β	Exponent
0.5	1.47(3)
1	1.32(4)
2	1.14(6)

Table 6.1: Exponents n computed from a numerical fit of the form $S_{\text{inst}} = A(1 - B/B_{\text{crit}})^n$ to the power-law regions of the curves in Fig. **??**. Errors are calculated using the covariance matrix of the least squares linear regression.

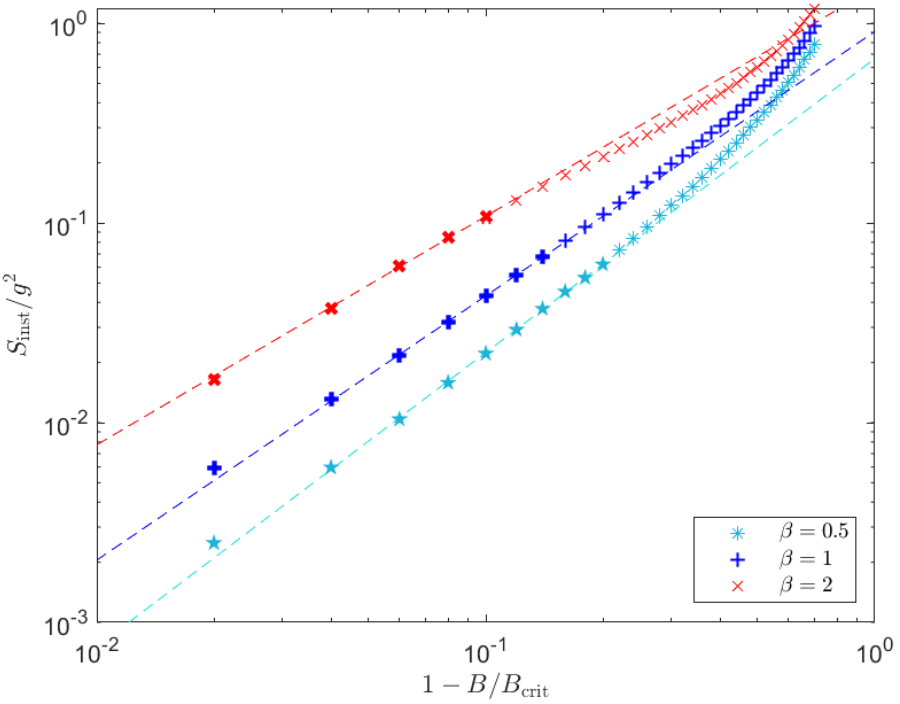

Figure 6.7: Logarithmic scale plot of scaled instanton action as the external field approaches B_{crit}. Dashed lines show fits to the power-law regions with exponents given in Table **??**. The points used to generate the fits are indicated with filled or thick markers.

constant magnetic fields. The Schwinger sphaleron energy can be used to estimate the rate of thermal Schwinger production of 't Hooft–Polyakov monopoles at high temperatures: $\Gamma \propto \exp(-E_{\text{sph}}/T)$. The Schwinger instanton determines the Schwinger pair production rate of these monopoles at zero temperature: $\Gamma \propto \exp(-S_{\text{inst}})$.

In both cases, we find that the barrier to pair production vanishes precisely at the Ambjørn-Olesen critical field strength

$$B_{\text{crit}} = \frac{m_{\text{v}}^2}{e}. \tag{6.43}$$

When the external field $B = B_{\text{crit}}$, the sphaleron and instanton both coincide with the vacuum, indicating that instead of decaying to a lattice of vortices as predicted in Ref. [**?**], the Ambjørn-Olesen instability leads to classical production of 't Hooft–Polyakov monopoles. This effect appears to be independent of the scalar boson mass; the critical field strength depends only on m_{v}, the mass of the charged vector boson.

It is interesting to note that the critical field strength we have found for classical monopole pair production agrees almost exactly with the field strength (**??**) at which quantum Schwinger pair production of pointlike monopoles becomes unsuppressed [**?**, **?**],

$$B_{\text{Schwinger}} = \frac{4\pi m^2}{g^3} = f(\beta)^2 B_{\text{crit}}, \tag{6.44}$$

where we have used Equation (**??**) for the monopole mass. Though this may seem like an unlikely coincidence, it is not entirely unexpected because this is the natural field strength given by dimensional analysis. This suggests that the Schwinger process turns continuously into the classical instability when the field exceeds the critical value.

As will be seen in Section **??**, in the case of electroweak theory—which does not admit finite-mass solitonic monopoles—the Ambjørn-Olesen vortex lattice is a stable solution to the equations of motion [**?**, **?**]. In future work it may be interesting to consider modifications to electroweak theory that do admit solitonic monopole solutions [**?**, **?**, **?**, **?**], to see if classical monopole production could occur in such a theory. If a similar phenomenon occurs at experimentally obtainable magnetic fields, future heavy ion collision data could be used to further constrain these models.

It is also worth considering if the classical production of monopoles could ever be observed in a laboratory. Electroweak theory does not permit solitonic monopoles, so the relevant mass m_{v} is not the electroweak W boson mass, but the mass of the charged gauge bosons associated with the 't Hooft–Polyakov monopole. Experimental searches for heavy charged bosons give a lower-bound mass of 5200 GeV [**?**], which implies a lower bound on the magnetic field

strength required to produce monopoles of 9×10^7 GeV$^2 \approx 4.5 \times 10^{23}$ T. As the fields in current LHC heavy ion collisions are of order 1 GeV^2 [**?**], classical monopole production is impossible to achieve with current technology. However, sufficiently strong magnetic fields may have been present in the early Universe [**?**]. Furthermore, even if such field strengths could be reached in experiments, one would expect monopoles to be produced by Schwinger pair creation at lower field strengths.

A key feature of the results of this chapter is that for fields where quantum Schwinger production is expected to occur, the sphaleron energy/instanton action is smaller than that predicted by the worldline approximation for all considered values of the boson mass ratio (see Figs. **??** and **??**). This means that monopole internal structure and strong coupling effects, which are considered fully by our lattice calculations, result in enhanced monopole production compared to worldline predictions. This suggests that cross sections computed from worldline approximations can be treated as lower bounds when applied to experimental monopole searches, and helps to justify our recommendations in Section **??**.

The next step, planned for future work, is to extend these calculations to electromagnetic fields with spacetime dependence, with the eventual aim of computing the Schwinger production rate of solitonic monopoles in the fields present in heavy ion collisions. This is a challenging task due to the decreased symmetry when compared to the homogeneous fields investigated in this chapter, but once the calculation is complete it will provide the first theoretically sound analysis of monopole pair production from particle collisions.

Chapter 7

Magnetic fields and electroweak baryogenesis

7.1 Lowering the sphaleron energy with an external magnetic field

The numerical techniques used and developed in earlier parts of this thesis are applicable to a wide range of physical phenomena beyond magnetic monopole production. One example of such a phenomenon is sphaleron-induced Electroweak baryogenesis [**?**, **?**]. The Electroweak sphaleron is a static, unstable solution to the field equations of Electroweak theory that mediates the violation of baryon number[1] B and lepton number L in the Standard Model—the energy of this configuration $E_{\rm sph}$ represents the barrier to $B + L$ violation. At finite temperature, the rate of these processes is suppressed by $\exp(E_{\rm sph}/T)$. The theoretical details of the Electroweak sphaleron are outlined in Section **??** and the references therein.

In this chapter, we focus on a numerical computation of the sphaleron solution in the presence of an external magnetic field. The motivation for this is the observation that—when the weak mixing angle $\theta_{\rm W}$ is nonzero—the sphaleron has a significant magnetic dipole moment [**?**, **?**, **?**, **?**]. According to Ref. [**?**] the main contribution to this dipole moment can be interpreted as coming from a small segment of Z string [**?**, **?**], which terminates on a Nambu monopole-antimonopole pair. The topological nature of the sphaleron may be interpreted as a relative "twist" between the monopole and antimonopole [**?**, **?**]. There is also

[1] Due to notational convention the same symbol is used for baryon number and magnetic field strength. As the contexts of the two uses are very different, this thesis does not explicitly distinguish between them unless there is a possibility of ambiguity.

a small contribution to the sphaleron dipole moment from a loop of electromagnetic current density [**?**].

The fact that the electroweak sphaleron has a nonzero dipole moment for the physical value of the weak mixing angle indicates that its energy may be lowered by the presence of a suitably aligned external magnetic field. This would increase the probability of a $B + L$ violating transition. For weak external fields, one can assume that this effect is linear: the change in energy is given by

$$\Delta E_{\rm sph} = -\vec{B}_{\rm ext} \cdot \vec{\mu}_{\rm sph}, \tag{7.1}$$

where $\vec{B}_{\rm ext}$ denotes the external magnetic field and $\vec{\mu}_{\rm sph}$ denotes the sphaleron dipole moment. However, for stronger magnetic fields nonlinear effects become important; these cannot be calculated analytically. A numerical study of the sphaleron in an external magnetic field was carried out by Comelli *et al.* in the weak-field limit [**?**]. However, this analysis only considered solutions where the fields did not have any angular dependence, so could not be extended far into the nonlinear regime. In this work we have carried out a numerical analysis over the full range of physically interesting external magnetic fields.

7.2 Ambjørn-Olesen condensation in Electroweak theory

In Section **??** we introduced the phenomenon of Ambjørn-Olesen condensation in Georgi-Glashow SU(2) theory. This is a classical instability of a homogeneous magnetic field in a theory containing charged vector bosons: at a field strength set by the vector boson mass scale, the constant field becomes unstable. In the previous chapter, we showed that in Georgi-Glashow SU(2) theory this instability leads to the classical production of 't Hooft–Polyakov monopoles.

In Electroweak theory, this instability occurs at the critical field strength [**?**]

$$B^{(1)}_{\rm crit} = \frac{m_{\rm W}^2}{e} \approx 2.1 \times 10^4 \ {\rm GeV}^2 \approx 1.1 \times 10^{20} \ {\rm T}, \tag{7.2}$$

where $m_{\rm W} \approx 80.4$ GeV is the W boson mass and e is the electric charge, both defined in Section **??**. As there is no possibility of a supercritical field decreasing in magnitude via creation of magnetic charges, the instability instead leads to a new stable solution, which consists of a periodic lattice of vortices [**?**, **?**] modulating both the gauge fields and the Higgs field. As the field strength increases further above $B^{(1)}_{\rm crit}$, the deviation from the homogeneous

vacuum increases in magnitude, and the mean magnitude of the Higgs field decreases. This continues until the external field strength reaches a second critical value

$$B_{\text{crit}}^{(2)} = \frac{m_{\text{H}}^2}{e} \approx 5.2 \times 10^4 \text{ GeV}^2 \approx 2.7 \times 10^{20} \text{ T}, \tag{7.3}$$

where $m_{\text{H}} \approx 125$ GeV is the Higgs mass. For field strengths above $B_{\text{crit}}^{(2)}$, it is energetically favourable for the Higgs field to be in the symmetric phase $|\phi| = 0$, and the magnetic field is pure hypercharge. This symmetry restoration has important consequences for the Electroweak sphaleron.

In the symmetric phase of the Higgs field the sphaleron field configuration is pure gauge, so it is expected that the energy of the sphaleron will be zero at this point. In Ref [**?**] it was shown that in this phase there is the potential for unsuppressed $B + L$ violation, meaning that strong magnetic fields could provide the first observations of this elusive phenomenon. However, the nature of the sphaleron in $B_{\text{crit}}^{(1)}$ and $B_{\text{crit}}^{(2)}$ has not previously been studied.

It is not immediately obvious that the sphaleron energy remains nonzero all the way up to $B_{\text{crit}}^{(2)}$. For example, if the Ambjørn-Olesen vortices can carry baryon number, there may be the potential for the instability at $B_{\text{crit}}^{(1)}$ to result in baryon number violation, in a similar fashion to the instability studied in Chapter **??** resulting in monopole production.

Another possibility for vanishing sphaleron energy below $B_{\text{crit}}^{(2)}$ is a regime where Z strings are (dynamically) stable. This was analysed in Ref. [**?**] for the unphysical case where $m_{\text{H}} < m_{\text{Z}}$. It was found that an infinite Z string is perturbatively stable above some field strength smaller than $B_{\text{crit}}^{(1)}$. As it has been shown that Z strings can carry baryon number [**?**] (though presumably not without an energy cost), an analogous phenomenon in a system with physical parameters could also provide a $B + L$ violation mechanism.

7.3 The Electroweak sphaleron in a strong magnetic field

7.3.1 Setup

For an overview of the electroweak sphaleron in the continuum, see Section **??** and the references therein. Here, we discuss the sphaleron on the lattice. As the sphaleron is a static solution, we can restrict the problem to three spatial dimensions, and set the timelike components of the gauge fields to zero. In order to perform numerical calculations we discretise the electroweak Lagrangian given in Section **??** (Eq. (**??**)), defining a 3D lattice of points

$\vec{x} = (n_x, n_y, n_z)a$ where n_x, n_y, n_z are integers and a is the lattice spacing. The Higgs field $\phi(\vec{x})$, which is a complex doublet, is defined on lattice points, whilst the gauge fields are defined by link variables $U_i^{\mathrm{W}}(\vec{x}) \in \mathrm{SU}(2)$ and $U_i^{\mathrm{Y}}(\vec{x}) \in \mathrm{U}(1)$. The discretised energy density (in units defined by a) is then

$$\begin{aligned}\mathcal{E}_{\mathrm{lat}} = &\frac{2}{g_{\mathrm{EW}}^2}\sum_{i<j}\left[2 - \mathrm{Tr}\, U_{ij}^{\mathrm{W}}(\vec{x})\right] + \frac{2}{g_{\mathrm{EW}}^2 \tan^2\theta_{\mathrm{W}}}\sum_{i<j}\left[1 - \mathrm{Re}\, U_{ij}^{\mathrm{Y}}(\vec{x})\right] \\ &+ 2\sum_i \left\{\phi^\dagger(\vec{x})\phi(\vec{x}) - \mathrm{Re}\left[\phi^\dagger(\vec{x})U_i^{\mathrm{Y}}(\vec{x})U_i^{\mathrm{W}}(\vec{x})\phi(\vec{x}+\hat{\imath})\right]\right\} \\ &+ V(\phi).\end{aligned} \tag{7.4}$$

Here U_{ij}^{W} and U_{ij}^{Y} respectively denote the SU(2) and U(1) Wilson plaquettes. The sum of this over all lattice sites $E_{\mathrm{lat}} = \sum_{\vec{x}} \mathcal{E}_{\mathrm{lat}}$ is the quantity we extremise.

In practice, we work in the unitary gauge, $\phi(\vec{x}) = (0\ h(\vec{x}))^T$, $h(\vec{x}) \in \mathbb{R}$.[2] Near the vacuum state the residual electromagnetic field then corresponds to the complex phase of the top left element $u_i(\vec{x}) \equiv [U_i(\vec{x})]_{11}$ of the combined link variable $U_i(\vec{x}) = U_i^{\mathrm{Y}}(\vec{x})U_i^{\mathrm{W}}(\vec{x})$. This agrees with the standard definition of the photon (**??**) in the continuum limit $a \to 0$. The electromagnetic field strength tensor is then given by the plaquette variable

$$f_{ij}(\vec{x}) = \frac{1}{e}\arg u_i(\vec{x})u_j(\vec{x}+\hat{\imath})u_i^*(\vec{x}+\hat{\jmath})u_j^*(\vec{x}), \tag{7.5}$$

and the magnetic field strength in the standard way as $B_i = \varepsilon_{ijk}f_{jk}/2a^2$.

A useful test of the lattice discretisation is computation of the ground state energy density in the Ambjørn-Olesen phase. This was carried out using gradient flow on a 64×64 grid (the solution is translation invariant along the axis parallel to the external field). An external magnetic field was enforced by exploiting periodic boundary conditions (see Chapter **??**) and varied incrementally by changing the Higgs VEV. The results are shown for Standard Model parameters in Fig. **??**, where the normalised, spatially-averaged ground state energy density is plotted against magnetic field strength. In line with the results of Refs. [**?**, **?**, **?**], the energy density interpolates between that of a homogeneous magnetic field in the broken Higgs phase for $B/B_{\mathrm{crit}}^{(1)} < 1$, and a pure hypercharge field in the symmetric Higgs phase for $B/B_{\mathrm{crit}}^{(1)} > m_{\mathrm{H}}^2/m_{\mathrm{W}}^2 \approx 2.42$.

7.3.2 Results

To generate the sphaleron solutions on the lattice, we used the Chigusa-Moroi-Shoji (CMS) gradient descent algorithm described in Section **??**. A similar method was also used in Ref. [**?**]

[2]Note that there are no issues with singularities on the lattice, as the points where the Higgs magnitude vanishes, and the positions of strings, are located between lattice sites.

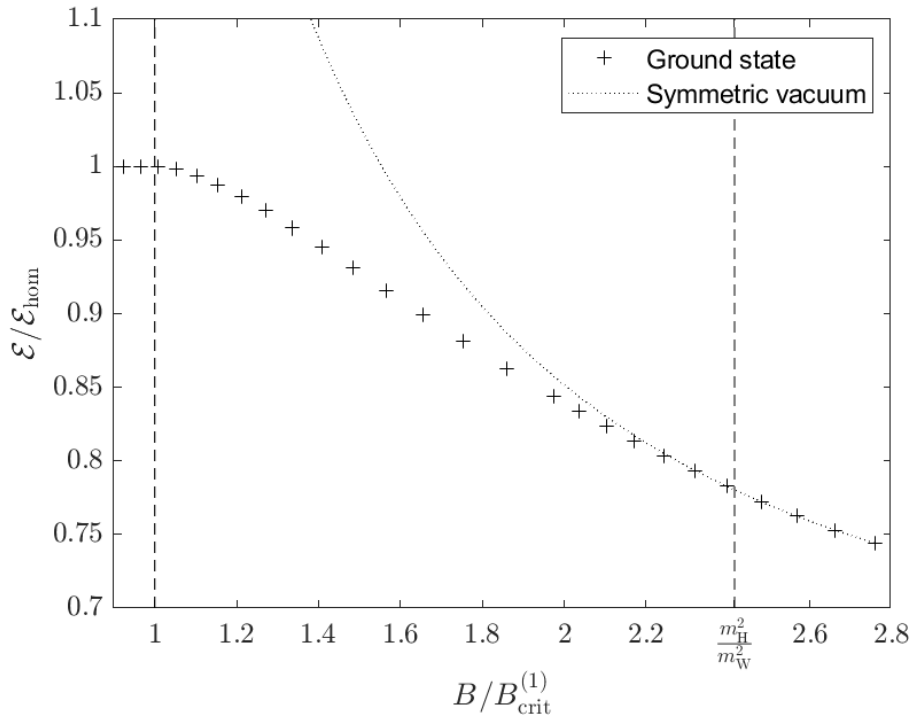

Figure 7.1: Plot of spatially-averaged ground state energy density (divided by that of a homogeneous magnetic field $\mathcal{E}_{\rm hom}$) against external field strength in units of the lower critical field, for Standard Model parameters. The dotted curve shows energy density of a pure hypercharge field in the symmetric Higgs phase. Dashed lines indicate the lower and upper critical fields.

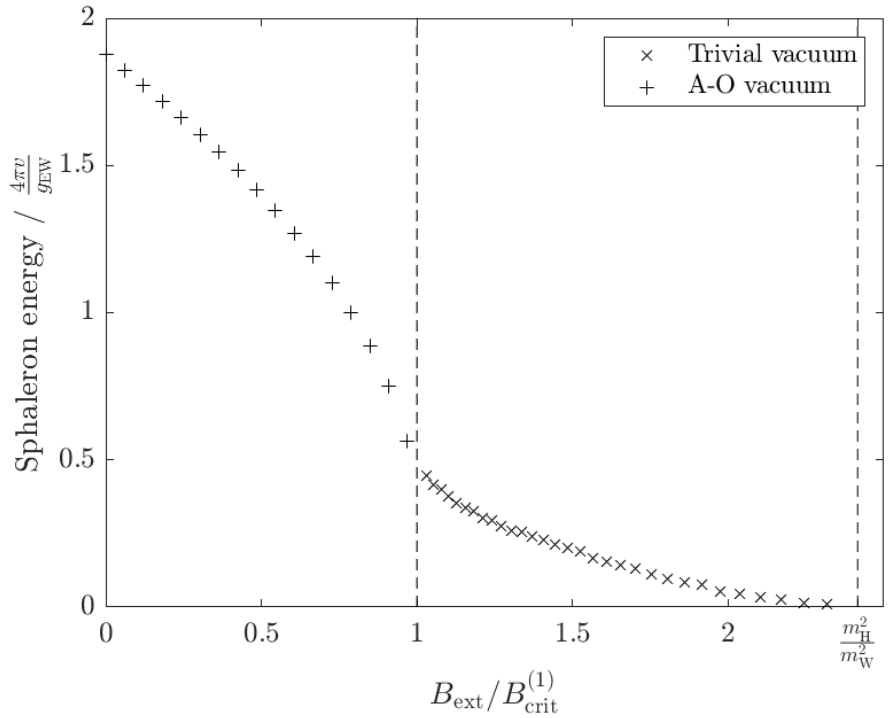

Figure 7.2: Plot of sphaleron energy (with the background field subtracted) against external field strength for physical values of the Standard Model parameters. Dashed lines indicate the lower and upper critical fields. In physical units, $4\pi v/g_{\mathrm{EW}} \approx 5$ TeV.

Parameter	Value
g_{EW}	0.5
λ	0.076
av	0.60-0.90
$\sin^2\theta_{\mathrm{W}}$	0.23

Table 7.1: Numerical values of the dimensionless parameters of Eq. (**??**) used in our calculations.

to compute the sphaleron in the limiting case $\theta_{\mathrm{W}} = 0$, without an external magnetic field present. The LATfield2 C++ library [**?**] was used to aid parallelisation and a Barzilai-Borwein adaptive step size [**?**] was used to speed convergence.

To find the sphaleron solution without an external field, we used the initial ansatz described in Ref. [**?**]. As detailed in Chapter **??**, periodic boundary conditions constrain the magnetic flux through the lattice in units of $4\pi/e$; this can be exploited to restrict the gradient flow to field configurations with an external magnetic field present. By linearly superposing a constant field on an existing sphaleron solution and using this as an initial condition for modified gradient flow, sphalerons in an external field were iteratively generated until the field strength was within one flux quantum of the first critical field $B^{(1)}_{\mathrm{crit}}$.

For $B > B^{(1)}_{\mathrm{crit}}$, a sphaleron solution with a nontrivial background field is sought. This was achieved by first using standard gradient flow to find the Ambjørn-Olesen vortex background, then "transplanting" a sphaleron solution with an incrementally weaker external field by replacing the field at lattice points outside the sphaleron core with the Ambjørn-Olesen vortex field. After smoothing using standard gradient flow, the CMS gradient flow could be used to find a saddle point solution of the fields that tends to the Ambjørn-Olesen vortex lattice at large distances. After the first sphaleron solution against an Ambjørn-Olesen background was found, the magnitude of the external field was increased further by changing the scalar field VEV. This was continued until the external field reached $B = B^{(2)}_{\mathrm{crit}}$.

Computation of the sphaleron for $B < B^{(1)}_{\mathrm{crit}}$ was carried out using a $64 \times 64 \times 192$ grid; for $B > B^{(1)}_{\mathrm{crit}}$ a $64 \times 64 \times 256$ grid was used. Table **??** gives the values or ranges of the dimensionless parameters of Eq. (**??**) used in our calculations. Note that the overall scale is set by the lattice spacing a, and the boson mass hierarchy is set by the ratios $\lambda/g^2_{\mathrm{EW}}$ and $\sin^2\theta_{\mathrm{W}}$, so matching these quantities to the Standard Model parameters ensures that our results reflect the physical Standard Model.

The sphaleron energy as a function of B is shown in Fig. **??**. For weak fields where

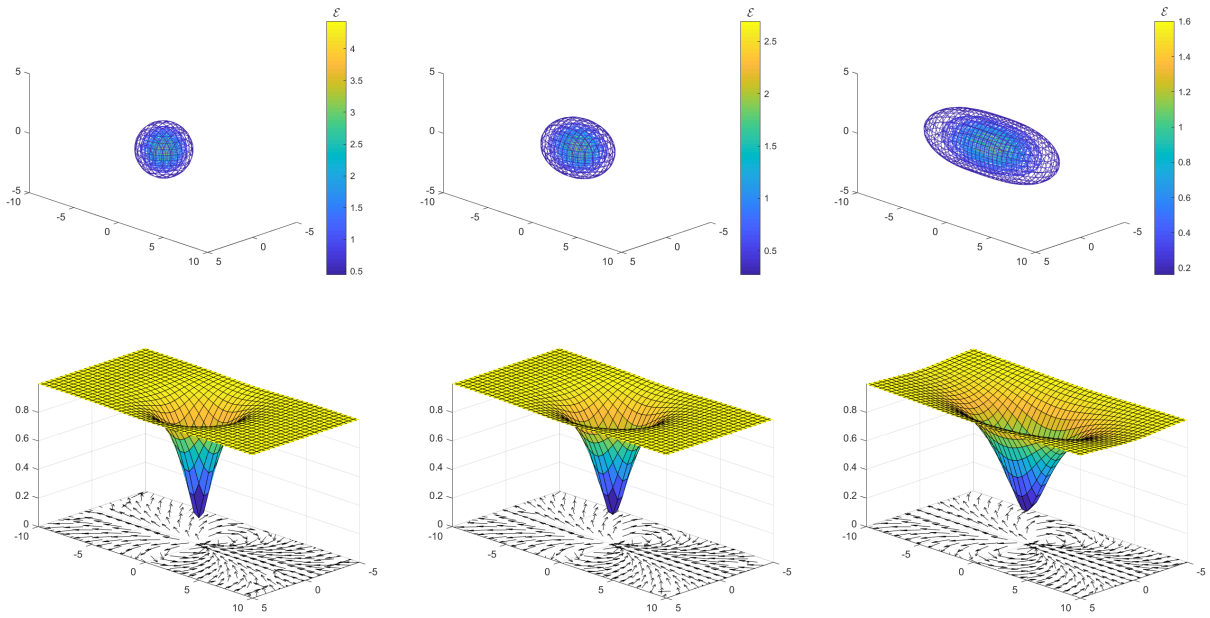

(a) $B/B^{(1)}_{\text{crit}} = 0$ (b) $B/B^{(1)}_{\text{crit}} = 0.48$ (c) $B/B^{(1)}_{\text{crit}} = 0.91$

Figure 7.3: Visualisations of sphaleron solutions for different subcritical magnetic field strengths. Top plots show energy density contours in units of $(g_{\text{EW}}v)^4$ in 3D space. Bottom plots show slices in a plane parallel to the magnetic field intersecting the sphaleron at its centre: the surface gives the scalar field magnitude in units of its VEV, whilst the vector plots give the direction of the magnetic field (with the background subtracted) through the same slice. Spatial axes have units of $(g_{\text{EW}}v)^{-1}$.

$B \ll B_{\mathrm{crit}}^{(1)}$, there is a linear relationship as expected from Eq. (**??**). The gradient in the linear region suggests a dipole moment of $\mu \approx 1.8\, e/(\alpha_{\mathrm{W}} m_{\mathrm{W}})$ (α_{W} denoting the weak fine structure constant), which agrees with interpolated results from other numerical studies of the sphaleron dipole moment [**?**, **?**, **?**] (these were carried out before the Higgs mass was known, so do not include data for the physical Higgs mass).

As the external field strength approaches $B_{\mathrm{crit}}^{(1)}$ from below, the sphaleron energy decreases at an increasing rate. Interpolating the values in Fig. **??** gives a sphaleron energy at the critical field of $E_{\mathrm{sph}}(B_{\mathrm{crit}}^{(1)}) \approx 2\pi v/g_{\mathrm{EW}} \approx 2.5$ TeV, significantly smaller than the sphaleron energy in the absence of an external field but significantly above zero.

Visualisations of sphaleron solutions for $B < B_{\mathrm{crit}}^{(1)}$ are shown in Fig. **??**. It can be clearly seen that the solution becomes more prolate as the field increases: for an external field of around half the first critical field the contours are still close to spherical (as the weak mixing angle is small, the prolation of the sphaleron in the absence of an external field is barely noticeable). However, the prolation becomes very pronounced at larger field strengths. It can be seen from Fig. **??** that the peak energy density of the sphaleron decreases monotonically with increasing field strength. The contours of the Higgs field magnitude also become more prolate, though there always remains a minimum close to zero at the centre of the sphaleron—this is due to the topologically nontrivial nature of the solution; in the continuum limit the Higgs field would vanish at the centre. The lower plots in Fig. **??** show the direction of the magnetic field as defined in Section **??**. The main observable feature is the dipole field due to a pair of Nambu monopoles as observed in Ref. [**?**]; the length of the segment of Z string is two lattice spacings for all $B < B_{\mathrm{crit}}$. The magnetic part of the Z field also shows a dipole-like configuration, though this decays much more rapidly with spatial distance as the Z boson is massive. Examination of the hypercharge field shows—again, as described in Ref. [**?**]—a loop of (electric) current density circling the centre of the sphaleron.

For $B > B_{\mathrm{crit}}^{(1)}$ the homogeneous vacuum develops a negative mode and is no longer the ground state. This makes computation of the sphaleron much more difficult.

By symmetry arguments, there should be a stationary point of the energy resembling the sphaleron in subcritical fields: an axisymmetric field configuration with a Chern-Simons number of one half. An argument for the existence of such a solution follows from the argument presented in Refs. [**?**, **?**]: the homogeneous vacuum is the lowest energy axisymmetric state for a given value of B, and one can construct a noncontractible loop from this vacuum to itself passing through a stationary point of the energy. However, such a stationary point would have two negative modes: in addition to the mode varying Chern-Simons number,

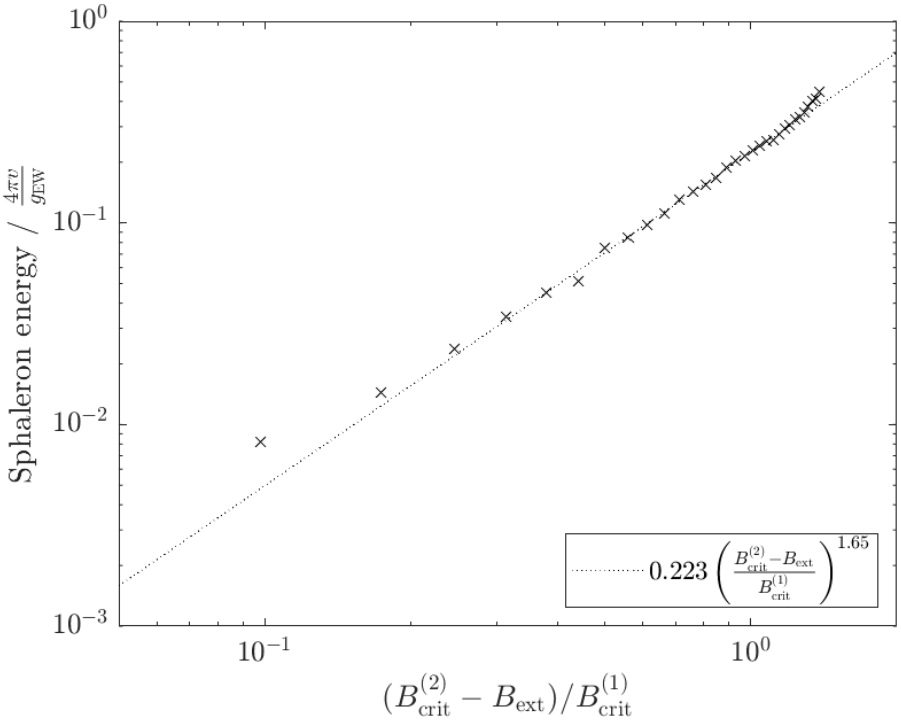

Figure 7.4: Logarithmic-scale plot showing sphaleron energy as the external field approaches $B^{(2)}_{\rm crit}$. The dotted line shows a power-law fit with the largest seven and smallest two points excluded.

there would also be the instability of the background field configuration. This would mean that this solution has multiple negative modes and would not be relevant for tunnelling processes, so we have not attempted to study it here.

Instead, the relevant sphaleron solution with a single negative mode should resemble the subcritical sphaleron at short distances but tend to the Ambjørn-Olesen vacuum at large distances. In this work we searched for and found such solutions. The key features are similar both above and below the first critical field: the energy contours trace a prolate spheroid, the Higgs field vanishes at the centre, and a pair of Nambu monopoles separated by a Z string are observed.

A surface plot of the Higgs field magnitude for a sphaleron solution with $B > B^{(1)}_{\text{crit}}$ is shown in Fig. **??**. The Higgs field in the ground state is also shown for comparison; it is clear that the solution consists of the sphaleron of Refs. [**?**, **?**] against the nontrivial background of Refs. [**?**, **?**, **?**].

While finding solutions for external fields very close to $B^{(1)}_{\text{crit}}$ is technically difficult due to the presence of the almost zero Ambjørn-Olesen mode, the points in Fig. **??** seem to indicate that the energy is continuous across the critical field. It can be seen that the energy of the sphaleron above the first critical field continues to decrease monotonically, though the acceleration of the decrease in energy with increasing field strength ceases.

The sphaleron energy remains greater than zero until the second critical field $B^{(2)}_{\text{crit}} = m_{\text{H}}^2/e$ is reached. At this point, the negative mode of the sphaleron "flattens" to a zero mode, and standard gradient flow from a sphaleron configuration at lower external field will converge upon a field configuration with the same energy as the vacuum, with a vanishing Higgs field magnitude. This solution still contains a Z string, but with no Higgs VEV this is purely a gauge object.

To quantify the critical scaling behaviour of the sphaleron energy as the field approaches $B^{(2)}_{\text{crit}}$, we show it on a logarithmic scale in Fig. **??**. For the strongest fields, the sphaleron solution is very close to the vacuum: the contribution to the total energy of the system due to the sphaleron is around one part in 10^5. For this reason, finding the exact solution is difficult and the value of the sphaleron energy may carry some error. This could explain the slight modulation of the curve visible on a logarithmic scale in Fig. **??**, especially in the smallest values of the energy. Unfortunately, as the errors are not statistical in nature, it is not possible to include error bars in this plot.

There appears to be a linear region on the log-log plot that suggests a power-law scaling: for B close to $B^{(2)}_{\text{crit}}$,

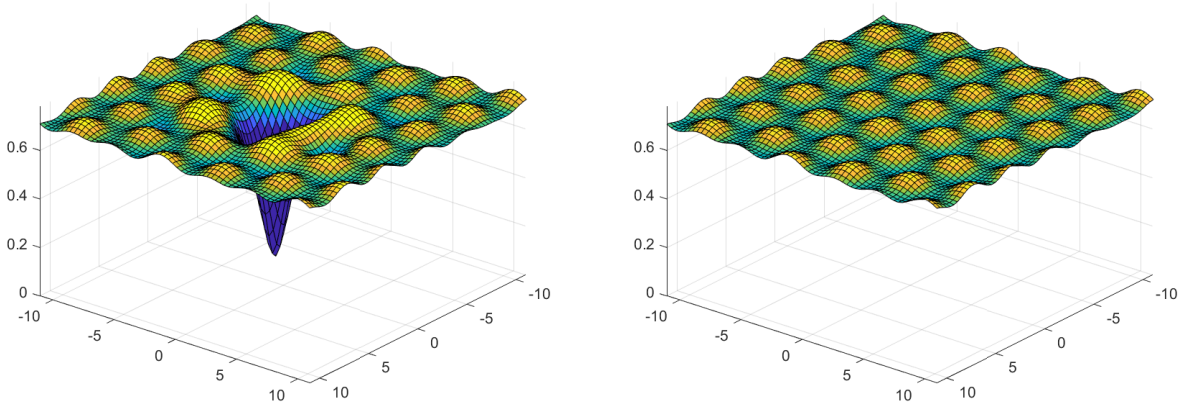

(a) (b)

Figure 7.5: Surface plots of Higgs field magnitude in units of the Higgs VEV. Left: sphaleron solution for $B/B^{(1)}_{\text{crit}} = 1.70$; a slice perpendicular to the external field passing through the centre of the sphaleron is displayed. Right: Ambjørn-Olesen condensate solution for the same external field. Spatial axes have units of $(g_{\text{EW}}v)^{-1}$.

$$\frac{g_{\text{EW}}E_{\text{sph}}}{4\pi v} \approx 0.223 \left(\frac{B^{(2)}_{\text{crit}} - B}{B^{(1)}_{\text{crit}}} \right)^{1.65} . \tag{7.6}$$

A numerical fit gives an exponent of 1.65 ± 0.04 and a coefficient of 0.223 ± 0.002. However, the errors in the data, especially for higher values of the field where the energy is very small, make the scaling relationship difficult to determine precisely. More investigation would be required to ascertain whether the power-law scaling is valid.

As the modified gradient descent method used in our calculations tends to converge to saddle points near to the initial field configuration, in principle there could be other saddle points for external fields between $B^{(1)}_{\text{crit}}$ and $B^{(2)}_{\text{crit}}$ that have a lower energy than the solutions we have found. However, our solution appears to be continuously connected to the standard zero-field sphaleron, suggesting that it is responsible for the same $B + L$ violating process. As even the zero-field sphaleron has not been shown rigorously to be the lowest energy saddle point of electroweak theory, we do not attempt to prove this here.

7.4 Summary

We have computed the electroweak sphaleron solution in an external magnetic field B ranging from zero up to the second Ambjørn-Olesen critical field $B_{\rm crit}^{(2)} = m_{\rm H}^2/e$ where the Higgs field symmetry is restored. We find that when $B_{\rm ext}$ is increased, the sphaleron energy initially decreases linearly for $B \ll B_{\rm crit}^{(1)}$, then more rapidly until $B = B_{\rm crit}^{(1)}$. For $B_{\rm crit}^{(1)} < B < B_{\rm crit}^{(2)}$, the sphaleron energy decreases gradually until it reaches zero when the Higgs symmetry is restored at $B_{\rm crit}^{(2)}$; above this the sphaleron ceases to exist.

The vanishing of the sphaleron energy at the second critical field confirms the result of Ref. [**?**] that if fields of this magnitude could be produced, they would result in a greatly enhanced rate of $B + L$ violation. A striking consequence of this is that any baryonic matter placed in such a magnetic field would spontaneously decay into leptons.

One potential avenue for observation of this field-induced baryon and lepton number violation is the heavy ion collisions much discussed in earlier parts of this thesis. As Eqs. (**??**) and (**??**) show, the scale of the magnetic field at which the enhancement becomes significant is of order 10^4 GeV^2. Numerical simulations [**?**, **?**] (see Section **??**) indicate that the fields in present day heavy ion collisions at the LHC are of the order 1 GeV^2, and scale linearly with energy, so collisions energies of around 10^5 TeV per nucleon would be needed. This regime is inaccessible to particle colliders in the near future. In a 10 TeV collision, the reduction in sphaleron energy due to the magnetic field is only of order 0.1%, and therefore baryon number violation is almost as strongly suppressed as at zero field. In addition, at high energies the magnetic field is highly localised in both space and time [**?**, **?**]: while according to Ref. [**?**] the spatial localisation has a suppressing effect, we showed in Chapter **??** that time dependence enhances a similar nonperturbative tunnelling phenomenon.

The results may also have relevance for cosmology. It is possible that strong magnetic fields were present in the early Universe [**?**, **?**, **?**]. If the field strength was still above or close to $B_{\rm crit}^{(1)}$ after the electroweak phase transition, it would have allowed baryon number violating sphaleron processes to continue for longer, thereby affecting the baryon asymmetry of the Universe. The required fields could be produced by exotic physics such as superconducting cosmic strings [**?**, **?**] or near-extremal magnetically charged black holes [**?**], but are not expected to arise in the simplest cosmological scenarios. An empirical observation, direct or indirect, of baryon number violation due to strong magnetic fields is therefore unlikely in the near future.

Chapter 8

Conclusions and outlook

In this thesis we have explored two main methods of computing the rate of magnetic monopole production from magnetic fields: the worldline approximation, and lattice discretisation.

Working in the worldline approximation, in Chapter **??** we computed the probability of producing a monopole-antimonopole pair via the Schwinger effect in the electromagnetic fields of an ultrarelativistic heavy ion collision. This calculation was performed analytically to leading order in worldline self-interactions, and numerically to all orders. Under conditions where the worldline approximation is valid, this is a truly nonperturbative result, applicable regardless of the magnitude of the monopole magnetic charge. Unfortunately, an analysis of the parameter regions where the worldline approximation holds shows that realistic heavy ion collisions do not satisfy the required conditions at any relativistic energy.

This roadblock is at first glance surprising: one might think that for sufficiently heavy monopoles, a worldline description should always be valid. The cause for dismay is the fact that while the effective size of the monopole decreases with increasing mass, it only decreases as $1/m$, while the minimum radius of curvature of the worldline instanton, due to the contracting effects of the time-dependent magnetic field, decreases as $1/m^2$. In the limit of light monopoles, on the other hand, the radius of curvature scales proportional to m; the

	Spacetime dependence	Monopole structure	Strong coupling
Worldline LCFA	✗	✗	✓
Worldline FPA	✓	✗	✗
Lattice	✗	✓	✓

Table 8.1: Comparison of the methods used in this thesis to analyse monopole production from magnetic fields.

worldline description is invalid in both limits.[1]

While, as this work has shown, the goal of computing a complete and reliable cross section for monopole production in ultrarelativistic heavy ion collisions cannot be achieved using worldline methods, our worldline results are far from useless. The first use of our results is in computing lower bounds on monopole cross sections. In Chapter **??** we identified two approximations that are expected to give conservative estimates of the cross section: the free particle approximation (FPA), which neglects worldline self-interactions while including the spacetime dependence of the magnetic fields to all orders, and the locally constant field approximation (LCFA), which accounts for worldline self-interactions to all orders but treats the spacetime dependence perturbatively. The FPA and LCFA have been used by the MoEDAL experiment in Ref. [**?**] in the first dedicated experiment searching for monopoles produced via the Schwinger effect, and have improved the previous Schwinger-derived mass bounds by almost two orders of magnitude.

The FPA and LCFA are not expected to provide an accurate theoretical model of Schwinger production in a heavy ion collision, but are suitable for computing conservative estimates that can be used to generate lower bounds on monopole masses. In this manner, there are parallels with the perturbative Drell-Yan and photon fusion cross sections [**?**] that are the standard for computing mass bounds from proton-proton collisions. However, unlike these calculations, it is known how to extend the results beyond their perturbative limits.

This is the other important result of our worldline investigations; we know exactly how the worldline instanton method breaks down. In the fields of heavy ion collisions, the worldline approximation is invalid because the radius of curvature of the instanton solution becomes small compared to the classical radius of the monopole. This is a problem both for solitonic monopoles—where to resolve smaller scales we must take the non-Abelian nature of the gauge fields into account—but also for elementary monopoles, due to the strong coupling effects causing the failure of the dilute instanton gas approximation. In the latter case, it is uncertain how to make progress, but for solitonic monopoles it is clear: we can perform an instanton calculation in the full field theory describing the monopole of interest.

This task is precisely what we have started in Chapter **??**. Using lattice field theory, we have successfully computed a sphaleron and an instanton solution responsible for determining the rate of pair production of 't Hooft–Polyakov monopoles from constant magnetic fields in Georgi-Glashow SU(2) theory. These solutions have been known to exist in the worldline

[1]The fact that there is no region of parameter space where the approximations are valid appears to be an frustrating coincidence of our Universe: if, for example, the atomic number of lead nuclei were a few orders of magnitude higher, the worldline approximation would hold at relativistic energies.

approximation for several decades [**?**,**?**], but to our knowledge we are the first to compute them explicitly beyond the limit of weak magnetic fields. We have extended the computation of these solutions to the Ambjørn-Olesen critical field strength [**?**], where both the sphaleron and instanton solutions coincide with the vacuum, which becomes unstable. This suggests that the Ambjørn-Olesen instability in Georgi-Glashow SU(2) theory leads to classical production of 't Hooft–Polyakov monopoles.

Most excitingly, the field-theoretic sphalerons and instantons of Chapter **??** have lower energies and actions, respectively, than their worldline counterparts. This means that accounting for the internal structure of the monopole results in an enhanced pair production probability compared to the worldline method. This is the reason that we believe the FPA and LCFA systematically underestimate the true cross section for monopole production; the evidence so far is that moving beyond the worldline approximation results in higher production probabilities for a given field.

8.1 Future research directions

As is to be expected, there are still many unanswered questions that have arisen over the course of completing this research. Some of them are summarised in the following.

8.1.1 Field-theoretic instantons in the fields of heavy ion collisions

As has been mentioned several times before, there are three factors that complicate the computation of the monopole-antimonopole pair production rate from the electromagnetic fields of heavy ion collisions. These are the spacetime dependence of the fields, the internal structure of the monopoles, and strong coupling effects. Table **??** summarises the approaches used so far in this thesis, showing that as yet, inclusion of all three complicating factors is out of reach.

In principle, the task is straightforward: generalise the instanton calculation of Section **??** from a constant magnetic field to the spacetime-dependent electromagnetic fields described in Section **??**. However, in practice, we expect there to be some difficulties in performing such a calculation.

This instanton solution of Section **??** had time dependence in the solution itself, but the magnetic field was homogeneous in both space and time. This resulted in a high level of symmetry in the solution, allowing us to use a three-dimensional lattice. In the full fields of a heavy ion collision, however, there are no continuous symmetries: all four spacetime

directions are different and the instanton solution will therefore require a four-dimensional lattice. This adds an extra degree of computational complexity to the problem, though with sufficient computational power and a good initial guess, there is no reason why the methods used in previous chapters should not be applicable. There may also be some simplifications that can be made in the ultrarelativistic limit, where the system becomes boost invariant.

Another nontriviality is the problem of exactly how to impose the external fields on the lattice. In the case of a constant magnetic field, one can exploit the fact that periodic boundary conditions quantise the flux through the lattice to generate solutions with a given flux at the boundary. This cannot be used to impose an inhomogeneous field with our current methods, as any initial inhomogeneity will be smoothed out by the gradient flow. It is possible that Dirichlet boundary conditions or source terms may be required. The introduction of the desired fields is further complicated by the fact that, in Euclidean time, the magnetic field from Section **??** is singular at $z = 0$, $\tau = \pm 1/\omega$. These poles are difficult to realise on the lattice, and it is not immediately obvious how to deal with them.

It is likely that there are still more stages to the problem, such as introducing temporal and spatial dependence separately. In the worldline approximation the time dependence results in an exponential enhancement of pair production, and understanding the extent to which this holds in the full field theory is of great interest. The localisation of the magnetic field in the beam direction (due to Lorentz contraction) is transverse to the direction of the magnetic field, so in the worldline approximation has no effect at leading order, as the interaction between the field and the worldline is local. This no longer holds with extended particles—understanding what happens when the monopole size becomes comparable to the field's spatial extent is again a key open question.

Another intermediate result that may be useful to investigate is a real-time simulation of classical monopole production from a time-dependent magnetic field. As we showed in Chapter **??**, magnetic fields in theories that admit 't Hooft–Polyakov monopoles become classically unstable to monopole-antimonopole production at a critical field strength set by the charged vector boson mass. The effect of time dependence on this effect could be investigated by computing the real time classical evolution of fields with appropriate initial conditions, and examining whether monopoles are produced. There are similarities between this proposed calculation and the calculation in Ref. [**?**], which simulated monopole creation from colliding classical wavepackets.

8.1.2 Sphalerons and instantons in other monopole models

The calculations of Chapter **??** were carried out in Georgi-Glashow SU(2) theory, which admits 't Hooft–Polyakov monopole solutions. This model is useful because, while relatively simple, it can be embedded in any Grand Unified Theory (GUT), meaning that our results are valid for all GUTs. However, GUT monopoles, if they exist, are expected to have very large masses, far greater than would be accessible in any particle accelerator in the foreseeable future, even with enhancements due to time dependence and strong coupling.

More experimentally relevant, perhaps, are theories modifying the electroweak interaction that predict solitonic monopoles at far lower masses [**?**, **?**, **?**, **?**], some at the TeV scale. These are much more likely to be accessible to particle accelerators, so calculations involving them may be of experimental interest. A fairly straightforward extension to the work in this thesis would be to find the Schwinger sphalerons and instantons in one or more of these theories. This would require a lattice formulation of a modified electroweak theory, and care must be taken to achieve this in a consistent manner with a sensible continuum limit.

In Georgi-Glashow theory, monopoles are produced via the Ambjørn-Olesen instability at a field strength set by the charged vector boson mass m_{v} and the electric charge e. Notably, the critical field strength does not depend on the scalar self-coupling, so is independent of the monopole mass (except through the shared dependence on m_{v} and e). In the modified electroweak theory models that admit monopoles, there are more free parameters, and the monopole mass can vary over a much greater scale by tuning these parameters. It would be interesting to see if the Ambjørn-Olesen instability still leads to monopole production in these theories, or if the phenomena decouple.

8.1.3 Other nonperturbative solutions in field theory

Finally, the techniques used and developed over the course of the research presented here are applicable to a wide range of problems involving nontrivial solutions in field theory. An example is presented in Chapter **??**, where we computed the energy of the electroweak sphaleron in an external magnetic field.

There are many more nonperturbative phenomena in field theory that our techniques could be applicable to, such as Skyrmions, cosmic strings and vacuum bubbles. As a specific example, in the Skyrme model, the only known saddle point solutions have a high degree of symmetry (e.g. the sphalerons found in Ref. [**?**]); our saddle point finding techniques may be able to find other, more complicated solutions. These would be theoretically interesting in their own right, but may also have physical interpretation as mediators of transitions in

atomic nuclei.

8.2 Final words

The theoretical study of magnetic monopole production is still very much in its infancy, due to the strong coupling between the monopole and the electromagnetic field, which severely complicates calculations. This work plays a small part in advancing our understanding of this phenomenon.

We have provided a new method of obtaining quantitative lower bounds on monopole masses, assuming that future heavy ion collision experiments do not produce monopoles.[2] We have pushed the worldline approximation to its limits, and shown how to move beyond it, generalising semiclassical results from weak fields to strong ones. In doing so, we have uncovered new features of the vacuum structure of non-Abelian gauge theories, describing them quantitatively for the first time.

The next steps that must be taken in order to obtain a complete theoretical description of monopole production in heavy ion collisions are clear, and while there are still practical obstacles to be overcome, we hope that the foundations we have laid with this work will precipitate further advances. In the not too distant future, we may see monopoles produced in heavy ion collisions for the first time—at least in a lattice simulation.

[2] If monopoles are discovered, we hope only that they do not oversaturate the bounds derived from our work.

Appendices

Appendix A

List of symbols and abbreviations

Latin symbols

a	Lie algebra index, lattice spacing, Woods-Saxon parameter
A	Woods-Saxon normalisation constant
A_μ	Gauge field
$\vec{A}$	3-vector potential
b	Impact parameter
$\vec{B}$	Magnetic field
B	Magnetic field magnitude, peak magnetic field strength, baryon number
c	Speed of light, generic coefficient
$\mathcal{C}$	Field configuration space
$\mathbb{C}$	Set of complex numbers
d	Number of dimensions
D	Exponential prefactor
e	Euler's number
e	Electric charge, gauge coupling
E	Energy, electric field magnitude, peak electric field strength
$\vec{E}$	Electric field
$\mathbf{E}$	Complete elliptic integral of the second kind
$\mathcal{E}$	Energy density
f	Generic function, monopole mass function, electroweak sphaleron gauge radial function
$f_{\mu\nu}$	Abelian field strength tensor

F	Flux
$F_{\mu\nu}$	Field strength tensor
$\mathcal{F}$	Electromagnetic invariant
g	Magnetic charge
g_{D}	Dirac charge quantum
g_{EW}	Electroweak SU(2) coupling constant
g'_{EW}	Electroweak U(1) hypercharge coupling constant
$G_{\mu\nu}$	Electroweak isospin field strength tensor, photon propagator
$\mathcal{G}$	Generic Lie group
$\mathcal{G}^2$	Gradient squared function
h	Electroweak sphaleron scalar radial function
$\hbar$	Reduced Planck's constant
H	't Hooft–Polyakov monopole scalar radial function
$H_{\alpha\beta}$	Hessian
$\mathcal{H}$	Generic Lie group
i	Imaginary unit, spatial index
$\mathbb{I}$	Identity matrix
j	Spatial index
$\vec{J}_{\mathrm{E}}$	Electric current density
$\vec{J}_{\mathrm{M}}$	Magnetic current density
k	Spatial index, CMS gradient descent parameter
k_{B}	Boltzmann's constant
$\vec{k}$	Kinetic 3-momentum
K	't Hooft–Polyakov monopole gauge radial function
$\mathbf{K}$	Complete elliptic integral of the second kind
L	Lattice size, Lagrangian, lepton number
$\mathcal{L}$	Lagrangian density
m	Monopole mass (without subscript), mass of particle specified by subscript
M	Generic matrix
n	Generic integer, generic index, momentum distribution
N	Number of lattice points, Lie group dimension
N_{CS}	Chern-Simons number
$\mathcal{N}$	Normalisation factor
$\vec{n}$	Generic unit vector

$\vec{p}$	Canonical 3-momentum
P	Probability
P_U	SU(2) projection operator
$\vec{q}$	Scaled Poynting flux
r	Polar radial coordinate
r_{M}	Monopole radius
R	Lie algebra representation, ion radius, generic radius, number of lattice points
$\mathbb{R}$	Set of real numbers
s	Particle spin, Schwinger parameter
$\sqrt{s}$	Centre of mass energy
S	Action
S^n	n-Sphere
t	Minkowski time
τ	Proper time
T	Temperature
u	Worldline parameter, generic function
U	Evolution operator
U^∞	Matrix rotating Higgs doublet of electroweak sphaleron at spatial infinity
U_μ	Link variable
$U_{\mu\nu}$	Plaquette variable
v	Scalar field vacuum expectation value, generic function, speed
$\mathbf{v}$	Generic eigenvector
V	Scalar potential, spatial volume
$\mathcal{V}$	Spacetime volume
w	Complex variable
W_μ	Electroweak SU(2) isospin field
x	Spatial coordinate, spacetime coordinate, generic variable
$\vec{x}$	Position 3-vector
x_μ	Position 4-vector, worldline path
$\mathbf{x}$	Generic vector
y	Spatial coordinate
Y_μ	Electroweak U(1) hypercharge field
$Y_{\mu\nu}$	Electroweak hypercharge field strength tensor

z	Spatial coordinate
Z	Atomic number
$\mathbb{Z}$	Set of integers

Greek symbols

α	Electric fine structure constant, vector index
α_{M}	Magnetic fine structure constant
α_{W}	Weak fine structure constant
β	Boson mass ratio in Georgi-Glashow SU(2) theory, speed in units of c, vector index
γ	Gradient descent step size, Lorentz factor
Γ	Generic path, pair production rate
δ	Kronecker symbol, Dirac distribution
ϵ	Small parameter
ε_0	Permittivity of free space
$\varepsilon_{i_1 \ldots i_n}$	Rank n Levi-Civita symbol
ζ	Integration variable
θ	Generic angle, spherical polar angle
θ_{W}	Weak mixing angle
κ	Semiclassicality parameter
λ	Scalar self-coupling, generic eigenvalue, Lagrange multiplier
μ	Spacetime index
$\vec{\mu}$	Magnetic dipole moment
μ_0	Permeability of free space
ν	Spacetime index
ξ	Keldysh parameter
π	π, homotopy group
Π	Lattice projection operator
ρ	Charge density, radial spacetime coordinate
ρ_{E}	Electric charge density
ρ_{M}	Magnetic charge density
σ	Cross section, Lagrange multiplier
σ_i	Pauli matrices

τ	Gradient flow time, Euclidean time
τ_i	SU(2) basis vectors
ϕ	Scalar field, generic field
Φ	Adjoint scalar field
φ	Azimuthal polar angle
χ	Angular spacetime coordinate
ω	Inverse decay time
Ω	Quantum state, inverse width, Lie group element

Abbreviations

ANITA	Antarctic Impulsive Transient Antenna
ANTARES	Astronomy with a Neutrino Telescope and Abyss environmental RESearch
AO	Ambjørn-Olesen
ATLAS	A Toroidal LHS ApparatuS
BPS	Bogomolny-Prasad-Sommerfeld
CDF	Collider Detector at Fermilab
CMS	Chigusa-Moroi-Shoji
CS	Chern-Simons
EW	Electroweak
GSD	Gradient squared descent
GUT	Grand Unified Theory
FPA	Free particle approximation
IceCube	Not an acronym; a literal cubic kilometre of ice
LCFA	Locally constant field approximation
LEP	Large Electron–Positron Collider
LHC	Large Hadron Collider
MACRO	Monopole, Astrophysics and Cosmic Ray Observatory
MODAL	Monopole Detector At LEP
MoEDAL	Monopole and Exotics Detector At the LHC
ODE	Ordinary differential equation
OPAL	Omni-Purpose Apparatus at LEP
QED	Quantum electrodynamics
QEMD	Quantum electromagnetodynamics
QFT	Quantum field theory

QGP	Quark-gluon plasma
RICE	Radio Ice Cherenkov Experiment
RHIC	Relativistic Heavy Ion Collider
RMSprop	Root mean square propagation
SGD	Stochastic gradient descent
STFC	Science and Technology Facilities Council
SPS	Super Proton Synchrotron
SQED	Scalar quantum electrodynamics
SU	Special unitary
U	Unitary
UK	United Kingdom
UV	Ultraviolet
VEV	Vacuum Expectation Value
WKB	Wentzel-Kramers-Brillouin

Appendix B

The locally constant field approximation

The locally constant field approximation (LCFA) is an approximation scheme for calculating the Schwinger pair production probability and momentum distribution in an inhomogeneous electromagnetic field. It is a leading order expansion in the spacetime derivatives of the external field, so is expected to be valid in the limit where the spatial and temporal inhomogeneities are small. Because it removes many of the complications introduced by field inhomogeneities, the LCFA has been widely used to study electron-positron Schwinger production theoretically: see Refs. [?, ?, ?] for recent discussions.

In this appendix, we review the application of the LCFA to compute the overall production probability, and the momentum distribution, of magnetic monopoles produced from electromagnetic fields.

B.1 Pair production probability

The starting point for the LCFA is the pair production probability per unit spacetime volume for a constant electromagnetic field. In fields where the electromagnetic invariant $F_{\mu\nu}\tilde{F}^{\mu\nu} = \vec{E}\cdot\vec{B}$ vanishes[1], for magnetic monopoles of mass m, charge g, and spin s, this is [?, ?]

$$\Gamma(x) = \frac{(2s+1)g^2}{8\pi^3}\mathcal{F}(x)^2 \exp\left(-\frac{\pi m^2}{g\mathcal{F}(x)} + \frac{g^2}{4}\right), \tag{B.1}$$

defining

$$\mathcal{F}(x) = \sqrt{|\vec{B}(x)|^2 - |\vec{E}(x)|^2} \tag{B.2}$$

[1] All fields considered in this thesis satisfy this condition

The overall production probability is then obtained by integrating over all spacetime:

$$P_{\mathrm{LCFA}} = \int \mathrm{d}^4x\, \Gamma(x). \tag{B.3}$$

This integration can be performed straightforwardly using numerical methods, or within a steepest descent approximation.

B.2 Momenta of produced particles

The LCFA can also be used to approximate the momentum distribution of particles produced via the Schwinger effect. There are two contributions to the measured momentum of the monopoles produced: the initial momentum they are produced at, which is probabilistically distributed, and the momentum they gain through classical evolution in the external field after production, which is deterministic. Note that in the free particle approximation (FPA), discussed in section **??**, these effects are combined by using canonical momenta.

The initial momentum distribution as a function of spacetime can be obtained by boosting to a frame where $\vec{E} = 0$ (which is always possible if $\vec{E}\cdot\vec{B} = 0$), and applying the constant field momentum distribution. This distribution was first identified in Ref. [**?**], and is identical to Eq. (**??**), with the mass m replaced by the "transverse mass" $\sqrt{m^2 + p_\perp^2}$, where $\vec{p}_\perp$ denotes the component of momentum transverse to the external magnetic field. Including the aforementioned boost gives the initial momentum distribution

$$n(t,\vec{x},\vec{p}) = \frac{g\mathcal{F}(t,\vec{x})}{2\pi^3}\exp\left(-\frac{\pi m^2}{g\mathcal{F}(t,\vec{x})} + \frac{g^2}{4}\right)\exp\left(-\frac{\pi}{g\mathcal{F}(t,\vec{x})}(p_\perp^2 + q_\perp(t,\vec{x})^2)\right)\delta(p_\parallel), \tag{B.4}$$

defining

$$\vec{q}_\perp(t,\vec{x}) = \frac{m}{|\vec{B}(t,\vec{x})|\mathcal{F}(t,\vec{x})}\vec{E}(t,\vec{x})\times\vec{B}(t,\vec{x}). \tag{B.5}$$

Note that in the LCFA, particles are assumed to be produced with zero longitudinal momentum $p_\parallel$; they gain longitudinal momentum via the classical evolution after production. This evolution follows the Lorentz force law for monopoles:

$$\frac{\mathrm{d}p^\mu}{\mathrm{d}\ell} g\tilde{F}^{\mu\nu}p_\nu, \tag{B.6}$$

where ℓ denotes proper time along the monopole worldline. This is straightforward to compute numerically.

Using the LCFA to compute a momentum distribution for monopoles produced in the fields studied in Chapter **??** gives a very different result to the FPA. Notably, the final

momenta of the particles is far lower, in the nonrelativistic regime. This suggests that if the LCFA accurately describes the momentum distribution, Schwinger-produced monopoles from heavy ion collisions may not have enough momentum to escape the beam pipe and interact with a detector. However, for ultrarelativistic collisions, the LCFA predicts a momentum distribution far narrower than allowed by the preparation-time energy uncertainty principle (whilst the FPA saturates the uncertainty principle, as discussed in Section **??**). For this reason, we do not expect the LCFA to provide a useful computation of the momentum distribution, and suggest that the FPA be used instead.

Appendix C

Worldline numerics

This appendix gives the details of the numerical worldline calculation presented in Section **??**, computing the worldline instanton solution, including worldline self-interactions to all orders. Our implementation of this algorithm was developed by Oliver Gould, adapting a previous implementation used in a constant field at finite temperature in Ref. [**?**].

The continuum action we seek to extremise is the worldline effective action

$$\begin{aligned} S[x,s;\tilde{A}_{\text{ext}}] = \frac{m^2 s}{2} + \frac{1}{2s}\int_0^1 \mathrm{d}u \dot{x}_\mu \dot{x}_\mu - ig\int_0^1 \tilde{A}^\mu_{\text{ext}} \dot{x}_\mu \mathrm{d}u \\ + \frac{g^2}{8\pi^2}\int_0^1 \mathrm{d}u \int_0^1 \mathrm{d}u' \frac{\dot{x}_\mu(u)\dot{x}_\mu(u')}{|x(u)-x(u')|^2}, \end{aligned} \tag{C.1}$$

given in Section **??**. The Schwinger parameter s is integrated out using steepest descents, and the worldline coordinates are scaled by gB/m to make them dimensionless. The worldline is then discretised into N points, evenly spaced in the worldline parameter u. Using finite differences to approximate the derivatives gives the discretised action

$$\begin{aligned} \frac{gB}{m^2}S[x] = \sqrt{N\sum_{\alpha,\mu}(x^{\alpha+1}_\mu - x^\alpha_\mu)^2} + \sum_{\alpha,\mu} A^\mu_{\text{ext}}(x^\alpha)(x^{\alpha+1}_\mu - x^\alpha_\mu) \\ - \frac{g^3 B}{2m^2}\sum_{\alpha,\beta}(x^{\alpha+1}_\mu - x^\alpha_\mu)(x^{\beta+1}_\mu - x^\beta_\mu) G_R(x^\alpha, x^\beta; a), \end{aligned} \tag{C.2}$$

where $\alpha, \beta = 0, \ldots, N-1$ index the discrete worldline points. Here the exponentially regularised propagator

$$G_R(x,y;a) = \frac{-1}{4\pi\left[(x-y)^2 + a^2\right]} + \frac{\sqrt{\pi}}{4\pi^2 a^2}\exp\left(-\frac{(x-y)^2}{a^2}\right) \tag{C.3}$$

is used in preference to a length counterterm [**?**] so that the bare mass is positive (see Ref. [**?**] for more details). Note that this form of discretisation is distinct from the lattice

discretisation described in Section **??** and used in Chapter **??**, as the background spacetime remains continuous.

The continuous symmetries of the external field A_μ result in zero modes which must be fixed in order to find a unique solution. The field used in Section **??** is spatially homogeneous, so there are three zero modes corresponding to spatial translations. These can be fixed by imposing the condition that the worldline centre of mass is at the origin, using the Lagrange multipliers λ_i, $i = 1, 2, 3$, adding the term

$$\sum_{\alpha,i} \lambda_i x_i^\alpha \tag{C.4}$$

to the action. There is also a zero mode due to reparametrisation invariance, which in Section **??** was fixed with the Lagrange multiplier term

$$\sigma(x_2^0 - x_2^{N/2-1}). \tag{C.5}$$

The equations of motion arising from this action, including the Lagrange multiplier terms, were solved using the Newton-Raphson method using the analytic approximation from Section **??** as an initial guess. In general, $N = 2^{12}$ points were used to describe the worldlines, though other values were used to check the $N \to \infty$ behaviour.

Bibliography

[1] Oliver Gould, David L.-J. Ho, and Arttu Rajantie. Towards Schwinger production of magnetic monopoles in heavy-ion collisions. *Phys. Rev.*, D100(1):015041, Jul 2019.

[2] Oliver Gould, David L.-J. Ho, and Arttu Rajantie. Schwinger pair production of magnetic monopoles: momentum distribution for heavy-ion collisions. *arXiv preprint arXiv:2103.14454*, 2021.

[3] B. Acharya et al. First experimental search for production of magnetic monopoles via the Schwinger mechanism. Jun 2021.

[4] David L.-J. Ho and Arttu Rajantie. Classical production of 't Hooft–Polyakov monopoles from magnetic fields. *Phys. Rev. D*, 101(5):055003, Mar 2020.

[5] David L.-J. Ho and Arttu Rajantie. Instanton solution for Schwinger production of 't Hooft–Polyakov monopoles. *Phys. Rev. D*, 103:115033, Jun 2021.

[6] David L.-J. Ho and Arttu Rajantie. Electroweak sphaleron in a strong magnetic field. *Phys. Rev. D*, 102(5):053002, 2020.

[7] Brian Scott Baigrie. *Electricity and magnetism: a historical perspective*. Greenwood Publishing Group, 2007.

[8] Petrus Peregrinus. The letter of Petrus Peregrinus on the magnet, 1269. Project Gutenberg. Retrieved March 15, 2021, from `https://www.gutenberg.org/files/50524/50524-h/50524-h.htm`.

[9] Paul A. M. Dirac. Quantised singularities in the electromagnetic field. *Proc. Roy. Soc. Lond.*, A133(821):60–72, 1931.

[10] G. 't Hooft. Magnetic monopoles in unified gauge theories. *Nucl. Phys. B*, 79(2):276–284, 1974.

[11] Alexander M. Polyakov. Particle spectrum in the quantum field theory. *JETP Lett.*, 20:194–195, 1974.

[12] T. W. B. Kibble. Topology of cosmic domains and strings. *Journal of Physics A Mathematical General*, 9(8):1387–1398, aug 1976.

[13] David J. Gross and Malcolm J. Perry. Magnetic monopoles in Kaluza-Klein theories. *Nucl. Phys. B*, 226:29–48, 1983.

[14] Rafael D. Sorkin. Kaluza-Klein monopole. *Phys. Rev. Lett.*, 51:87–90, Jul 1983.

[15] John Preskill. Magnetic monopoles. *Ann. Rev. Nucl. Part. Sci.*, 34:461–530, 1984.

[16] Fritz Sauter. Uber das Verhalten eines Elektrons im homogenen elektrischen feld nach der relativistischen Theorie Diracs. *Z. Phys.*, 69(11-12):742–764, 1931.

[17] Julian S. Schwinger. On gauge invariance and vacuum polarization. *Phys. Rev.*, 82:664–679, 1951. [,116(1951)].

[18] Jan Ambjorn and P. Olesen. Antiscreening of large magnetic fields by vector bosons. *Phys. Lett.*, B214:565–569, 1988.

[19] Jan Ambjorn and P. Olesen. A magnetic condensate solution of the classical electroweak theory. *Phys. Lett.*, B218:67, 1989. [Erratum: Phys. Lett.B220,659(1989)].

[20] Jan Ambjorn and P. Olesen. A condensate solution of the electroweak theory which interpolates between the broken and the symmetric phase. *Nucl. Phys.*, B330:193–204, 1990.

[21] Tai Tsun Wu and Chen Ning Yang. Concept of nonintegrable phase factors and global formulation of gauge fields. *Phys. Rev. D*, 12:3845–3857, Dec 1975.

[22] Joseph Polchinski. Monopoles, duality, and string theory. *Int. J. Mod. Phys.*, A19S1:145–156, 2004. [,145(2003)].

[23] P. A. M. Dirac. The theory of magnetic poles. *Phys. Rev.*, 74:817–830, Oct 1948.

[24] N. Cabibbo and E. Ferrari. Quantum electrodynamics with Dirac monopoles. *Nuovo Cim.*, 23:1147–1154, 1962.

[25] Julian S. Schwinger. Magnetic charge and quantum field theory. *Phys. Rev.*, 144:1087–1093, 1966.

[26] Daniel Zwanziger. Local Lagrangian quantum field theory of electric and magnetic charges. *Phys. Rev.*, D3:880, 1971.

[27] Richard A. Brandt, Filippo Neri, and Masa-aki Sato. Renormalization of loop functions for all loops. *Phys. Rev.*, D24:879, 1981.

[28] M. Blagojevic and P. Senjanovic. The quantum field theory of electric and magnetic charge. *Phys. Rept.*, 157:233, 1988.

[29] Yakov M. Shnir. *Magnetic Monopoles*. Text and Monographs in Physics. Springer, Berlin/Heidelberg, 2005.

[30] P Goddard and D I Olive. Magnetic monopoles in gauge field theories. *Reports on Progress in Physics*, 41(9):1357–1437, sep 1978.

[31] Nicholas Manton and Paul Sutcliffe. *Topological Solitons*. Cambridge Monographs on Mathematical Physics. Cambridge University Press, 2004.

[32] David Tong. TASI lectures on solitons: Instantons, monopoles, vortices and kinks. In *Theoretical Advanced Study Institute in Elementary Particle Physics: Many Dimensions of String Theory*, 6 2005.

[33] David Tong. Line operators in the Standard Model. *Journal of High Energy Physics*, 2017(7):1–15, 2017.

[34] E. B. Bogomolny. Stability of classical solutions. *Sov. J. Nucl. Phys.*, 24:449, 1976.

[35] M. K. Prasad and Charles M. Sommerfield. An exact classical solution for the 't Hooft Monopole and the Julia-Zee dyon. *Phys. Rev. Lett.*, 35:760–762, 1975.

[36] P. Forgács, N. Obadia, and S. Reuillon. Numerical and asymptotic analysis of the 't Hooft-Polyakov magnetic monopole. *Phys. Rev. D*, 71:035002, Feb 2005.

[37] John P. Preskill. Cosmological production of superheavy magnetic monopoles. *Phys. Rev. Lett.*, 43:1365–1368, Nov 1979.

[38] Alan H. Guth. Inflationary universe: A possible solution to the horizon and flatness problems. *Phys. Rev. D*, 23:347–356, Jan 1981.

[39] L. Patrizii and M. Spurio. Status of searches for magnetic monopoles. *Annual Review of Nuclear and Particle Science*, 65(1):279–302, 2015.

[40] M Fairbairn, AC Kraan, DA Milstead, Torbjörn Sjöstrand, Peter Skands, and Terry Sloan. Stable massive particles at colliders. *Physics Reports*, 438(1):1–63, 2007.

[41] E. N. Parker. The origin of magnetic fields. *The Astrophysical Journal*, 160:383, May 1970.

[42] V.A. Rubakov. Adler-Bell-Jackiw anomaly and fermion-number breaking in the presence of a magnetic monopole. *Nuclear Physics B*, 203(2):311–348, 1982.

[43] Curtis G. Callan. Dyon-fermion dynamics. *Phys. Rev. D*, 26:2058–2068, Oct 1982.

[44] Sergey Burdin, Malcolm Fairbairn, Philippe Mermod, David Milstead, James Pinfold, Terry Sloan, and Wendy Taylor. Non-collider searches for stable massive particles. *Physics Reports*, 582:1–52, 2015.

[45] Nick E. Mavromatos and Vasiliki A. Mitsou. Magnetic monopoles revisited: Models and searches at colliders and in the cosmos. *Int. J. Mod. Phys. A*, 35(23):2030012, 2020.

[46] P.A. Zyla et al. Review of particle physics. *PTEP*, 2020(8):083C01, 2020.

[47] Hunmoo Jeon and Michael J Longo. Search for magnetic monopoles trapped in matter. *Physical review letters*, 75(8):1443, 1995.

[48] Michael S. Turner, E. N. Parker, and T. J. Bogdan. Magnetic monopoles and the survival of galactic magnetic fields. *Phys. Rev. D*, 26:1296–1305, Sep 1982.

[49] Fred C. Adams, Marco Fatuzzo, Katherine Freese, Gregory Tarlé, Richard Watkins, and Michael S. Turner. Extension of the Parker bound on the flux of magnetic monopoles. *Phys. Rev. Lett.*, 70:2511–2514, Apr 1993.

[50] Oliver Gould and Arttu Rajantie. Magnetic monopole mass bounds from heavy-ion collisions and neutron stars. *Phys. Rev. Lett.*, 119(24):241601, Dec 2017.

[51] Michelangelo Ambrosio et al. Final results of magnetic monopole searches with the MACRO experiment. *The European Physical Journal C-Particles and Fields*, 25(4):511–522, 2002.

[52] Leonard P. Gamberg, George R. Kalbfleisch, and Kimball A. Milton. Direct and indirect searches for low mass magnetic monopoles. *Found. Phys.*, 30:543–565, 2000.

[53] MG Aartsen, K Abraham, M Ackermann, J Adams, JA Aguilar, M Ahlers, M Ahrens, D Altmann, T Anderson, I Ansseau, et al. Searches for relativistic magnetic monopoles in IceCube. *The European Physical Journal C*, 76(3):1–16, 2016.

[54] Georges Aad, Brad Abbott, Dale Charles Abbott, A Abed Abud, K Abeling, DK Abhayasinghe, SH Abidi, OS AbouZeid, NL Abraham, H Abramowicz, et al. Search for magnetic monopoles and stable high-electric-charge objects in 13 TeV proton-proton collisions with the ATLAS detector. *Physical review letters*, 124(3):031802, 2020.

[55] B. Acharya et al. Magnetic monopole search with the full MoEDAL trapping detector in 13 TeV pp collisions interpreted in photon-fusion and Drell-Yan production. *Phys. Rev. Lett.*, 123(2):021802, 2019.

[56] G Abbiendi, C Ainsley, PF Åkesson, G Alexander, G Anagnostou, KJ Anderson, S Asai, D Axen, I Bailey, E Barberio, et al. Search for Dirac magnetic monopoles in e+ e- collisions with the OPAL detector at LEP2. *Physics Letters B*, 663(1-2):37–42, 2008.

[57] H1 Collaboration. A direct search for stable magnetic monopoles produced in positron-proton collisions at HERA. *The European Physical Journal C-Particles and Fields*, 41:133–141, 2005.

[58] Y. D. He. Search for a Dirac magnetic monopole in high energy nucleus-nucleus collisions. *Phys. Rev. Lett.*, 79:3134–3137, Oct 1997.

[59] Daniel P Hogan, Dave Z Besson, John P Ralston, Ilya Kravchenko, and D Seckel. Relativistic magnetic monopole flux constraints from RICE. *Physical Review D*, 78(7):075031, 2008.

[60] M. Detrixhe, D. Besson, P. W. Gorham, P. Allison, B. Baughmann, J. J. Beatty, K. Belov, S. Bevan, W. R. Binns, C. Chen, P. Chen, J. M. Clem, A. Connolly, D. De Marco, P. F. Dowkontt, M. A. DuVernois, C. Frankenfeld, E. W. Grashorn, D. P. Hogan, N. Griffith, B. Hill, S. Hoover, M. H. Israel, A. Javaid, K. M. Liewer, S. Matsuno, B. C. Mercurio, C. Miki, M. Mottram, J. Nam, R. J. Nichol, K. Palladino, A. Romero-Wolf, L. Ruckman, D. Saltzberg, D. Seckel, G. S. Varner, A. G. Vieregg, and Y. Wang. Ultrarelativistic magnetic monopole search with the ANITA-II balloon-borne radio interferometer. *Phys. Rev. D*, 83:023513, Jan 2011.

[61] P. B. Price, E. K. Shirk, W. Z. Osborne, and L. S. Pinsky. Evidence for detection of a moving magnetic monopole. *Phys. Rev. Lett.*, 35:487–490, Aug 1975.

[62] Blas Cabrera. First results from a superconductive detector for moving magnetic monopoles. *Phys. Rev. Lett.*, 48:1378–1381, May 1982.

[63] Y. M. Cho and D. Maison. Monopoles in Weinberg-Salam model. *Phys. Lett.*, B391:360–365, 1997.

[64] John Ellis, Nick E. Mavromatos, and Tevong You. The price of an electroweak monopole. *Phys. Lett.*, B756:29–35, 2016.

[65] Suntharan Arunasalam and Archil Kobakhidze. Electroweak monopoles and the electroweak phase transition. *Eur. Phys. J. C*, 77(7):444, 2017.

[66] P.Q. Hung. Topologically stable, finite-energy electroweak-scale monopoles. *Nucl. Phys. B*, 962:115278, 2021.

[67] Georges Aad et al. Search for magnetic monopoles and stable particles with high electric charges in 8 TeV *pp* collisions with the ATLAS detector. *Phys. Rev.*, D93(5):052009, 2016.

[68] B. Acharya et al. Search for magnetic monopoles with the MoEDAL prototype trapping detector in 8 TeV proton-proton collisions at the LHC. *JHEP*, 08:067, 2016.

[69] B. Acharya et al. Search for magnetic monopoles with the MoEDAL forward trapping detector in 2.11 fb^{-1} of 13 TeV proton-proton collisions at the LHC. *Phys. Lett.*, B782:510–516, 2018.

[70] J.L. Pinfold, R. Du, K. Kinoshita, B. Lorazo, B. Price, and M. Regimbald. A search for highly ionizing particles produced at the OPAL intersection point at LEP. *Physics Letters B*, 316(2):407–411, 1993.

[71] A Abulencia, D Acosta, J Adelman, T Affolder, T Akimoto, MG Albrow, D Ambrose, S Amerio, D Amidei, A Anastassov, et al. Direct search for Dirac magnetic monopoles in p p collisions at s= 1.96 TeV. *Physical review letters*, 96(20):201801, 2006.

[72] GR Kalbfleisch, W Luo, KA Milton, EH Smith, and MG Strauss. Limits on production of magnetic monopoles utilizing samples from the D0 and CDF detectors at the Fermilab Tevatron. *Physical Review D*, 69(5):052002, 2004.

[73] Edward Witten. Baryons in the 1/n expansion. *Nucl. Phys.*, B160:57–115, 1979.

[74] A. K. Drukier and S. Nussinov. Monopole pair creation in energetic collisions: Is it possible? *Phys. Rev. Lett.*, 49:102–105, Jul 1982.

[75] C. J. Goebel. The spatial extent of magnetic monopoles. In P. G. O. Freund, C. J. Goebel, and Y. Nambu, editors, *Quanta: Essays in Theoretical Physics Dedicated to Gregor Wentzel*, pages 338–344. University of Chicago Press, 1970.

[76] Alfred S. Goldhaber. Monopoles and gauge theories. In Richard A. Carrigan and W. P. Trower, editors, *Magnetic Monopoles. Proceedings, NATO Advanced Study Institute, Wingspread, USA, October 14-17, 1982*, volume 102, pages pp.1–16. Elsevier B.V., 1983.

[77] Sidney R. Coleman. The magnetic monopole fifty years later. In *Particles and Fields 2. Proceedings, Summer Institute, Banff, Canada, August 16-27, 1981*, pages 461–552, 1982. [,461(1982)].

[78] Oliver Gould. *Magnetic monopole creation*. PhD thesis, Imperial Coll., London, 2017.

[79] S. Baines, N. E. Mavromatos, V. A. Mitsou, J. L. Pinfold, and A. Santra. Monopole production via photon fusion and Drell–Yan processes: MadGraph implementation and perturbativity via velocity-dependent coupling and magnetic moment as novel features. *Eur. Phys. J.*, C78(11):966, 2018.

[80] Xu-Guang Huang. Electromagnetic fields and anomalous transports in heavy-ion collisions — a pedagogical review. *Rept. Prog. Phys.*, 79(7):076302, 2016.

[81] Gabriele Inghirami, Mark Mace, Yuji Hirono, Luca Del Zanna, Dmitri E Kharzeev, and Marcus Bleicher. Magnetic fields in heavy ion collisions: flow and charge transport. *The European Physical Journal C*, 80:1–26, 2020.

[82] Ian K. Affleck and Nicholas S. Manton. Monopole pair production in a magnetic field. *Nucl. Phys.*, B194:38–64, 1982.

[83] Ian K. Affleck, Orlando Alvarez, and Nicholas S. Manton. Pair production at strong coupling in weak external fields. *Nucl. Phys.*, B197:509–519, 1982.

[84] LA Ljusternik. The topology of the calculus of variations in the large (Amer. Math. Soc. Transl. 16). *Providence, RI: American Mathematical Society*, 1966.

[85] N. S. Manton. Topology in the Weinberg-Salam theory. *Phys. Rev.*, D28:2019, 1983.

[86] F. R. Klinkhamer and N. S. Manton. A saddle-point solution in the Weinberg-Salam theory. *Phys. Rev. D*, 30:2212–2220, Nov 1984.

[87] H.G. Liddell, F. Passow, R. Scott, and H. Drisler. *A Greek-English Lexicon: Based on the German Work of Francis Passow.* A Greek-English Lexicon: Based on the German Work of Francis Passow. Harper & brothers, 1859.

[88] N. S. Manton. The inevitability of sphalerons in field theory. *Phil. Trans. Roy. Soc. Lond.*, A377(2161):20180327, 2019.

[89] Clifford Henry Taubes. The existence of a non-minimal solution to the SU(2) Yang-Mills-Higgs equations on $\mathbb{R}^3$. part I. *Communications in Mathematical Physics*, 86(2):257–298, Jun 1982.

[90] Burkhard Kleihaus and Jutta Kunz. Multi - sphalerons in the weak interactions. *Phys. Lett. B*, 329:61–67, 1994.

[91] Burkhard Kleihaus and Jutta Kunz. Multi - sphalerons in the Weinberg-Salam theory. *Phys. Rev. D*, 50:5343–5351, 1994.

[92] Steven Weinberg. A model of leptons. *Phys. Rev. Lett.*, 19:1264–1266, Nov 1967.

[93] Abdus Salam. Weak and electromagnetic interactions. *Conf. Proc. C*, 680519:367–377, 1968.

[94] S-H Henry Tye and Sam SC Wong. The Chern-Simons number as a dynamical variable. *arXiv preprint arXiv:1601.00418*, 2016.

[95] G. 't Hooft. Symmetry breaking through Bell-Jackiw anomalies. *Phys. Rev. Lett.*, 37:8–11, Jul 1976.

[96] G. 't Hooft. Computation of the quantum effects due to a four-dimensional pseudo-particle. *Phys. Rev. D*, 14:3432–3450, Dec 1976.

[97] Stephen L. Adler. Axial-vector vertex in spinor electrodynamics. *Phys. Rev.*, 177:2426–2438, Jan 1969.

[98] J. S. Bell and R. Jackiw. A PCAC puzzle: $\pi^0 \to \gamma\gamma$ in the σ model. *Nuovo Cim. A*, 60:47–61, 1969.

[99] Graham Albert White. *A Pedagogical Introduction to Electroweak Baryogenesis*. 2053-2571. Morgan & Claypool Publishers, 2016.

[100] Burkhard Kleihaus, Jutta Kunz, and Yves Brihaye. The electroweak sphaleron at physical mixing angle. *Physics Letters B*, 273(1):100–104, 1991.

[101] Margaret E. R. James. The sphaleron at nonzero Weinberg angle. *Z. Phys.*, C55:515–524, 1992.

[102] Valerii A Rubakov and Mikhail E Shaposhnikov. Electroweak baryon number non-conservation in the early universe and in high energy collisions. In *AIP Conference Proceedings*, volume 419, pages 347–412. American Institute of Physics, 1998.

[103] Claudio Rebbi and Robert L. Singleton, Jr. Computational study of baryon number violation in high-energy electroweak collisions. *Phys. Rev.*, D54:1020–1043, 1996.

[104] F. L. Bezrukov, D. Levkov, C. Rebbi, V. A. Rubakov, and P. Tinyakov. Semiclassical study of baryon and lepton number violation in high-energy electroweak collisions. *Phys. Rev.*, D68:036005, 2003.

[105] F. L. Bezrukov, D. Levkov, C. Rebbi, V. A. Rubakov, and P. Tinyakov. Suppression of baryon number violation in electroweak collisions: Numerical results. *Phys. Lett.*, B574:75–81, 2003.

[106] S. H. Henry Tye and Sam S. C. Wong. Baryon number violating scatterings in laboratories. *Phys. Rev.*, D96(9):093004, 2017.

[107] Yu-Cheng Qiu and S. H. Henry Tye. The role of Bloch waves in baryon-number violating processes. 2018.

[108] Frans R. Klinkhamer and R. Laterveer. The sphaleron at finite mixing angle. *Z. Phys.*, C53:247–252, 1992.

[109] Jutta Kunz, Burkhard Kleihaus, and Yves Brihaye. Sphalerons at finite mixing angle. *Phys. Rev. D*, 46:3587–3600, Oct 1992.

[110] Mark Hindmarsh and Margaret James. The origin of the sphaleron dipole moment. *Phys. Rev.*, D49:6109–6114, 1994.

[111] Sidney Coleman. *Aspects of Symmetry: Selected Erice Lectures*. Cambridge University Press, Cambridge, U.K., 1985.

[112] Jr. Curtis G. Callan and Sidney R. Coleman. The fate of the false vacuum. 2. first quantum corrections. *Phys. Rev.*, D16:1762–1768, 1977.

[113] M. Stone. The lifetime and decay of excited vacuum states of a field theory associated with nonabsolute minima of its effective potential. *Phys. Rev.*, D14:3568, 1976.

[114] Sidney R. Coleman. The fate of the false vacuum. 1. semiclassical theory. *Phys. Rev.*, D15:2929–2936, 1977. [Erratum: Phys. Rev.D16,1248(1977)].

[115] Sidney Coleman. Quantum tunneling and negative eigenvalues. *Nuclear Physics B*, 298(1):178–186, 1988.

[116] Alexander M. Polyakov. Quark confinement and topology of gauge groups. *Nucl. Phys. B*, 120:429–458, 1977.

[117] A. A. Belavin, Alexander M. Polyakov, A. S. Schwartz, and Yu. S. Tyupkin. Pseudoparticle solutions of the Yang-Mills equations. *Phys. Lett. B*, 59:85–87, 1975.

[118] W Heisenberg and H Euler. Folgerungen aus der Diracschen Theorie des Positrons. *Zeitschrift für Physik*, 98(11-12):714–732, 1936.

[119] Seungyong Hahn, Kwanglok Kim, Kwangmin Kim, Xinbo Hu, Thomas Painter, Iain Dixon, Seokho Kim, Kabindra R Bhattarai, So Noguchi, Jan Jaroszynski, et al. 45.5-Tesla direct-current magnetic field generated with a high-temperature superconducting magnet. *Nature*, 570(7762):496–499, 2019.

[120] SA Olausen and VM Kaspi. The McGill magnetar catalog. *The Astrophysical Journal Supplement Series*, 212(1):6, 2014.

[121] Wei-Tian Deng and Xu-Guang Huang. Event-by-event generation of electromagnetic fields in heavy-ion collisions. *Phys. Rev.*, C85(4):044907, 2012.

[122] John Bloczynski, Xu-Guang Huang, Xilin Zhang, and Jinfeng Liao. Azimuthally fluctuating magnetic field and its impacts on observables in heavy-ion collisions. *Physics Letters B*, 718(4-5):1529–1535, 2013.

[123] Richard P. Feynman. An operator calculus having applications in quantum electrodynamics. *Phys. Rev.*, 84:108–128, 1951.

[124] Gerald V. Dunne and Christian Schubert. Worldline instantons and pair production in inhomogeneous fields. *Phys. Rev. D*, 72:105004, 2005.

[125] Gerald V Dunne, Qing-hai Wang, Holger Gies, and Christian Schubert. Worldline instantons and the fluctuation prefactor. *Physical Review D*, 73(6):065028, Mar 2006.

[126] Cesim K. Dumlu and Gerald V. Dunne. Complex worldline instantons and quantum interference in vacuum pair production. *Phys. Rev.*, D84:125023, 2011.

[127] Christian Schneider. *Worldline instantons and the Sauter-Schwinger effect*. PhD thesis, May 2019.

[128] V. S. Dotsenko and S. N. Vergeles. Renormalizability of phase factors in the NonAbelian gauge theory. *Nucl. Phys.*, B169:527–546, 1980.

[129] Alexander M. Polyakov. Gauge fields as rings of glue. *Nucl. Phys.*, B164:171–188, 1980.

[130] Alexander M. Polyakov. Gauge fields and strings. *Contemp. Concepts Phys.*, 3:1–301, 1987.

[131] Oliver Gould and Arttu Rajantie. Thermal Schwinger pair production at arbitrary coupling. *Phys. Rev.*, D96(7):076002, 2017.

[132] Olindo Corradini and Christian Schubert. Spinning particles in quantum mechanics and quantum field theory. 2015.

[133] K Bardakci and S. Samuel. Local field theory for solitons. *Phys. Rev.*, D18:2849, 1978.

[134] N. S. Manton. An effective Lagrangian for solitons. *Nucl. Phys.*, B150:397–412, 1979.

[135] M. Creutz. *Quarks, Gluons and Lattices*. Cambridge Monographs on Mathematical Physics. Cambridge University Press, 1983.

[136] I. Montvay and G. Münster. *Quantum Fields on a Lattice*. Cambridge Monographs on Mathematical Physics. Cambridge University Press, 1994.

[137] David Tong. Gauge theory, 2018. Lecture notes.

[138] Kenneth G. Wilson. Confinement of quarks. *Phys. Rev. D*, 10:2445–2459, Oct 1974.

[139] David E Rumelhart, Geoffrey E Hinton, and Ronald J Williams. Learning representations by back-propagating errors. *nature*, 323(6088):533–536, 1986.

[140] Geoffrey Hinton, Nitish Srivastava, and Kevin Swersky. Neural networks for machine learning lecture 6a overview of mini-batch gradient descent, 2012. Lecture notes.

[141] John Duchi, Elad Hazan, and Yoram Singer. Adaptive subgradient methods for online learning and stochastic optimization. *Journal of machine learning research*, 12(7), 2011.

[142] Diederik P Kingma and Jimmy Ba. Adam: A method for stochastic optimization. *arXiv preprint arXiv:1412.6980*, 2014.

[143] Sebastian Ruder. An overview of gradient descent optimization algorithms. *arXiv preprint arXiv:1609.04747*, 2016.

[144] W.H. Press, W. H, S.A. Teukolsky, W.T. Vetterling, S. A, and B.P. Flannery. *Numerical Recipes 3rd Edition: The Art of Scientific Computing*. Cambridge University Press, 2007.

[145] So Chigusa, Takeo Moroi, and Yutaro Shoji. Bounce configuration from gradient flow. *Phys. Lett.*, B800:135115, 2019.

[146] R. D. Mawhinney. Confinement and saddle point configurations. *Nucl. Phys. B Proc. Suppl.*, 26:444–446, 1992.

[147] Anthony Duncan and Robert D. Mawhinney. Lattice saddle point configurations in SU(2) in three-dimensions. *Phys. Lett. B*, 282:423–427, 1992.

[148] A. J. van der Sijs. Gauge invariant extremization. *Nucl. Phys. B Proc. Suppl.*, 30:893–896, 1993.

[149] Bert Speelpenning. Compiling fast partial derivatives of functions given by algorithms. Technical report, Illinois Univ., Urbana (USA). Dept. of Computer Science, 1980.

[150] Iulia M. Comsa, Moritz Firsching, and Thomas Fischbacher. So(8) supergravity and the magic of machine learning. *JHEP*, 08:057, 2019.

[151] Atılım Günes Baydin, Barak A Pearlmutter, Alexey Andreyevich Radul, and Jeffrey Mark Siskind. Automatic differentiation in machine learning: a survey. *The Journal of Machine Learning Research*, 18(1):5595–5637, 2017.

[152] Juliana Duncan, Qiliang Wu, Keith Promislow, and Graeme Henkelman. Biased gradient squared descent saddle point finding method. *The Journal of Chemical Physics*, 140(19):194102, 2014.

[153] David L.-J. Ho. davidho95/tfmonopoles: First release, June 2021.

[154] Martín Abadi, Ashish Agarwal, Paul Barham, Eugene Brevdo, Zhifeng Chen, Craig Citro, Greg S. Corrado, Andy Davis, Jeffrey Dean, Matthieu Devin, Sanjay Ghemawat, Ian Goodfellow, Andrew Harp, Geoffrey Irving, Michael Isard, Yangqing Jia, Rafal Jozefowicz, Lukasz Kaiser, Manjunath Kudlur, Josh Levenberg, Dandelion Mané, Rajat Monga, Sherry Moore, Derek Murray, Chris Olah, Mike Schuster, Jonathon Shlens, Benoit Steiner, Ilya Sutskever, Kunal Talwar, Paul Tucker, Vincent Vanhoucke, Vijay Vasudevan, Fernanda Viégas, Oriol Vinyals, Pete Warden, Martin Wattenberg, Martin Wicke, Yuan Yu, and Xiaoqiang Zheng. TensorFlow: Large-scale machine learning on heterogeneous systems, 2015. Software available from tensorflow.org.

[155] Wit Busza, Krishna Rajagopal, and Wilke van der Schee. Heavy ion collisions: The big picture and the big questions. *Annual Review of Nuclear and Particle Science*, 68(1):339–376, 2018.

[156] M. Harrison, T. Ludlam, and S. Ozaki. RHIC project overview. *Nucl. Instrum. Meth. A*, 499:235–244, 2003.

[157] John Jowett et al. The 2018 heavy-ion run of the LHC. In *10th International Particle Accelerator Conference*, page WEYYPLM2, 2019.

[158] Dmitri E. Kharzeev, Larry D. McLerran, and Harmen J. Warringa. The effects of topological charge change in heavy ion collisions: 'event by event P and CP violation'. *Nucl. Phys.*, A803:227–253, 2008.

[159] H. De Vries, C. W. De Jager, and C. De Vries. Nuclear charge and magnetization density distribution parameters from elastic electron scattering. *Atom. Data Nucl. Data Tabl.*, 36:495–536, 1987.

[160] Jaroslav Adam et al. Centrality dependence of particle production in p-Pb collisions at $\sqrt{s_{\rm NN}}$= 5.02 TeV. *Phys. Rev.*, C91(6):064905, 2015.

[161] Greger Torgrimsson, Johannes Oertel, and Ralf Schützhold. Doubly assisted Sauter-Schwinger effect. *Phys. Rev.*, D94(6):065035, 2016.

[162] E. Brezin and C. Itzykson. Pair production in vacuum by an alternating field. *Phys. Rev.*, D2:1191–1199, 1970.

[163] A. I. Nikishov. Barrier scattering in field theory removal of Klein paradox. *Nucl. Phys.*, B21:346–358, 1970.

[164] Sang Pyo Kim and Don N Page. Schwinger pair production in electric and magnetic fields. *Physical Review D*, 73(6):065020, 2006.

[165] LV Keldysh et al. Ionization in the field of a strong electromagnetic wave. *Sov. Phys. JETP*, 20(5):1307–1314, 1965. [Zh. Eksp. Teor. Fiz. 47, No. 5, 1945 (1965)].

[166] Chen Lan, Yi-Fan Wang, Huifang Geng, and Alexander Andree. Holographic Schwinger effect of dynamic fields. 2018.

[167] Christian Schneider, Greger Torgrimsson, and Ralf Schützhold. Discrete worldline instantons. *Phys. Rev.*, D98(8):085009, 2018.

[168] Nikolay Borisovich Narozhny, SS Bulanov, Vadim Davydovich Mur, and Vladimir Stepanovich Popov. On e+ e- pair production by colliding electromagnetic pulses. *Journal of Experimental and Theoretical Physics Letters*, 80(6):382–385, 2004.

[169] S.P. Gavrilov and D.M. Gitman. Vacuum instability in slowly varying electric fields. *Phys. Rev. D*, 95(7):076013, 2017.

[170] I. A. Aleksandrov, G. Plunien, and V. M. Shabaev. Locally-constant field approximation in studies of electron-positron pair production in strong external fields. *Phys. Rev.*, D99(1):016020, 2019.

[171] Christian Kohlfürst. Phase-space analysis of the Schwinger effect in inhomogeneous electromagnetic fields. *Eur. Phys. J. Plus*, 133(5):191, 2018.

[172] SA Smolyansky, G Röpke, S Schmidt, D Blaschke, VD Toneev, and AV Prozorkevich. Dynamical derivation of a quantum kinetic equation for particle production in the Schwinger mechanism. *arXiv preprint hep-ph/9712377*, 1997.

[173] S Schmidt, D Blaschke, G Röpke, SA Smolyansky, AV Prozorkevich, and VD Toneev. A quantum kinetic equation for particle production in the Schwinger mechanism. *International Journal of Modern Physics E*, 7(06):709–722, 1998.

[174] Yuval Kluger, Emil Mottola, and Judah M Eisenberg. Quantum Vlasov equation and its Markov limit. *Physical Review D*, 58(12):125015, 1998.

[175] Iwo Bialynicki-Birula, Pawel Górnicki, and Johann Rafelski. Phase-space structure of the Dirac vacuum. *Phys. Rev. D*, 44:1825–1835, Sep 1991.

[176] Florian Hebenstreit, Reinhard Alkofer, and Holger Gies. Schwinger pair production in space-and time-dependent electric fields: Relating the Wigner formalism to quantum kinetic theory. *Physical Review D*, 82(10):105026, 2010.

[177] Florian Hebenstreit, Anton Ilderton, Mattias Marklund, and Jens Zamanian. Strong field effects in laser pulses: the Wigner formalism. *Physical Review D*, 83(6):065007, 2011.

[178] V. S. Popov. Production of e+e- pairs in an alternating external field. *JETP Lett.*, 13:185–187, 1971. [Pisma Zh. Eksp. Teor. Fiz.13,261(1971)].

[179] VS Popov. Pair production in a variable and homogeneous electric field as an oscillator problem. *Soviet Journal of Experimental and Theoretical Physics*, 35, 1972.

[180] M. S. Marinov and V. S. Popov. Electron-positron pair creation from vacuum induced by variable electric field. *Fortsch. Phys.*, 25:373–400, 1977.

[181] F. Hebenstreit, R. Alkofer, and H. Gies. Particle self-bunching in the Schwinger effect in spacetime-dependent electric fields. *Phys. Rev. Lett.*, 107:180403, 2011.

[182] I. A. Aleksandrov, G. Plunien, and V. M. Shabaev. Momentum distribution of particles created in space-time-dependent colliding laser pulses. *Phys. Rev. D*, 96(7):076006, 2017.

[183] Q. Z. Lv, S. Dong, Y. T. Li, Z. M. Sheng, Q. Su, and R. Grobe. Role of the spatial inhomogeneity on the laser-induced vacuum decay. *Phys. Rev. A*, 97(2):022515, 2018.

[184] Christian Kohlfürst. Effect of time-dependent inhomogeneous magnetic fields on the particle momentum spectrum in electron-positron pair production. *Phys. Rev. D*, 101(9):096003, 2020.

[185] Ivan A. Aleksandrov and Christian Kohlfürst. Pair production in temporally and spatially oscillating fields. *Phys. Rev. D*, 101(9):096009, 2020.

[186] W. a Heisenberg. Uber den anschaulichen Inhalt der quantentheoretischen Kinematik und Mechanik. *Z. Phys.*, 43:172–198, 1927.

[187] M. Bauer and P. A. Mello. The time-energy uncertainty relation. *Annals Phys.*, 111:38–60, 1978.

[188] Paul Busch. *The Time–Energy Uncertainty Relation*, pages 73–105. Springer Berlin Heidelberg, Berlin, Heidelberg, 2008.

[189] S. Agostinelli et al. GEANT4–a simulation toolkit. *Nucl. Instrum. Meth. A*, 506:250–303, 2003.

[190] C. Montonen and D. Olive. Magnetic monopoles as gauge particles? *Physics Letters B*, 72(1):117–120, 1977.

[191] Howard Georgi and Sheldon L. Glashow. Unified weak and electromagnetic interactions without neutral currents. *Phys. Rev. Lett.*, 28:1494–1497, May 1972.

[192] N. K. Nielsen and P. Olesen. An unstable Yang-Mills field mode. *Nucl. Phys. B*, 144:376–396, 1978.

[193] Oliver Gould, Arttu Rajantie, and Cheng Xie. Worldline sphaleron for thermal Schwinger pair production. *Phys. Rev.*, D98(5):056022, 2018.

[194] Ayush Saurabh and Tanmay Vachaspati. Monopole-antimonopole interaction potential. *Phys. Rev. D*, 96:103536, Nov 2017.

[195] A. C. Davis, T. W. B. Kibble, A. Rajantie, and H. Shanahan. Topological defects in lattice gauge theories. *JHEP*, 11:010, 2000.

[196] Arttu Rajantie. Mass of a quantum't hooft-polyakov monopole. *Journal of High Energy Physics*, 2006(01):088, 2006.

[197] Jonathan Barzilai and Jonathan M. Borwein. Two-point step size gradient methods. *IMA Journal of Numerical Analysis*, 8(1):141–148, 01 1988.

[198] David Daverio, Mark Hindmarsh, and Neil Bevis. Latfield2: A C++ library for classical lattice field theory. 2015.

[199] Michael S. Turner and Lawrence M. Widrow. Inflation produced, large scale magnetic fields. *Phys. Rev.*, D37:2743, 1988.

[200] Y. Nambu. String-like configurations in the Weinberg-Salam theory. *Nuclear Physics B*, 130(3):505–515, 1977.

[201] Tanmay Vachaspati. Vortex solutions in the Weinberg-Salam model. *Phys. Rev. Lett.*, 68:1977–1980, Mar 1992.

[202] Tanmay Vachaspati and George B. Field. Electroweak string configurations with baryon number. *Phys. Rev. Lett.*, 73:373–376, Jul 1994.

[203] Ana Achucarro and Tanmay Vachaspati. Semilocal and electroweak strings. *Phys. Rept.*, 327:347–426, 2000. [Phys. Rept.327,427(2000)].

[204] D. Comelli, D. Grasso, M. Pietroni, and A. Riotto. The sphaleron in a magnetic field and electroweak baryogenesis. *Phys. Lett.*, B458:304–309, 1999.

[205] P. H. Damgaard and D. Espriu. Anomalous electroweak processes in a strong magnetic field. *Phys. Lett.*, B256:442–450, 1991.

[206] Jaume Garriga and Xavi Montes. Stability of Z strings in strong magnetic fields. *Phys. Rev. Lett.*, 75:2268–2271, 1995.

[207] Yu Hamada and Kengo Kikuchi. Sphaleron from gradient flow. 2020.

[208] M. Joyce and Mikhail E. Shaposhnikov. Primordial magnetic fields, right-handed electrons, and the abelian anomaly. *Phys. Rev. Lett.*, 79:1193–1196, 1997.

[209] Ruth Durrer and Andrii Neronov. Cosmological magnetic fields: Their generation, evolution and observation. *Astron. Astrophys. Rev.*, 21:62, 2013.

[210] Edward Witten. Superconducting strings. *Nucl. Phys. B*, 249:557–592, 1985.

[211] Juan Maldacena. Comments on magnetic black holes. *JHEP*, 04:079, 2021.

[212] Tanmay Vachaspati. Creation of magnetic monopoles in classical scattering. *Phys. Rev. Lett.*, 117(18):181601, 2016.

[213] Steffen Krusch and Paul Sutcliffe. Sphalerons in the Skyrme model. *Journal of Physics A: Mathematical and General*, 37(38):9037, 2004.

[214] A.I. Nikishov. Pair production by a constant external field. *Sov. Phys. JETP*, 30(4):660, 1970. [Zh. Eksp. Teor. Fiz. 57, No. 4, 1210 (1969)].